EVALUATION AND USE OF REGENERATIVE MULTI ELECTRODE INTERFACES IN PERIPHERAL NERVES

By

VIDHI DESAI

Presented to the Faculty of the Graduate School of

The University of Texas at Arlington in Partial Fulfillment

of the Requirements

for the Degree of

DOCTOR OF PHILOSOPHY

THE UNIVERSITY OF TEXAS AT ARLINGTON

August 2014

Dedication

- *To the spirit of the land where dreams come true!*

“…..The value of a college education is not the learning of many facts, but the training of the mind to think.” Albert Einstein

“…..A scientist in his laboratory is not merely a technician; he is also a child confronting natural phenomena that continue to impress him as though they were fairy tales.” Marie Curie

Acknowledgements

Many individuals have contributed to the extensive experiments involved in this work, and I would not be able to complete my part without their sincere efforts. Reflecting back on my graduate school journey, I do acknowledge this dissertation to be part of a learning experience in scientific research and yet I hope that the compiled information is useful to others pursuing similar future endeavors.

I am very thankful to my advisor, Dr. Mario Romero-Ortega, who encouraged me to pursue a career in science and provided me with an exceptional beginning opportunity in the field of neural engineering that ultimately resulted in this dissertation. He is an incredible mentor who ensured that, over the years, I receive comprehensive tutelage in research, teaching and communication skills as well as leadership and management principles. He has constantly motivated me to identify my personal limitations and address them.

I am extremely grateful to Dr. Edward Keefer who has relentlessly helped me at several different stages of my doctorate project. His continuous guidance enabled me to ward off intimidation from the chaotic “world of electrophysiology”, persist through challenging recording sessions, and understand the associated practical and theoretical intricacies. Most valuably, he taught me to look beyond the realm of mysticism and steadily develop an attitude of logical reasoning.

I extend my gratitude to Stanisa Raspopovic, Marco Capogrosso, and Professor Silvestro Micera, at the École Polytechnique Fédérale de Lausanne (EPFL) in Switzerland, who graciously accepted me as part of their lab and took genuine interest in enhancing my doctorate training, making sure that I learnt the maximum possible during the short time I spent with them.

I am also very thankful to Dean Khosrow Behbehani, Dr. Yuan Peng, and Dr. Samarendra Mohanty for taking the time and effort to serve as my committee members, provide their valuable insight, and in particular, point out aspects that needed improvisation from my side.

I reiterate the importance of each and every individual who worked with me on the different experiments towards the accomplishment of this dissertation; unfortunately I cannot list everyone due to space restriction. Sanjay Anand deserves special thanks for simply surviving my often stubborn and almost paranoid ways during experiments, and just being the amazingly supportive friend he is.

The people who work behind the scenes are always the most difficult to thank. This includes all the beautiful friends that I made over the last few years, especially Charan Satish, Sonia Santimano and Sumeet Pawaskar, who stood by me from the start to the very end of this process and never allowed me to give up through its ups and downs.

A warm appreciation goes to the silent, unquestioning and protective support of my dear brother, sister-in-law, and family back in India. The people who remain most oblivious to their contribution are my parents, Hitendra and Kirtida Desai, who inculcated in me the two paramount values that, I believe, have served as a beacon to my thought process throughout the undertaken journey. I thank my papa for instilling the importance of independent thinking; the unparalleled conviction he holds has always been my aspiration. I thank my mummy for showing me that sincerity and perseverance are very important work ethics, but above all, for just making sure that the early foundation of my education never got compromised through some of the most difficult years of her life.

July 18, 2014.

Abstract

EVALUATION AND USE OF REGENERATIVE MULTIELECTRODE INTERFACES IN PERIPHERAL NERVES

Vidhi Desai, PhD

The University of Texas at Arlington, 2014

Supervising Professor: Mario Ignacio Romero-Ortega

Peripheral nerves offer unique accessibility to the innate motor and sensory pathways that can be interfaced with high degree of selectivity for intuitive and bidirectional control of advanced upper extremity prosthetic limbs. Several peripheral nerve interfaces have been proposed and investigated over the last few decades with significant progress made in the area of sensory feedback. However, clinical translation still remains a formidable challenge due to the lack of long term recordings. Prominent causes include signal degradation, eventual interface failures, and lack of specificity in the low amplitude nerve signals. This dissertation evaluates the capabilities of the newly developed Regenerative Multi-electrode Interface (REMI) by the characterization of signal quality progression, the identification of interfaced axon types, and the demonstration of “functional linkage” between acquired signals and target organs.

Chapter 2 details the chronic recording and characterization of high quality signals from REMI in sciatic nerve which remained stable over a 120 day implantation period indicative of minimal ongoing tissue response with no detrimental effects on the recording ability. The dominant cause of failures was attributable to abiotic factors pertaining to the connector/wire breakage, observed in 76% of REMI implants. Also, the REMI implants had 20% higher success rate and significantly larger signal to noise ratio in comparison to the Utah Slanted Electrode

Array (USEA). **Chapter 3** describes the successful feasibility of interfacing with motor and sensory axons by REMI implantation in the tibial and sural fascicles of the sciatic nerve. A characteristic sampling bias towards recording signals from medium-to-large diameter axons that are primarily involved in mechanoception and proprioception sensory functions was uncovered. Specific bursting units (Inter Spike Interval of 30-70ms) were observed most frequently from the tibial fascicle during bipedal locomotion. **Chapter 4** explores the discrimination between motor and proprioceptive origin of this bursting activity and reports on the identified efferent motor nature, as well as the demonstration of a significant and stable correlation with the activity of distal muscle involved in locomotion. In summary, sensory-motor neural activity was recorded chronically by REMI electrodes with high signal to noise ratio which serves as a tool for evaluating firing patterns of specific axon types during voluntary movement or sensory stimulation. In turn, this interface can be used to improve motor control and sensory feedback in closed loop systems for robotic prosthesis.

Table of Contents

List of Illustrations

List of Tables

Chapter 1

Introduction

1.1 Overview

Evidences of electrical activity recorded from the central and peripheral nervous system, since the early 19th and 20th centuries have led to a longstanding yet continually evolving goal in neuroscience, aimed at a fundamental understanding of its functioning and application of the deciphered mechanisms towards restoration and replacement of lost functions. Neural interfaces have a broad spectrum and are defined as “systems operating at the intersection of the nervous system and an internal or external device” by the National Institute of Health. The historical roots of neural interfaces can be traced back to the year 1787 when Luigi Galvani, an Italian physician, uncovered the concept of “animal electricity” by showing that nerves could be stimulated to induce muscle contractions. Emil DuBois-Reymond demonstrated in the year 1843 that the fundamental unit of “animal electricity”, i.e. action potential could be recorded which led to the advent of the field of electrophysiology. In the early 1900s, the works of Edgar Adrian and Charles Sherrington followed by that of Erlanger and Gasser gave insight into the fundamental principles of nerve conduction and its implication on the percepts of sensation. Simultaneously, electrical signals from the skeletal muscles were recorded as Electromyogram (EMG) and Electroencephalography (EEG) was developed by Hans Berger to measure electrical activity of the human brain for diagnosis of neurological disorders. Although, EEG and EMG are more commonly used as clinical diagnostic tools, extensive interdisciplinary research between neuroscience and engineering over the decades has led to promising avenues of voluntary skeletal movement and missing sensation replacement in the burgeoning field of neural interfaces. Cochlear implants that provide a sense of sound by direct electrical stimulation of the auditory nerve have been implanted in 324,200 patients worldwide as of December 2012 (source: NIH) and currently are the most successfully clinical translated neural interfaces. Deep Brain

Stimulation has been employed in 80,000 patients worldwide (source: Medtronic) since its inception in 2003 to alleviate symptoms associated with movement disorders in Parkinson's disease and its therapeutic application in other neurological disorders such as epilepsy and Obsessive Compulsive Disorders (OCD) are being investigated. More recently, a wireless retinal implant that can restore partially the sense of vision in patients suffering from congenital blindness by stimulation of optic nerve has been approved for clinical use by the Food and Drug Administration (FDA).

One of the most challenging yet coveted applications of neural interfaces is to drive robotic prostheses with electrical signals of the innate nervous system. Potential beneficiaries of this technology include people suffering from debilitating effects of paralysis of the upper and lower extremities, Locked-in syndrome, limb loss, and neurodegenerative diseases. An estimated of 1.6 million people suffered from major limb loss in the United States as of 2005, with projections up to 3.6 million by 2050, caused by diseases like diabetes and cancer or catastrophic personal injuries from war and accidents [1]. Recent research initiatives by the Defense Advanced Research Projects Agency (DARPA) have been extensively directed towards improved quality of life of returning war veterans with a special emphasis on mitigating disabling conditions of upper limb loss. These efforts have given an impetus to the development of neural interfaces that can provide intuitive control of sophisticated anthropomorphic prosthetic hands.

The following sections of this introductive chapter will provide a synopsis on upper extremity amputation, review the current state of the art prostheses and discuss different strategies for alternative control mechanisms leading into an outline of the specific aims of this research project.

1.2 Upper Limb Amputation

1.2.1 Prevalence and Etiology

Approximately 150,000 amputation surgeries with 10% comprised of mostly trauma related upper limb amputation are performed every year in the United States alone [2]. As of December 2013, a total of 1458 major limb amputations were reported among US troops over a thirteen year period spanning the military operations in Iraq and Afghanistan (Fischer, Hannah. "US Military Casualty Statistics: Operation New Dawn, Operation Iraqi Freedom, and Operation Enduring Freedom." (2013)). A study of smaller cohort in 2009 reported that 50% of extremity amputation seen at the Naval and Marine treatment facilities during a 1-year period were related to upper limb [3]. Although, the incidences of lower limb amputation are more common in both civilian and military population, the disabling effects and compromised quality of life are far more intense with upper limb loss [4] accounting for 76% permanent retirement in the US service members [5].

The functional sensory and motor deficits, consequent to damage of underlying nerves in the arm, and the type of prostheses prescribed vary depending on the level of amputation. Upper limb amputations are broadly classified on the level of injury into ranging from loss of one or more fingers (trans-metacarpal) to that of an entire arm (trans-humeral or forequarter) as shown in Figure 1.1. Trans-radial (through the forearm) and trans-humeral (above elbow) amputations are most commonly represented in 47 % and 34 % cases of upper limb loss in military population [5]. However, amputations at levels greater than the trans-carpal would contribute to an almost complete loss of sensation from the hand.

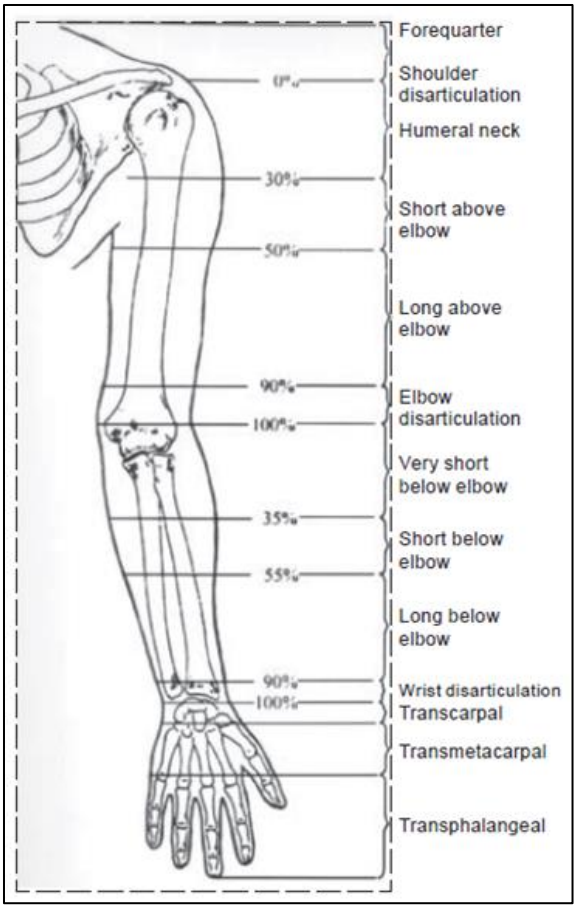

Figure 1.1 Nomenclature of upper limb amputation defined by length of residual limb relative to that of uninjured arm. Percentage indicates relative length and broad classification includes shoulder disarticulation as complete loss, Above Elbow (AE) or trans-humeral, Below Elbow (BE) or trans-radial, and trans-carpal (below wrist) at a 100% length of the uninjured arm. [6]

1.2.2 Artificial Prostheses for Arm Replacement

The earliest examples of prosthetic limbs date back to the 15th century BC as revealed by the finding of a leather and wood made toe on the foot of an Egyptian mummy. However, the beginning of modern prosthetic development is generally attributed to the works of Ambroise Pare´ (1510-1590), a French army surgeon, who first designed and used mechanical hands made of

iron, wood, copper and operated by springs and catches [6]. Subsequently, the vast number of limb losses that occurred during the Second World War along with the advancements in material and manufacturing industry at the time catalyzed the development of new generation prostheses made from plastics, aluminum, metals, and other composites. Since then, the components of modern upper extremity prosthetic arm primarily consist of a socket that attaches a Terminal Device (TD) to the residual stump of the amputated arm and allows for additional connections with harnesses, and artificial elbow and wrist units, depending on the type of prosthetic used.

TDs attached to the distal end of the prosthetic, serving primarily for the prehensile or grasping function, are broadly classified as passive or active. Passive devices include silicon made artificial hands for cosmetic restoration and hooks that assist functional tasks by using them to stabilize or push/pull objects. Active or powered terminal devices include mechanical and electric powered hooks and artificial hands that can perform simple tasks of picking and holding objects by opening/closing movements. While mechanical hooks are light in weight and operation wise similar to a pair of tweezers, electric powered hooks and hands can produce finger prehensile force up to 20-24 lbs similar to that of natural adult hand (Billock, J. N. Hands versus Hooks. Clinical prosthetics and Orthotics.1986.10 (2): 57-65). In lieu of the limited functionalities of these traditional prostheses, technological advancements in the field of material science and electro-mechanical device fabrication have led to the development of light weight anthropomorphic robotic hands that can perform complex movements with 22 degrees of freedom[7]. Touch Bionics, a Scottish company, was the first to commercialize in 2007 an articulated prosthetic hand capable of multiple grasping actions (iLimb), which is reported to have been implanted in 1200 patients worldwide (Source: Touch Bionics Inc). The 18 degree of freedom capable Luke Arm developed by Deka Research & Development Company and the Applied Physics Laboratory at Johns Hopkins University is adjustable to use with any level of

amputation and recently received approved for clinical use by the Food and Drug Administration (FDA).

1.2.3 Conventional Sources of Prosthetic Arm Control

All active terminal devices can be controlled currently by three main available mechanisms which are described further.

1.2.3.1 Bowden Cable Control:

These systems were largely developed around the 1950s in the United States and harness the forces generated by “gross” body movements such as arm flexion (gleno-humeral flexion) or shoulder shrug (scapular or bi-scapular abduction) to operate a Bowden cable that actuates and control mechanical terminal devices. Durability and ease of user learning are some of the advantages of these systems. Although forces sufficient for operation of an artificial hand, hook, or elbow can be developed by body motions in normal BE or AE amputees, at higher amputation levels such as the shoulder or forearm disarticulation these body motions may be absent or insufficient [8].

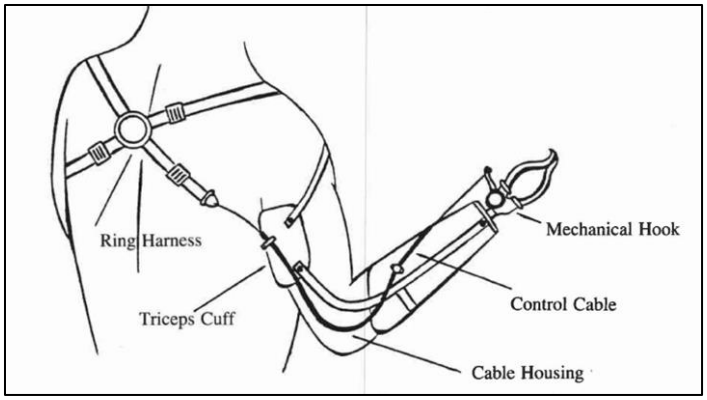

Figure 1.2 Illustration of a typical body or Bowden cable controlled Below Elbow (BE) prostheses with components as labeled. (Billock, J. N. Hands versus Hooks. Clinical prosthetics and Orthotics.1986.10 (2): 57-65)

1.2.3.2 Switch Control:

These systems utilize switches activated by “fine” body movements of remnant digit, part of a bony structure or by a pull on the suspension harness. Typically, they require less force and excursion in comparison to body controlled systems. Varieties of incorporated switches include pull, rocker, push-bottom or toggle types for activation of electric powered terminal devices (Billock, J. N. Hands versus Hooks. Clinical prosthetics and Orthotics.1986.10 (2): 57-65).

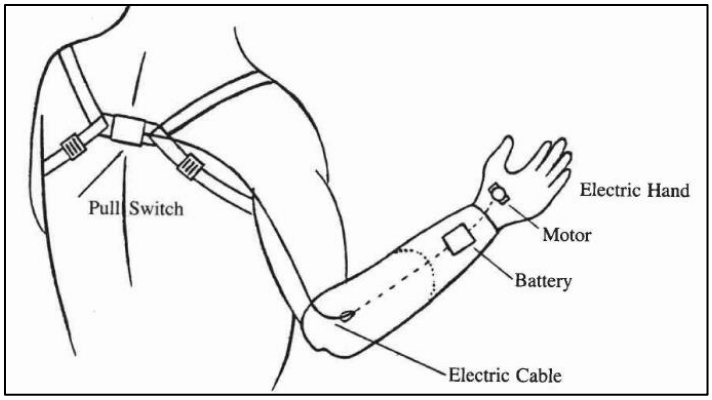

Figure 1.3 Illustration of a typical switch controlled Below Elbow (BE) prostheses with components as labeled. (Billock, J. N. Hands versus Hooks. Clinical prosthetics and Orthotics.1986.10 (2): 57-65)

1.2.3.3 Myoelectric Control:

Conceptualized first in Germany in 1948 and rapidly developed with the advent of micro-electronics from the 1960s to 1980s, these systems utilize the remaining existing neuromuscular system to generate forces and commands that actuate and control an electro-mechanical terminal device. As seen in the block diagram of Figure 1.4, EMG signals recorded with surface electrodes placed over appropriate muscle or muscle groups within the residual limb are amplified and used for either digital or proportional control of the terminal device. The speed or force of the prosthetic action is determined by the magnitude of the myoelectric signal in proportional control and by the duration of muscle contraction up to a preset limit in digital control systems [9]. The wider range of motion enabled by the elimination of the restrictive harness assembly was a major advantage of the initial systems leading to wide spread acceptance such that, by the year 1985, after further development of advanced myoelectric arms like the Otto Bock hand, the Italian arm, and the Utah arm [10], an estimated of 10,000 to 20,000 worldwide were implanted with myoelectric controlled

devices (Kritter AE. Current concepts review: myoclectric prostheses. JBJS (Am Vol) 1985 ;62A:654-7).

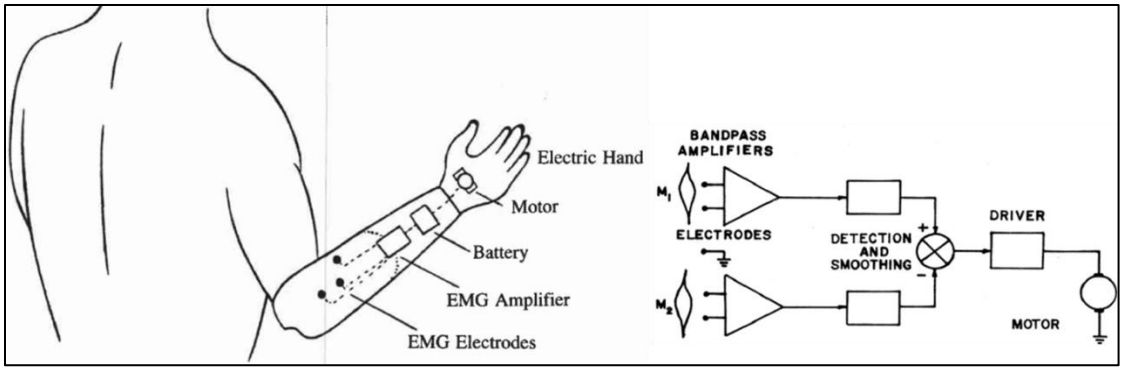

Figure 1.4 Illustration of a typical myo-electric controlled Below Elbow (BE) prostheses with components as labeled. Simplified block diagram shows principle of operation where two muscles M1 and M2 control one degree of freedom movement [8] (Billock, J. N. Hands versus Hooks. Clinical prosthetics and Orthotics.1986.10 (2): 57-65)

1.2.4 Abandonment Reasons and Desired Features

Use of prostheses in upper limb amputee population is very limited compared to the people suffering from lower limb loss. For example, with the aid of prostheses, lower limb amputees have participated in marathon runs while soldiers and civilian alike discard currently available robotic prosthetic hands only to use passive hooks or cosmetic silicon hands or none at all. One of the reasons for this contradiction is the complexity of versatile functions of the human hand such as in daily activities of hygiene, eating, grooming, and dressing versus simple sit-to-stand and ambulatory tasks of the lower extremities.

One in five individuals with the past use of prosthetic arms are reported to permanently reject further use, with a striking 89% feeling that they would be more functional without prosthetic

intervention and 72% willing to reconsider use only if certain requirements were met [11]. Rejection rates are highly dependent on level of amputation, with a survey of prosthetic use among veterans reporting abandonment rates of 40-42% associated with trans-humeral and more proximal amputations and overall lowest rate among trans-radial levels [12][13]. A similar review reported rejection rates of 23-35% and 26-45% for electric and body-powered upper limb prosthetic devices in pediatric and civilian adult and user populations [11]. Major reasons for dissatisfaction with body controlled terminal devices include limited range and speed of motion due to the harness, high energy expenditure and consequent fatigue, lack of comfort and pain, and debilitating shoulder issues as well as anterior muscle imbalances leading to cases of nerve entrapment within the contralateral axilla. Areas reported to need improvements in myoelectric prostheses comprise of durability of device, reliability of electrodes, longer lasting batteries, heavy weight, pain, dependency of visual feedback, and array of executable functions [13][11][14]. Additional caveats to rejection also include time to surgical intervention and delay between injury and amputation[15], “choking” of residual limb stump by improper fit with socket [9], initial cost of device and subsequent maintenance expenditures, gender and age bias [16], expertise of rehabilitative care provider, and individual motivation and emotional support system.

Overall, major identified priorities for future design improvement of prosthetic control based on studies by [17][18] are:

- Multiple dexterous wrist level movements such as spherical grasp for holding a ball, tip pinch for needle and lateral grasp for a dollar bill
- Varied modalities of sensory feedback and less dependency on vision
- High energy batteries that can deliver high power to prosthetics within short time period
- Durable, light weight and comfortable devices

1.2.5 Promising Contemporary Control Mechanisms

Despite the advances made in the fields of applied neuroscience and electrical/mechanical engineering since the 1950s, current clinical standards for prosthetic arms are widely limited to the use of surface EMG based control of one Degree Of Freedom (DOF) (opening/closing) movement. Control of multi-DOF prosthetic is slow, counter-intuitive entailing high cognitive burden due to its sequential rather than parallel fashion of operation wherein mode switching by hardware switches or brief co-contractions of muscles is required to change control from one DOF to the next [19] [20]. The use of myoelectric controlled prosthetics is further complicated by issues related to muscle fatigue, effects of skin temperature and resistivity on signal quality, and lesser availability of independent muscle groups for physiological control of distal movements with higher level of amputations [21]. To address these issues of traditional surface EMG (sEMG) based control, two promising novel surgical techniques have been developed over the past decade and are discussed further.

1.2.5.1 Targeted Muscle and Sensory Re-innervation

To address the need of more independent information from muscle groups, researchers at the Northwestern University in Chicago developed a surgical technique known as Targeted Muscle Re-innervation (TMR) of redirecting intact residual nerves from the amputated limb stump to alternative surgically denervated remnant muscles (usually chest or upper-arm) which are not biomechanically functional after limb loss. The re-innervated muscles serve as biological amplifiers of motor commands from the nerves and thus provide physiologically appropriate sEMG signals to control robotic hands [22] [23]. Apart from the one time necessary surgery, this approach is completely non-invasive and has been reported to provide simultaneous control of two to three DOFs (opening/closing, wrist pronation/supination, and elbow extension/flexion) in 40 patients worldwide as of the year 2011 [21].

Complimentary to this approach, was the unexpected benefit of sensory nerve re-innervation to the skin overlying the transfer muscle sites and has enabled percepts of light touch, graded pressure, vibration, sharp/dull stimuli, and hot/cold stimuli related sensations on the missing hand or arm [24][25]. Although widely successful, this technique has possible complications associated with phantom limb pain and sensations, lack of proprioceptive feedback, possibility of neuroma formations, and muscle fatigue due to repetitive contractions [26].

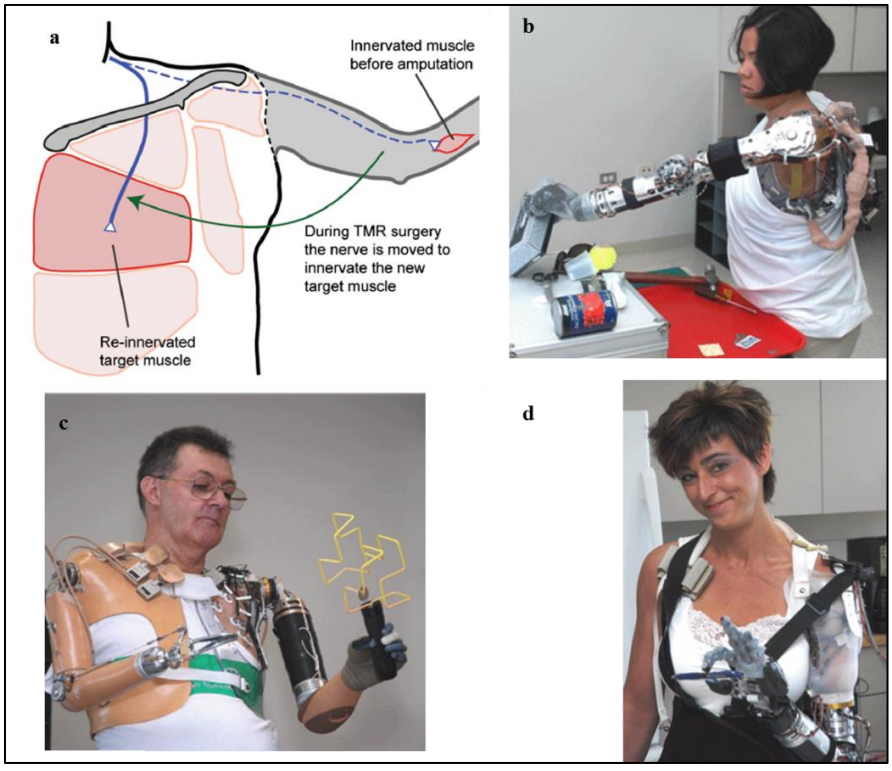

Figure 1.5 Targeted Muscle Re-innervation. (a) Schematic illustration of a typical TMR surgery [27]. (b-d) Photographs of volunteer subjects performing three different grasps to reach a tissue box, move a ring across a geometric wire, and hold a pen respectively[28].

1.2.5.2 Implantable Myo-Electric Sensors (IMES)

Researchers at the Alfred Mann Foundation have developed a wireless Implantable Myo-Electric Sensor (IMES) system that can alleviate the limited robustness of sEMG recording due to associated complications of motion artifacts, electrode movement and lack of repeatable placement after donning and doffing prostheses, wire breakage, and infection related to percutaneous leads. This approach exploits the availability, after trans-radial amputation, of most of the 18 extrinsic muscles in the forearm related to the control of the hand and wrist by implantation of fine-wire or needle EMG electrodes in the targeted muscles. Thus, high count of independent signals can be reliably obtained from a relatively dense group of muscles [29] [19]. Additionally, the incorporation of magnetic field coupling for power generation, on-board amplification and digitization, and Radio Frequency (RF) telemetry make this implant favorable for clinical acceptance.

The proof-of-concept of this approach has been verified by the successful decoding of seven different finger movements (individual and combined) from nine implanted IMES over a span of 2 years in rhesus monkeys [30] [31], simultaneous control of 2 DOF in wrist prosthesis [32], and recently 12 hand postures with 4 DOF in real-time from four able bodied human volunteers [33]. Identified areas of improvement from reported studies include generation of undesired movements due to cross talk among signals and muscle co-activations especially with target postures that involved alternate full closure / opening of one or more DOFs. Clinical trials to evaluate the feasibility of IMES to control electromechanical prosthetics for trans-radial amputee subjects were approved by the FDA in December 2013 and are currently underway.

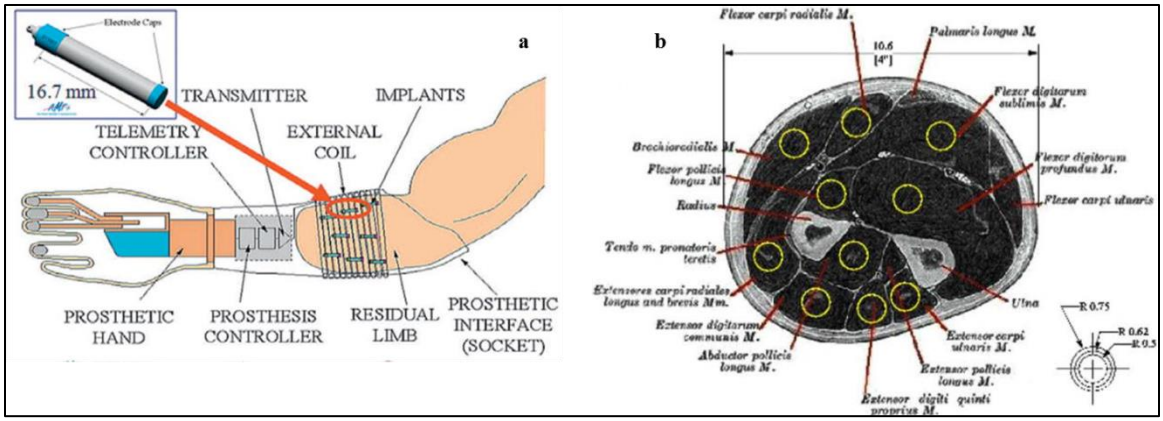

Figure 1.6 Implantable Myo-Electric Sensors (IMES). Schematic of a typical implant system (B) Projected signal pickup area superimposed on an appropriately scaled section through the proximal forearm[19]

1.2.5.3 Pattern Recognition

The pattern recognition branch of Artificial Intelligence (AI) has been successfully used in diverse commercial applications, e.g. voice recognition, Optical Character Recognition (OCR), finger print and face detection. Introduced to the area of prosthetic control in 1970, pattern recognition is used as a computational approach to discriminate multiple degrees of freedom from acquired EMG signals and increase the amount of information, thus reducing the need for independent muscle sites. A typical pattern recognition system consists of feature extraction from detected signals which are used as inputs to multi-dimensional classifiers that further probabilistically assigns “class” to different movements and finally predicts muscle activation or grasp intent. The classifier output is then used to control actuators in terminal devices and execute desired movement [20][21]. A thorough review of the different documented features used to define EMG signal characteristics (time and frequency domains, or combination) and various employed classification strategies such as Artificial Neural Network, Support Vector Machines (SVM), linear discriminant analysis (LDA), Gaussian Mixture Models (GMMs), Hidden Markov Models (HMM), and fuzzy logic based approaches is detailed in [34] [35].

Although not yet commercially available for clinical incorporation, it has largely shown promising results when used in conjunction with traditional sEMG, TMR, and IMES techniques in research studies. Indeed, among many others [36] [37], a study showed that a patient with shoulder disarticulation was able to discriminate 27 classes of upper-limb function translating to a total of 8 DOF movements with greater than 97 percent accuracy[38]. Translation of offline prediction accuracy to practical performance of prosthetic device is limited by the lack of online adaptability of the trained classifier algorithm and consequent computational requirements which has been recognized to limit its clinical implementations [39][27].

1.3 Alternative Thought Based Control Sources

To summarize the review of existing upper limb prostheses, only one to two DOF simultaneous movements are possible in clinically available myoelectric systems which are insufficient for volitional control of sophisticated multi-DOF robotic prosthetic arms (e.g. DEKA arm, Proto2). Electrical signals from the sensori-motor cortex, dorsal and ventral roots of spinal cord, and peripheral nerves have been proposed as alternative sources to obtain more natural, stable, and wider array of movement related information. Figure 1.7 shows the conceptual schematic of a neural interface driven prosthetic arm where information extracted from recorded and conditioned neural activity is used to control actuators and execute a desired movement.

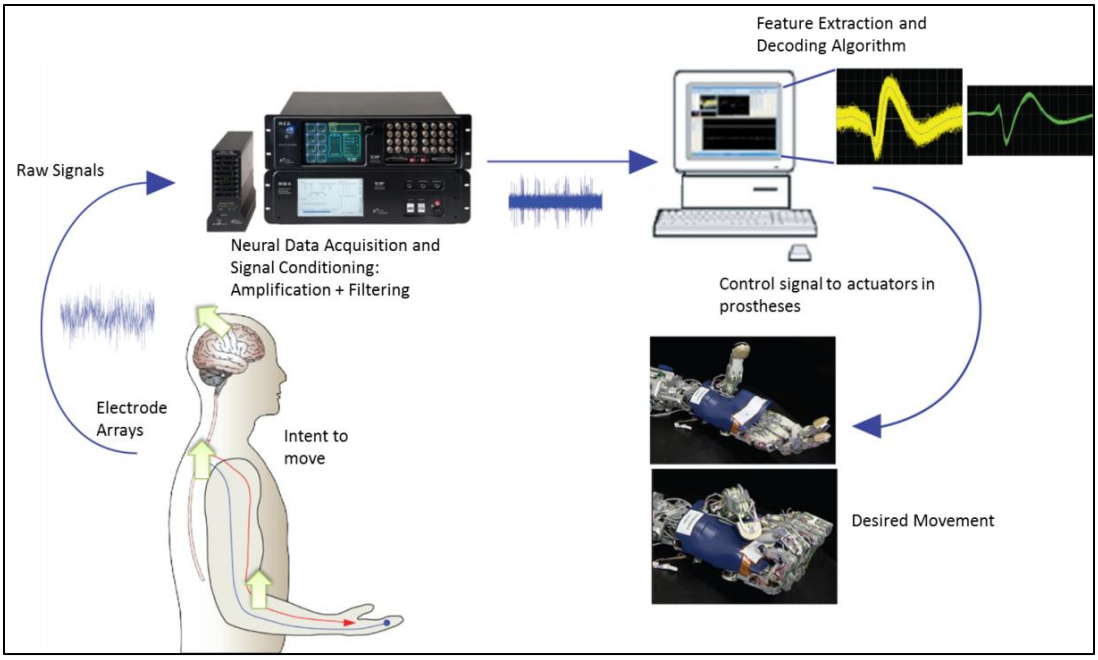

Figure 1.7 Conceptual schematic of steps involved in the process of controlling movements in a prosthetic arm with electrical signals of the nervous system.

1.3.1 Cortical Interfacing

Electrophysiological information can be obtained from the brain using invasive high impedance micro-electrodes in the intra-parenchymal region, large grid (~ 4mm) of low impedance subdural electrodes in the lesser invasive Electro-Corticogram (ECoG) interfaces, and scalp electrodes in non-invasive Electro-Encephalogram techniques. Types of recorded signals include: 1) Distinct individual action potentials as Single Unit (SU) spikes (frequency bandwidth 1-3 KHz) recorded from a single neuron within 50-100 µm distance of micro-electrode tip, 2) Multi Unit (MU) activity derived from aggregate spikes of multiple undistinguishable distant (100-200 µm) neurons [40], and 3) Local Field Potentials from micro-electrodes (0.1-200 Hz) and ECoG (up to 1Khz) representing the cumulative electric potentials generated in the extra-cellular space mainly due to synaptic interactions between axons and dendrites of neurons. EEG activity (0.1-200 Hz) represents macroscopic electrical field generated by almost the entire brain with spectral

peaks concentrated at different frequencies for different EEG rhythms (delta, theta, alpha, sigma, beta, and gamma) [41] [42][43]. ECoG and EEG interfaces have shown promising results in animal and human studies as neural correlates of speech [44] and epileptic seizures [45], and provide up to 2-D thought control of computer cursor [46] [47]. However, the limited information throughput (usually up to 1 bit/sec) of such complex higher cognition signals has been anticipated to make them unsuitable for use in prosthetic arm control [48]. In contrast, the extra-cellular spiking activity recorded by micro-electrodes is usually confined to the vicinity of the implantation site and offers specific information with higher temporal resolution.

Feasibility of recording SU spikes from various cortical regions was demonstrated in the early 1950s using Stainless Steel [49] and Tungsten [50] micro-electrodes having tip sizes in the 0.4 – 2 micron range. The first chronic long term SU recording in unrestrained awake animals was demonstrated [51] using Stainless Steel micro-wire electrodes (80µm diameter). Over the next two decades, arrays consisting of multiple micro-wires (20-50 µm tip sizes) made from noble bio-compatible materials such as Platinum (Pt),and Iridium (Ir) [52] [53] were designed. With progresses in micro-fabrication and semi-conductor technology, micro-machined Silicon (Si) substrate based electrodes arranged in 3-D grid fashion (Utah Array) [54][55] and 2-D planar structure (Michigan probe) [56] were developed and have become a popular multi-electrode array (MEA) choice for Brain Machine Interfaces (BMIs). Indeed, chronic SU recordings from large ensembles of neurons in the sensorimotor cortex of rodents and non-human primates [57][58][59] have been demonstrated using different BMIs.

BMIs operate on the premise that movement related information is encoded in the firing rate of recorded SU spikes which can be modulated by various bio-feedback strategies as established by several studies [60][61]. Typically, in an open-loop system, the instantaneous binned (10-100 milliseconds) firing rate of multiple SU spikes is fed as an input to a classification or decoding

algorithm with desired hand movements or trajectories as the end output [62]. The parallel neurophysiological breakthrough of population coding evidence in cortical neurons where it was shown that movement direction can be predicted by joint activity of group of neurons led to further advancements in BMI research [63][64][65][66]. The first successful real time control of a robotic device was demonstrated in a rodent study where signals recorded from 21-46 individual neurons controlled the position of a one-degree-of-freedom lever [67]. Subsequently, the real time prediction of monkey arm positions [68], Non-Human Primate (NHP) control of computer cursor and 3-D robotic arm movements [69][70] led to revolutionizing clinical trials in which paralyzed patients could volitionally control the position and velocity of a computer cursor [71][72]. Closed loop studies showed that NHP could control robotic arms to reach and grasp virtual objects as well as feed itself [73] [74] and paved way to the possibility of incorporating sensory feedback by direct electrical stimulation of the sensory cortex [75].

While recent clinical trials of BMI (mostly Utah arrays) in patients with chronic tetraplegia have successfully demonstrated the three dimensional control of advanced anthropomorphic robotic hands with up to 7 DOF movements[76][77], immediate wide-spread practical use is challenged by the reported inability of such BMIs to maintain consistent high level of performance primarily due to loss in signal quality [78]. Broadly, BMI failure mechanisms are classified into acute mechanical, biological and material categories (Figure 1.8). A recent comprehensive study evaluating failure mechanisms associated with the Utah array in NHPs concluded that majority of arrays failed within a year of implantation primarily due to acute mechanical failures (54%) and a progressive meningeal reaction that pushed the array out of cortical regions (14.5%). A significant number of chronic arrays (that lasted up to 5 years) in that study were determined to have failed from electrode insulation damage [79].

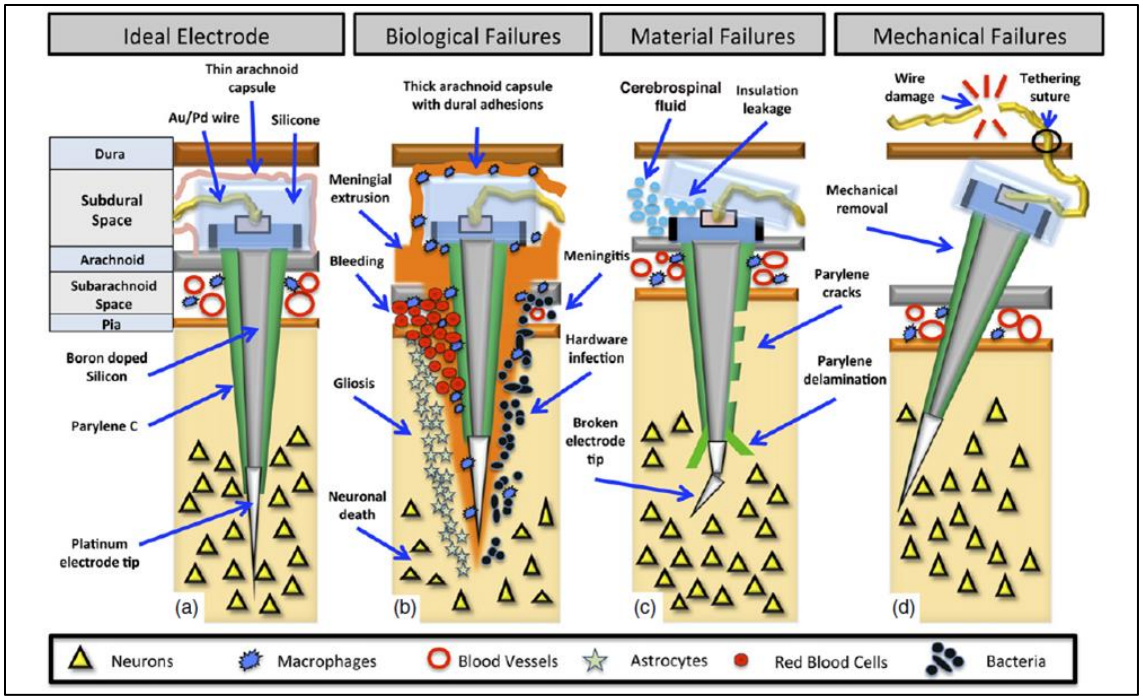

Figure 1.8 Schematic of documented BMI failure mechanisms. (a) Ideal electrode placed in the intra-parenchymal region and stabilized by a thin arachnoid or connective tissue layer. (b) Biological failures primarily due to glial tissue encapsulation, neuro-inflammation, cell death, and infection of the meninges. (c) Material failures from insulation and electrode tip damages. (d) Mechanical or catastrophic failures due to expulsion of array, and connector/wire breakage. [79]

Other researchers have postulated the prominent hurdle in longevity of intra-cortical signals to be one of the elicited foreign body response which is dependent on the electrode geometry, surface characteristics, insertion method and is exacerbated by micro-motion due to the compliance mismatch between the metallic electrode and soft neuronal tissue [80][81]. This response typically involves formation of a ‘glial scar’ consisting mainly of Neural Precursor Cells

(NPC) and astrocytes which encapsulates the electrode tips and forms a highly resistive barrier [82]. A theoretical circuit model of this phenomenon has been explained in detail [83]. Additionally, a state of “frustrated phagocytosis” leading to prolonged neuro-inflammation is also hypothesized to create a “kill zone” within the 100 μm recording zone of the electrode tip, thus causing inability to record SU spikes leading to interface failure [84].

Thus, despite significant progress achieved in the field of Brain Machine Interfacing, the bottleneck of long-lasting signal quality for consistent high performance remains a challenge. Another prime concern is the risks associated with an invasive craniotomy surgery which is necessary for its implantation currently. This issue might not alarm patients with paralysis due to spinal cord lesions who may invariably gain better quality of life by the incorporation of volitional control to the current assistive technology for their different daily needs. However, for upper limb amputee populations who have functions and mobility retained in all other limbs might not readily accept the invasive implantation of foreign devices into their brain for the simple addition of limited functions achieved by present prosthetic arm control.

1.3.2 Peripheral Nerve Interfacing

Apart from the invasive nature of BMI, detected intra-cortical signals are highly encoded as they have not undergone diverse sensory integration and processing in the neural circuitry of spinal cord and thalamus; hence require complex decoding algorithms to extract motor intent. Also, with the significant re-organization that occurs in the sensory cortex after limb loss, it is currently unknown if Intra Cortical Micro Stimulation (ICMS) can provide distinct percepts of diverse tactile and proprioceptive modalities without any adverse side effects. Even in the event of successful sensory feedback, questions regarding its stability and implications on mapped topography of motor cortex remain unexplored. Peripheral Nerve Interfaces (PNI) have garnered

much interest as an alternative to BMI for patients with an intact spinal cord due to its relatively low invasiveness, and the persistence of functional sensory and motor neural pathways in residual peripheral nerves despite several years of amputation. In contrast to the higher cognitive signals acquired from BMI, simplified movement specific signals can be directly recorded from motor axons, and stimuli delivered through innate afferent axonal pathways undergo multiple levels of “natural” processing along the somatosensory neuraxis making them easily comprehensible; thus promising a true intuitive bidirectional control of prosthetic arm [85]. Incorporation of near-natural tactile feedback has the additional benefit of enabling the subject to perceive the artificial hand as part of his “self”, a concept termed as mind body ownership that is much similar to the well-known rubber hand illusion [86][87]. Potential of multichannel micro-stimulation of residual nerves to assuage the pain associated with Phantom Limb Syndrome are also being explored [88] [89].

PNI are classified on the basis of a tradeoff between the invasiveness and selectivity/sensitivity of recorded signals associated with the design and technique of implantation in the peripheral nerves (Figure 1.9). Implant specific advantages, challenges and achieved progress so far are discussed in the following sub-sections.

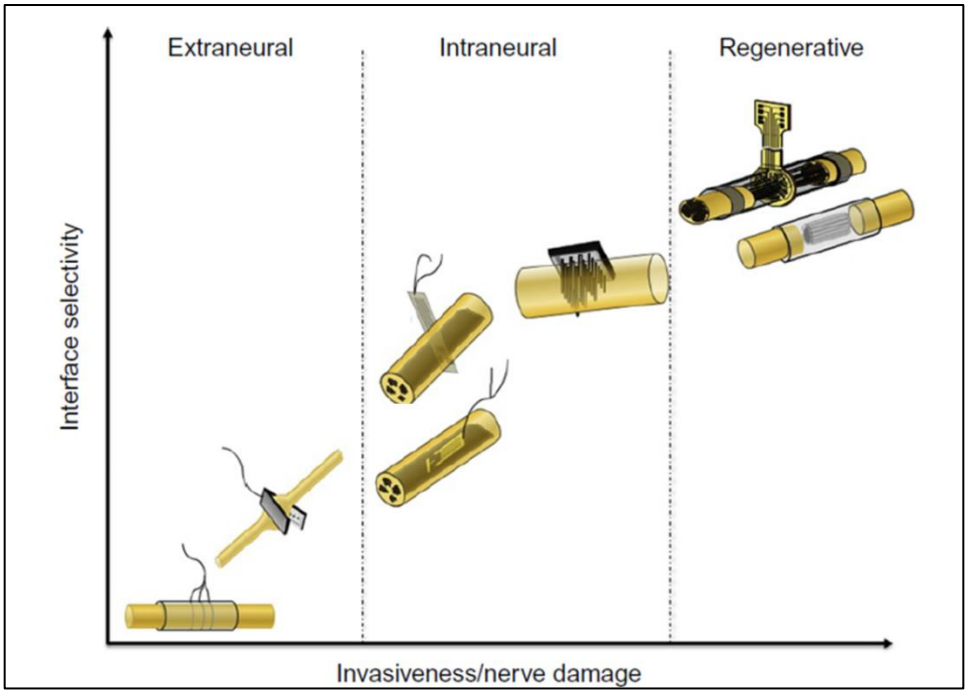

Figure 1.9 Classification of PNI in the order of invasiveness and selectivity as extra-neural (Cuff/FINE), intra-neural or inra-fascicular (LIFE, TIME, USEA), and regenerative interfaces (sieve, REMI, microchannel) [90].

1.3.2.1 Extra-neural Electrodes

These interfaces involve wrapping of the nerve around its circumference with a silicon or polyimide material that is embedded with circumferential or discrete electrode contacts usually made of Pt or SS wires[91][92]. Studies conducted in awake and behaving animals have shown the acquisition of differentially recorded signals in a bipolar or tri-polar configuration (to avoid EMG interference from adjacent musculature) which typically represent averaged cumulative activity of electric potentials generated by the entire nerve with a 5 to 40μV amplitude range [93] [94] [95]. Using artificial intelligence classifiers, proprioceptive, mechanical, and nociceptive types of afferent sensory signals have been discriminated offline in a rat sciatic nerve model [96]. However, recorded compound nerve signals generally have low information specificity and are restricted to the detection of sensory event onset for the closed-loop control of Functional

Electrical Stimulation (FES) systems [97]. On the contrary, this interface has gained significant clinical success in stimulation based applications such as foot drop correction [98], owing to its stable recruitment properties that last over the span of multiple years [99][100][101].

To improve the specificity of signals recorded by cuffs, researchers at the Case Western University modified the approach to a Flat Interface Nerve Electrode (FINE) design that slowly reshapes the enclosed nerve into a flat structure thereby forcing the underlying fascicles closer to the electrode contacts and potentially reducing the infiltration of connective tissue within the inner circumference of the cuff [102]. Biocompatibility studies revealed no chronic changes in the nerve physiology and Blood Nerve Barrier (BNB) permeability with only minor decrease in axon count and associated myelin damage [103][104]. Despite promising results shown in the selective activation of tibial and peroneal nerve of human subjects, long term specificity in recorded information is yet to be demonstrated[105].

1.3.2.2 Intra-neural or Intra-fascicular Electrodes

This category of interfaces has been developed to increase the selectivity of stimulation and Signal to Noise Ratio (SNR) of signals in comparison to extra-neural approaches. As the name suggests, they are aimed to be placed in close proximity of axons within distinct individual fascicles (bundle of axons) overcoming the highly resistive epineurium and perineurium layers of the nerve. Three prominent proposed designs with different surgical implantation techniques have been extensively studied over the last two decades which include the Longitudinal Intra-Fascicular Electrode (LIFE), the Transverse Intra-fascicular Multi-channel Electrode (TIME), and the Utah Slanted Electrode Array (USEA), a variant of the popular BMI.

The LIFE interface was designed to exploit the somatotopic and functional organization of peripheral nerves at the fascicular level. Specifically, motor and sensory axons originating from

the dorsal and ventral roots of the spinal cord are grouped in fascicles (bundles), remain localized for long distances, and eventually give origin to branches of the nerve that innervate distinct destined targets. This functional “modularity” of axon groups facilitates selective interfacing of different fascicles within a given common mixed nerve [48]. The implantation procedure involves threading thin insulated conducting wires made from Pt/Ir or metallized Kevlar® (polymer) fibers through a nerve longitudinally. The active recording/stimulating site is a short de-insulated (250–1,500 μm) region of the wire [106]. Signals acquired represent multi-unit activity from axon bundles of nerve with peak-to-peak amplitudes in 5-20μV range and spectral peaks at about 2 KHz [107][108]. The feasibility of these interfaces in animal models was demonstrated early in 1990s using single channel LIFEs [109], followed by multiple studies characterizing its stimulation and recording abilities, biocompatibility evident by minimal axonal damage, and development of interfaces with increased electrode contacts [110][111][112]. In 2004, LIFEs were implanted in the median nerves of six amputee subjects and controlled a one DOF device demonstrating for the first time that viable motor signals can be recorded from residual nerves [113] [114]. More recently, the same group of researchers showed that amputee subjects could perform object recognition by receiving sensations of touch in the hand delivered by electrical stimulation through the LIFEs [115]. In another independent study, four thin film substrate LIFEs (tf-LIFE) with higher flexibility were implanted in the median and ulnar nerves of an amputee volunteer who was able to voluntarily execute three distinct hand movements with the use of Wavelet de-noising and classification algorithms [116]. While these results underscore the potential of LIFE as a bidirectional interface, limitations of low signal strength, high amplitude EMG interference, lead wire and connector breakage, and the possibility of electrode contacts to be placed outside of the fascicles during surgery or eventual post-implantation migration have been recognized as critical factors that need to be addressed.

The TIME interface is implanted in a transverse rather than parallel direction to the cross sectional area of the nerve. The idea for this implant orientation stemmed from the need to achieve higher spatial selectivity in recruitment of axon subsets within different fascicles than within the same fascicle as is mostly achieved by LIFEs[117]. Indeed, this interface has shown superior selectivity in activation of different muscles innervated by distinct branches of the rat sciatic nerve [118], and also those within the same fascicle (e.g. Plantaris versus Gastrocnemius Medialis innervated by tibial branch) [119]. Histological evaluation of the nerve post 2 months of implantation have not shown any signs of morphological or functional damages [120]. The stimulation capacity has also been verified by the selective activation of dense muscle groups in a pig median nerve model [121]. However, no study has reported on the recording abilities of this interface yet.

USEAs are Multi-electrodes arrays (MEAs) composed of needle shaped electrodes with different heights arranged in multiple rows on a silicon substrate and inserted perpendicularly to the nerve using a pneumatic force device [122]. Originally designed with 100 electrodes and highly popular for use in the cortex [123], its recording and stimulating abilities were further tested in the Dorsal Root Ganglions (DRGs) of animals over a series of experiments [124][125]. The need to reduce redundant electrodes and to increase chances of accessing multiple fascicles across the nerve led to the development of the modified “slanted” and more recently the High Density (HD) versions which have shown promise in recording and low injection current based selective stimulation in animal models [126] [127][128][129] as well in a human volunteer [130]. This technology has been proposed for diverse potential applications in vision restoration [131], bladder control[132], and prosthetic limb interfacing. High amplitude (15-200 μV) Single Unit (SU) spiking activity representative of action potentials derived from a single axon have been acquired using this interface, albeit on a marginal 10-20 % of total electrodes and with high EMG interference. Additionally, all studies report on the difficulty to record SUs beyond a “few days”

and occasionally last up to a month in awake unrestrained animals which is in stark contrast to its superior long term stable stimulation abilities. Identified biocompatibility issues that might affect its recording abilities include potential traumatic nerve injury caused due to pneumatic insertion, mechanical compliance mismatch between the rigid MEA structure and soft nerve tissue, and tethering forces produced by transcutaneous connector lead wires and need to be further evaluated.

1.3.2.3 Regenerative Electrodes

Peripheral nerves are intrinsically able to spontaneously regenerate after injury to a certain extent. The concept of utilizing this natural mechanism to record from axons re-growing through electrodes was initially proposed in 1969 by the demonstration of successful regeneration in severed nerve stumps across a tube embedded with an array of holes, each lined with conducting contacts. This laid the foundation of initial regenerative devices that were made from non-semiconductor materials and commonly referred as sieve interfaces. With the early evidence of signals recorded from Xenopus sciatic motor fibers [133] using implantable regenerative devices, a rapid surge was initiated in the investigation of their potential to serve as a bidirectional link with the remnant peripheral nerves in amputees. Subsequently, SU spiking activity (100-600 μV) was successfully recorded from silicon based implantable sieve interfaces in rabbit tibial [134] and sciatic nerves [135], fish cranial nerves [136], and rat glossopharyngeal nerves [137][138][139] in mostly acute and very few chronic preparations. However, the rigid constitution of such silicon interfaces was reported as an issue and polyimide sieve interfaces were introduced in 1996 with the incorporation of the electrodes, conducting cables, and external contact pads as a single flexible micro-fabricated entity [140]. Despite the proposed improvements, very limited success was achieved in acquiring SU signals by the use of polyimide sieves in animal models [141] [142]. This further shifted the research focus to the long-term evaluation of regenerated axonal quality and functional recovery of distal target muscles after allowing sufficient time for re-innervation

[143][144][145]. Such biocompatibility studies revealed minimal foreign body response to the device as a whole; however in spite of several efforts to increase the restricted space available in the porous design, frequent signs of axonopathy due to the compressive forces acting on maturing axons that enlarge in diameter have been indicated.

Newer designs have explored the idea of restricting the action current leaving the nodes of Ranvier and forcing it to flow longitudinally within the confines of the channel, parallel to the axon, by the encapsulation of regenerating axons within multiple microfluidic channels embedded with electrodes, aimed at extracellular recording amplification and lowering of injection charge required for selective stimulation. Preliminary results have shown the feasibility of obtaining high SNR signals in anesthetized rats [146][147] and more recently a closed loop spinal neuro-prosthesis for bladder control in animal models was accomplished [148]. However, detailed characterization of recorded signals and stimulation abilities are yet to be conducted.

In summary, interfacing with the peripheral nerves in amputees has been recognized since several decades as a feasible strategy to record multiple specific motor signals necessary to drive a prosthetic arm with high degrees of freedom. While theoretical benefits of using PNI for the volitional control of robotic prostheses outweigh those of BMI, thorough experimental validation and wide spread clinical translation remains to be achieved.

In 2008, our laboratory developed a novel Regenerative Multi-electrode Interface (REMI) with an open-space design wherein a 3D multi-electrode array (originally developed for BMI use) is fixed within the lumen of a hollow polyurethane conduit. Preliminary animal studies showed robust regeneration in transected peripheral nerves, whether acutely injured or after months of chronic amputation, when placed between the two ends of the REMI conduit. Re-growing axons were determined to be in close proximity (12.13 – 28.28 μm) of the electrode tips and immuno-

histochemical analysis confirmed presence of unmyelinated (pain fibers) and thickly myelinated axon sub-types with minimal inflammatory response [149]. Recently, we demonstrated that high SNR signals can be recorded using this interface as early as seven days post implantation. Further, evaluation of nerve injury related gene expressions determined that the presence of rigid electrode array in the path of re-growing axons does not alter the involved molecular mechanisms of regeneration [150].

1.4 Research Objective and Dissertation Organization

Based on the review of current prosthetic control techniques and state-of-the-research measures described in previous sections, it is concurred that any prospective neural interface would need to achieve at least some salient features to be usefully integrated with prosthetic limbs. Few imperative considerations include durability or robustness of interface reflected in long-lasting signal fidelity, specificity of motor control and sensory feedback, and deliverability of increased physiological functions.

The overall purpose of this dissertation project is to evaluate the potential of the newly developed Regenerative Multi-electrode Interface (REMI) in context of the above guidelines.

In **Chapter 2**, with the specific aim of evaluating the long term reliability of the REMI, an in-depth characterization of the signal quality of obtained recordings and encountered failure mechanisms in a longitudinal study will be described. A comparison was made with the quality of signals obtained with an extensively studied electrode array to ensure relevance with the current field. The results obtained highlight the long term stable quality of REMI signals in a rodent

model, the dominant cause of failure, and indications towards potential challenges in chronic implementations.

Chapter 3 examines the neurophysiological features of REMI acquired signals from the heterogeneous population of sensory and motor axons in a mixed nerve and from its fascicles that predominantly sub serve distinct functions of movement and cutaneous sensation. The specific aim was to ascertain if signals from axons of discrete modalities can be interfaced with the REMI in peripheral nerves and the results highlight a distinctive sampling bias in its recording ability.

Chapter 4 extends the approach used in Chapter 3 to identify the nature of a subset of signals that exhibited distinct neurophysiological signature in a locomotion paradigm. The functional utility of identified signals was evaluated by analyzing the stability and extent of correlation with target muscles. The results obtained answer the specific question of whether the REMI can record from functional signals from regenerated motor axons.

Chapter 2

Signal Quality from Regenerative Multi-electrode Interfaces

2.1 Abstract

Our laboratory has developed a novel Regenerative Multi-electrode Interface (REMI) and we recently demonstrated its feasibility in a rodent peripheral nerve model [149][150]. The purpose of this study is to elucidate dominant failure mechanisms and its implications on the quality of electrophysiological signals acquired from REMI interfacing of peripheral nerves. We characterized the quality of Single Unit (SU) recorded from awake and unrestrained animals over time by quantification of metrics such as peak to peak amplitude, signal to noise ratio, array yield and number of SU per implant; and delineated the types of failures encountered. Furthermore, a direct comparison was made with the quality of signals acquired from a relatively well characterized peripheral nerve interface, albeit fundamentally different, the Utah Slanted Electrode Array (USEA). Large cohorts of animals, specifically n=43 for REMI and n=34 for USEA, were used to ensure statistical confidence in quantification of signal quality metrics and incidence rates of failures. 46% of REMI and 26% of USEA implants were successful in yielding SU activity. While REMI displayed a higher Signal to Noise Ratio (SNR), the total number of SU acquired per implant was comparable in both interface types. The recording ability of REMI was determined to be stable in terms of peak to peak amplitude, SNR, and total number of signals available over a 120 day period of REMI implantation. Mechanical failures i.e. pedestal detachment and wire breakage hindered long term chronic signal acquisition in 76% of successful REMI implants. Results of this study provide an insight into the capabilities of REMI as a potential peripheral nerve interface and aspects that need improvements towards its increased efficiency and longevity.

2.2 Background

To achieve the desired feature of durability and reliability, neural interfaces are expected to record high fidelity signals consistently over long periods of time, preferably a decade in human patients. Despite recent advances in demonstrations of intuitive control of robotic prosthesis using spiking activity of neurons in the cortex of rodents [58][67], non-human primates [151] as well as human patients [77], deterioration of signal quality over time is reported thereby making long term reliability a formidable task. This instability has an impact on real-time performance in terms of accuracy of decoding movement intent and also accounts for frequent recalibration of involved algorithms, which is impractical for clinical use [152].

The causes for signal deterioration are broadly categorized into abiotic and biotic factors. Electrode implants elicit a certain degree of inflammatory response from the immune system, leading to gliosis wherein a tissue sheath of glial cells and fibroblasts is formed around the electrodes [8]. This encapsulation is suggested to result in isolation of recording site from the neuronal tissue [9], decrease in conductivity of ions [10], thereby reducing the sensitivity for recorded signals. Neuronal degeneration from infiltration of pro-inflammatory cells and neurotoxic cytokines, led by the chronic breach of the blood brain barrier at the electrode implantation site, has also been correlated with electrode failure [11]. Additional factors recognized to exacerbate tissue response include the shape of the electrode (planar vs 3-D), the mode of implantation (tethered vs untethered), and micro-motion of electrodes within the neuronal tissue [12][13]. Documented abiotic factors include integrity of device hardware, delamination of the insulating layer and corrosion leading to changes in electrochemical properties of electrode recording sites [14]. Although no consensus for the most dominant cause of signal failures (biotic vs. abiotic)

exists, their presentation as eventual decrease of Signal to Noise Ratio (SNR), Peak to Peak amplitude (P-P) or total number of signals detected is a common observation.

In contrast to the literature pertaining neural interfacing of the brain, reports on Peripheral Nerve Interfaces (PNI) are generally limited to electrode development, material characterization, and demonstrations of sensory feedback by electrical stimulation. In fact, testing of recording ability has been limited to few animal subjects and neither progression of signal quality nor along with failure mechanisms and incidence rates are rarely stated (refer Table 2.1). Nevertheless, some issues are similar to those observed in cortical interfaces, in addition to a set of challenges unique to the peripheral nervous system. Specifically, it is extremely difficult to record strong stable peripheral nerve signals from conscious behaving animals. The average strength of signals recorded from axons is comparatively lower than that from cell bodies in the spinal cord and cerebral cortex due to the spatial arrangement of nodes of Ranvier along axon fibers, and signals are easily confounded by high amplitude Electromyographic (EMG) activity in the periphery[153]. This explains why the vast majority of experiments on peripheral nerve recording have been limited to anesthetized animals (Table 2.1). Since testing in unconscious state bears little relevance to the eventual use of such interfaces, i.e. control robotic prostheses, this study attempts to evaluate the recording ability of REMI in awake and freely behaving animals by the characterization of signal quality progression over time.

Table 2.1 Summary of selected published studies reporting characteristics of recorded signals and failures observed in peripheral nerve interfaces. (“n/r”, “Y”, “N” indicates not reported, yes, and no, respectively; mechanical failures representative of connector loss and wire breakage.)

Electrode Type	Species/Model	Recording		Single Units	Quality over time	Failures/ Concerns	Reference
		Condition	Period				
Cuff	Cat / sciatic (n=8)	Wake	63 days	**N**	**N**	Mechanical / Connective tissue growth	[154]
Cuff	Rat / sciatic (n=5)	Anesthetized	At time of implantation	**N**	**N**	n/r	[155]
LIFE	cat / sciatic (n=6)	Anesthetized	180 days	**Y**	**Y**	Mechanical	[109]
LIFE	human / median (n=3) and (n=1)	Wake	14 and 28 days	**N**	**N**	n/r	[156] and [157][158]
LIFE	cat / dorsal rootlets (n=6)	Anesthetized	70 days	**N**	**N**	Insulation delamination	[159]
USEA	cat / sciatic (n=12)	Anesthetized	60 hours	**Y**	**N**	Mechanical/ EMG contamination	[160]
USEA	cat / sciatic (n=4)	Anesthetized/wake	120 days	**Y**	**N**	Electrodes in inter-fascicular space	[128]
USEA	rat / sciatic (n=1)	Anesthetized	10 hours	**Y**	**N**	n/r	[129]
Sieve	rabbit / tibial (n=2)	Wake	Single instance at 224 days	**Y**	**N**	n/r	[134]
Sieve	rat / glossopharyngeal (n=5)	Anesthetized	91-118 days	**Y**	**N**	25 % regeneration	[137]
Sieve	Rat / sciatic (n=30)	Anesthetized	30-360 days	**N**	**N**	Compressive axonopathy	[161]
MCRE	rat / sciatic (n=8)	Anesthetized	Single Instance at 90 day	**Y**	**N**	Limited open space for regeneration	[146]
REMI	rat /sciatic (n=41)	Anesthetized/wake	7 – 120 days	**Y**	**Y**	Mechanical	This study

2.3 Materials and Methods

2.3.1 Peripheral Nerve Interfaces

2.3.1.1 Regenerative Multi-electrode Interface (REMI)

A custom made Floating Micro-electrode Array (FMA) consisting of sixteen recording electrodes, a reference electrode, and a ground Platinum/Iridium (70/30%) electrode (Microprobes Inc., Gaithersburg, MD) secured within a polyurethane conduit constitutes the REMI assembly. Electrodes were arranged in a 5-4-5-4 pattern and 400 µm uniform inter electrode spacing on a 125µm thick ceramic base of 2.45 mm X 1.95 mm X 0.45 mm physical dimensions. Individual electrode shafts had a conical structure with approximately 50 µm base diameters and alternately varying in height from 0.7 to 1.0 mm to maximize contact with axons regenerating in different planes of the conduit. All electrodes were coated with a 3µm thick insulating layer of Parylene-C, and precisely laser ablated at the tip to yield an exposed recording surface area of approximately 400 μm^2 and with impedances between 100 and 300 kΩ at 1 KHz, i.e. the neuronal spike frequency range. Ground and reference electrodes were exposed to have < 5kΩ and 10-20 kΩ impedances respectively. Eighteen Parylene-C insulated gold wires, each 25 µm in diameter, were wound in a helix and micro-welded to the shaft of individual electrodes to form a 4.5 cm cable which was sonically bonded to an 18 channel connector (A8141-001, Omnetics, Minneapolis, MN). Details on micro-fabrication and array manufacturing are described in [162]. The connector was housed within a titanium pedestal and the electrode array placed within one side of a 5-7 mm long polyurethane conduit (Micro-Renathane, Braintree Scientific Inc., Braintree, MA; OD 3 mm, ID 1.75 mm). The entire assembly was sterilized with 70% ethanol and exposure to UV light and then the lumen of conduit was filled with sterile collagen I/III (0.3%; Chemicon, Temecula, CA).

2.3.1.2 Utah Slanted Electrode Array

Custom made silicon wafer based 3D electrode arrays were purchased from Blackrock Microsystems (Salt Lake City, UT). Each array consisted of thirty two recording electrodes arranged in a 6 by 6 square grid with an inter-electrode spacing of 400 μm in a unique “slanted” architecture wherein length of electrodes increased from 0.5 to 1.0 mm in one direction, while being constant in length in the other. Electrodes comprised of conductive sharpened Silicon conical needles with Platinum coated tips yielding impedances between 100 and 400 kΩ. The entire electrode array, except for recording tips, was coated with Parlyene-C. A 4.5 cm cable consisting of 25 μm Pt/Au lead wires served as a transmission link from the electrodes in the USEA to a 36 channel connector (Omnetics, Minneapolis, MN) which was housed in a titanium pedestal.

2.3.2 Surgical Implantation

Adult female Lewis rats, weighing ~220g, were implanted with REMIs (n=43) and USEAs (n=34) in the sciatic nerve with a connector/pedestal affixed to the pelvis bone. Animals were prepared for surgery by anesthetizing with isoflurane (5% induction, 2.5 % maintenance) in 100% oxygen, keeping eyes moist with ophthalmic ointment, and shaving and disinfecting the field of surgical operation with 70% ethanol and Povidine-iodine. A muscle sparing incision was made between the semitendinosus and biceps muscles and after gently spreading them apart, the unbranched portion of the sciatic nerve was exposed. For REMI implants, a transection injury was introduced and the proximal and distal nerve stumps inserted into and sutured at the opposing ends of the REMI conduit. In case of USEA implants, the nerve was not transected; rather the array was inserted into the nerve using a pneumatic insertion device at a constant pressure of 12 psi [163]. The gold wire cable from the arrays was routed subcutaneously from the leg to the pelvic area. A second incision was made on the pelvis area above the spinal segments L5-S2 and the underlying muscle tissue and tips of dorsal processes, thus exposed, removed. The

pelvic bone was cleaned and dried, after which the titanium pedestal housing the connector was attached using bone cement (Biomet, Warsaw, IN). The incisions were closed using surgical staples and antibiotics (cephazolin; 5 mg/kg, IM) and analgesics (buprenorphine; 0.05-0.1mg/kg, SC) were administered post-surgery once every 24 hours for three consecutive days. All procedures were performed in accordance with the guidelines of the Institutional Animal Care and Use Committee of the University of Texas Arlington.

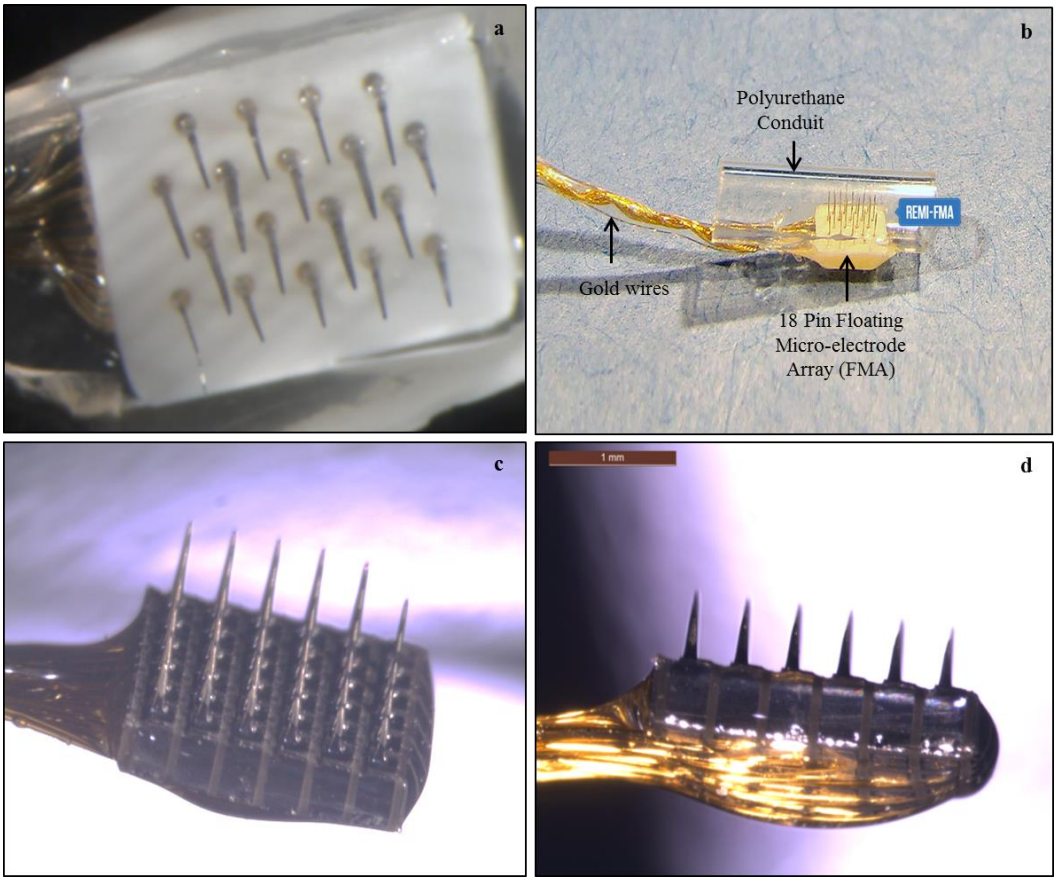

Figure 2.1 Peripheral Nerve Implants. (a) Ceramic Base holding 18 Platinum electrodes of FMA. (b) REMI consisting of 18 pin Floating Micro-electrode Array (FMA) in a polyurethane conduit; Image source- Microprobes Inc. (c) (d) Utah Slanted Electrode Array (USEA) Scale Bar = 1mm.

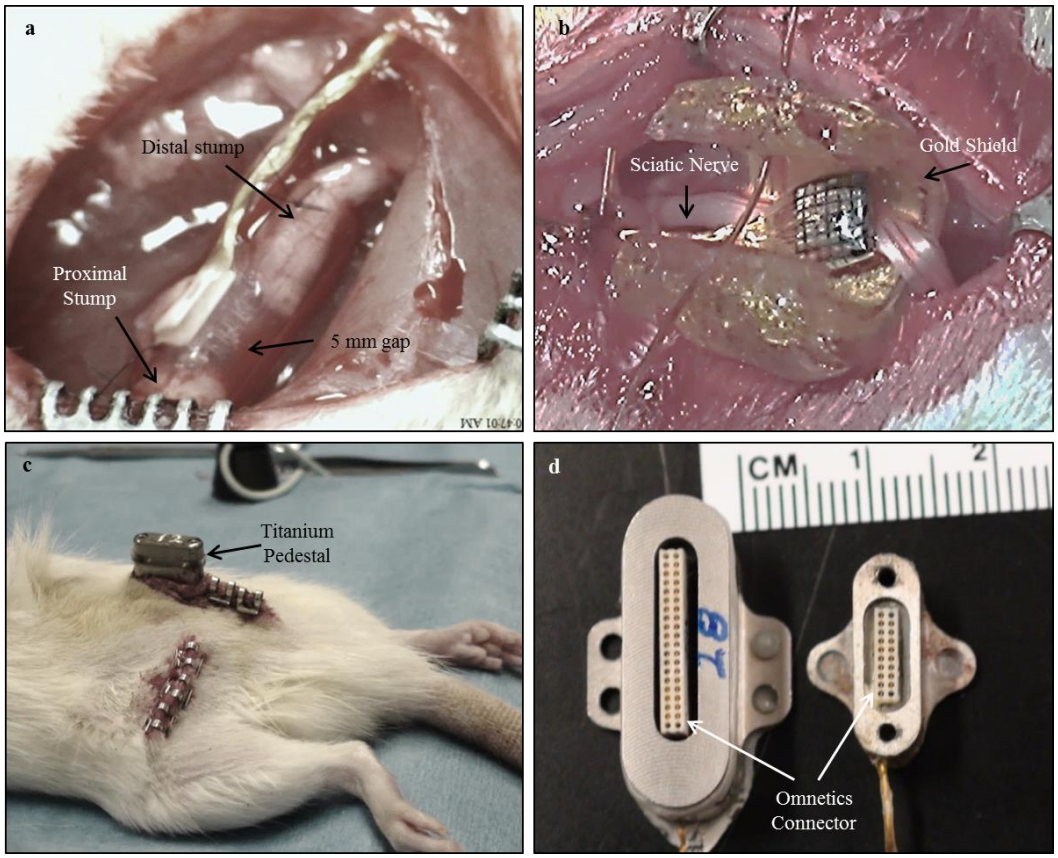

Figure 2.2 Surgical implantation of (a) REMI in a transected sciatic nerve with proximal and distal stumps inserted into a 7 mm long polyurethane conduit and effective gap of 5 mm. (b) USEA inserted in sciatic nerve with gold shield wrapped around it. (c) Titanium pedestal implanted on the pelvis. (d) Titanium pedestals with Omnetics connectors of 36 channels (USEA) and 18 channels (REMI).

2.3.3 Electrophysiological Recordings

Seven days after implantation, neural activity was acquired weekly from awake, unrestrained animals freely moving in a small confined space. Recordings were obtained simultaneously from all electrodes in the implanted array using Omniplex Data Acquisition System (Plexon Inc., Dallas, USA) at a sampling frequency of 40 kHz in a bandwidth of 100-8000 Hz using a Bessel 4-

pole analog filter. Neural signals were differentially amplified using a reference signal generated by a low impedance electrode within the REMI or a buffered ground signal generated by the preamplifier head-stage unit (HST/16V-G20, Plexon). The animal was grounded by connecting the common ground in the amplifier to a screw on the titanium pedestal. All recording sessions were at least five minutes in duration and conducted inside a Faraday cage to reduce external electromagnetic interference.

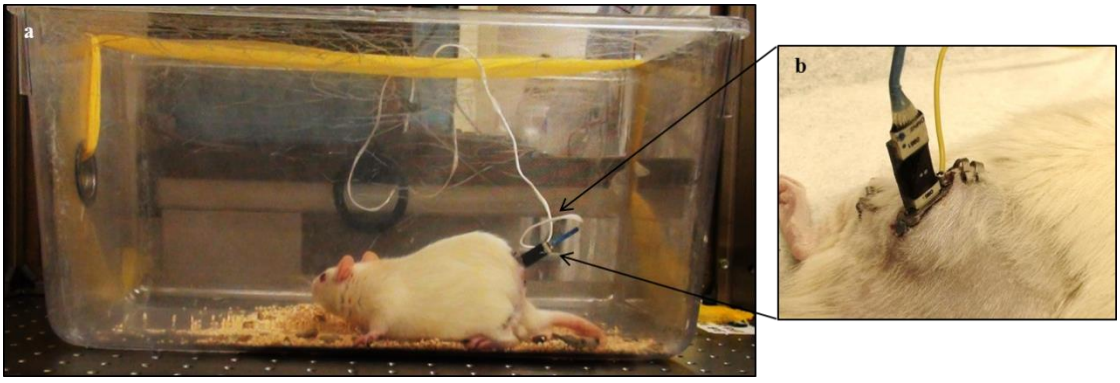

Figure 2.3 Illustration of a typical recording set up. (a) Peripheral Nerve Interface implanted animal with a pelvis mounted connector fit with Headstage (HST) and cables for transmission linked to the data acquisition system. (b) Inset showing magnified view of the HST fit with Omnetics connector and a ground wire wound around a screw in the titanium pedestal.

2.3.4 Gross Tissue Examination

Animals were euthanized by an intraperitoneal injection of sodium pentobarbital (100 mg/kg) followed by transcardial perfusion with saline (0.9%) and paraformaldehyde (4%). Peripheral nerve implants (REMI and USEA), along with several millimeters of sciatic nerve from proximal and distal sides, were harvested, post-fixed overnight in 4% paraformaldehyde (PFA) and transferred to 1X PBS (Phosphate Buffered Solution). Later, the conduit (REMI) or surface of array – nerve interface (USEA) was freed from connective tissue by careful dissection and the

nerve electrode-array interface examined under the microscope to quantify the number of electrodes embedded within and outside of the nerve tissue.

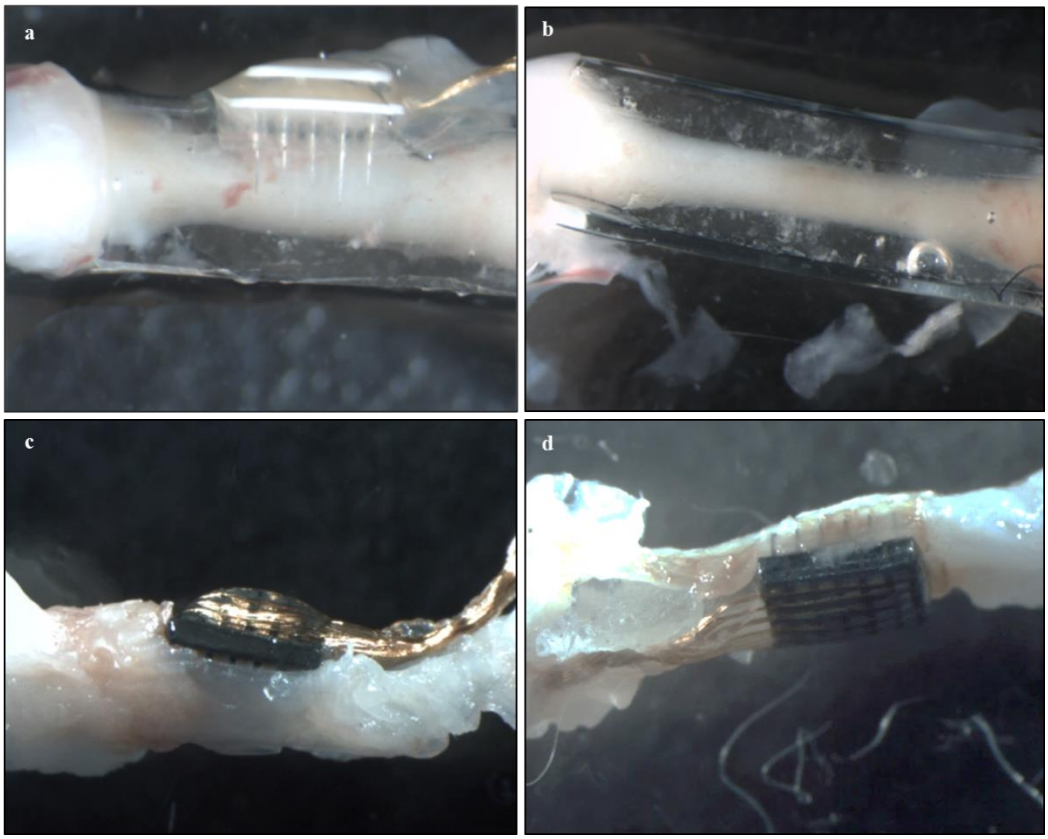

Figure 2.4 Microscopic evaluation of the explanted Electrode-Nerve Interface. Representative images of (a) 30 day explanted REMI depicting a regenerated nerve tissue embedded with FMA electrodes (b) 30 day explanted polyurethane conduit without FMA electrodes and (c) (d) USEA embedded in explanted nerve tissue.

2.3.5 Neural Signal Analysis

Acquired signals were digitally filtered using Offline Sorter (Plexon) by high pass filter (Butterworth, 4 pole) with at 800 Hz cut off frequency to attenuate EMG contamination and power line interference. Waveforms that crossed a fixed threshold (- 4.5 standard deviation) from the

mean distribution of signal were extracted in windows of 1400 µsec. Large amplitude movement artifacts were removed after visual inspection and remaining waveforms were manually sorted into Single Unit (SU) spikes based on the similarity of their shapes. This entire process was done by a single investigator in order to minimize variability in spike sorting of SU [164]. Further, to distinguish SU from Multi Unit (MU) activity, putative spike waveforms were subjected to the uniform criteria [165] of having a) repetitive consistent biphasic or triphasic shape and b) less than 1% waveforms within an Inter Spike Interval (ISI) of less than 3 msec confirming the presence of a refractory period of at least 3 msec. c) Signal-to-Noise Ratio > 3 to exclude poorly discriminable units [166][167]. Single Units were then imported into MATLAB (MathWorks, Natick, MA) for further determination of signal quality metrics.

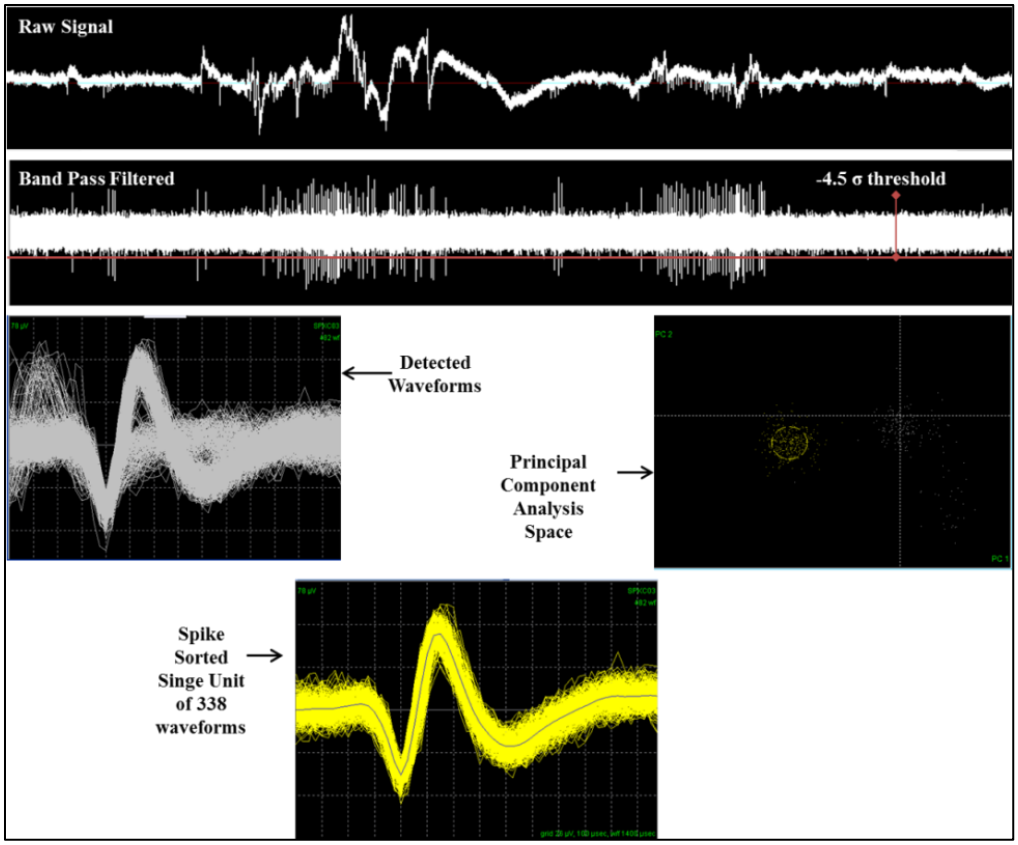

Figure 2.5 Illustration of signal preprocessing and spike sorting steps involved in the typical detection of a single unit.

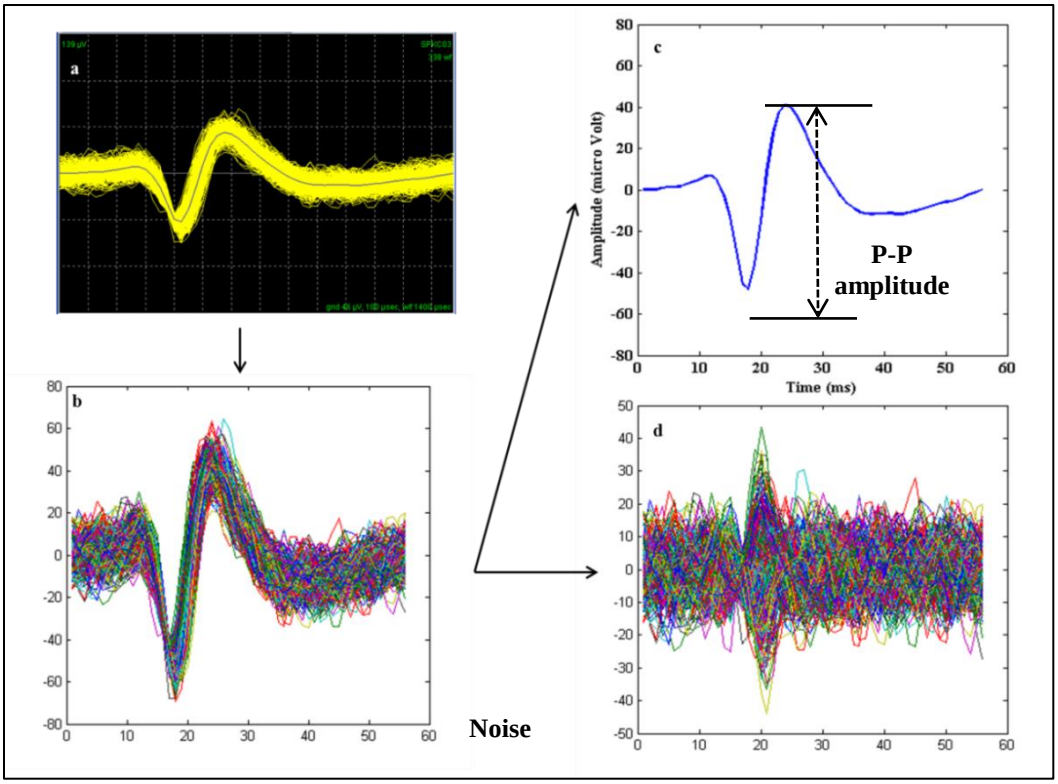

Figure 2.6 Steps of signal quality metric extraction. Representative examples of (a) Spike-sorted Single Unit (SU) of 338 individual action potential waveforms (b) SU imported in MATLAB (c) Mean waveform calculated as an average of the 338 waveforms (d) Noise as a collection of residual waveforms obtained after subtracting the mean waveform (c) from each individual waveform in (b).

2.3.5.1 Signal Quality Metrics

2.3.5.1.1 Peak to Peak (P-P) Amplitude:

All waveforms within an individual SU were averaged to create a mean waveform for each SU. The difference between the maximum and minimum voltage of the mean waveform was defined as P-P amplitude of the SU.

2.3.5.1.2 Signal to Noise Ratio (SNR):

We defined noise as the collection of residual waveforms obtained after subtracting the mean waveform from each individual waveform within the SU [167], since the spectral properties of residual waveforms and background activity in neuronal recordings have been shown to be similar [168]. Noise was quantified by the standard deviation measure (~ to Root Mean Square value) rather than the peak-peak amplitude (mostly used for deterministic signals). This is because of the inherent random nature of noise which makes the peak amplitude ambiguous due to the presence of multiple peaks where any one is not representative of the overall amplitude. Noise in electrophysiological recordings is generally approximated to have a Gaussian distribution (white noise) where the instantaneous amplitude is within $\pm$ 2σ, 98.5% of time. Thus, it is a general practice to use standard deviation of the noise as its measures, and to include the maximal probability estimation, researchers typically multiply the standard deviation by a factor ranging from 2 to 6 [167][169][170][166]. We selected the more commonly used factor of 2 to aid the comparison of results obtained in this work with that of other published studies[171].

SNR of each SU was subsequently defined as:

$$SNR = \frac{P - P\ Amplitude\ (Volt)}{2X\ Standard\ Deviation\ of\ Noise\ Waveforms}$$

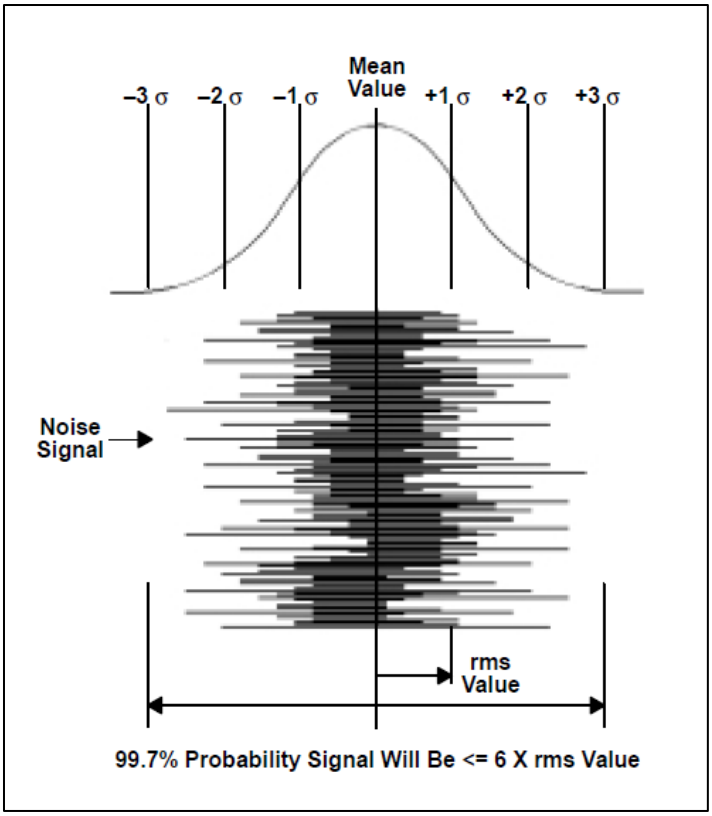

Figure 2.7 Gaussian distribution of noise (included from [172])

2.3.5.1.3 Number of SU per implant:

The total number of single units obtained across all electrodes from each peripheral nerve implant was determined. In order to compare across different time points, the mean of individual data points of total number of SU per implant at each time point was reported.

2.3.5.1.4 Array Yield:

The percentage of electrodes that recorded SU from the average number of electrodes embedded within nerve tissue per implant was defined as the array yield. The average number of electrodes whose tips were found to be positioned outside the regenerated nerve tissue upon REMI explant examination was four electrodes (4.1 $\pm$ 2.3; Mean $\pm$ SD; n=16) (Figure 2.7a,b); thus

the fraction of electrode tips embedded in nerve was determined to be an average of fourteen. In order to compare across different time points, the mean of individual array yield data points was reported at each time point.

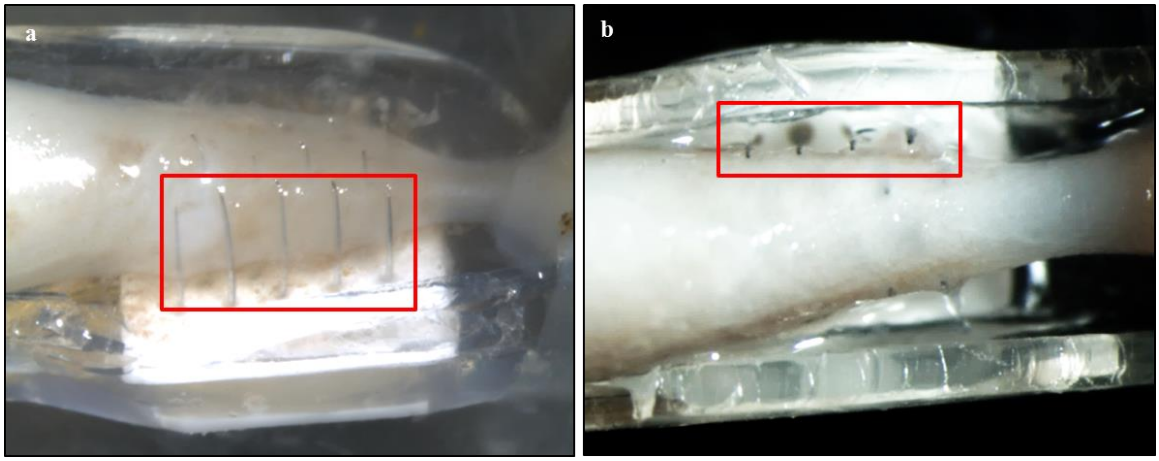

Figure 2.8 Examination of REMI explanted tissue at (a) 15 days and (b) 60 days post implantation. Area in red shows typical example of electrode tips that were considered to be positioned out of nerve tissue while remaining electrode tips were well embedded within nerve tissue.

2.4 Results

All animals (n=43) implanted with REMI were confirmed post-mortem to have the presence of an end to end regenerated nerve cable within the REMI conduit. Two animals were observed to have an improper incorporation of the connector within the pedestal resulting in a mismatched fit between the recording “head-stage” unit and the array connector, hence were excluded from further analysis. This reduced the number of eligible animals considered to forty one.

2.4.1 Classification of Failure Modes

Broadly, failures were classified as mechanical or regenerative due to poor electrode-nerve contact. Observed mechanical causes included expulsion of the pedestal due to detachment from the pelvis, and cable breakage which impeded further neural signal acquisition beyond their manifestation (Figure2.8a,b). In addition to the noted mechanical failures, upon REMI explant examination, we uncovered a second type of failure, one that relates to suboptimal nerve regeneration. Specifically, despite the presence of an end to end regenerated nerve cable, some electrode tips penetrated through the regenerated tissue while some were positioned completely outside the path of regenerating nerve. REMI explants that had less than 50% electrode tips in contact with the nerve tissue were classified as “Electrode-nerve contact failures” (Figure 2.8c).

Figure 2.9 Classification of observed failures. Illustrations of typical failures related to mechanical issues of (a) Occurrence of wire breakage at base of pedestal-connector assembly indicated by red circle and (b) Site of pedestal expulsion from pelvis indicated by area marked in red circle, and (c) electrode-nerve contact where some or all electrode recording tips inside REMI conduit are positioned out of the regenerated nerve tissue as highlighted by region marked in red circle.

2.4.1.1 Failure distribution in implants with no SU yield:

Twenty two of the forty one eligible implants (22/41; ~54%) failed completely to yield SU spikes throughout the experimental observation period. Eight of these failed implants (8/22; ~36%) suffered from loss of pedestal or visible wire breakage by 28 days post implantation. Ten implants (10/22; ~46%) were identified to have failures resulting from poor electrode nerve interface, i.e. less than 50% of electrode tips were in contact with the regenerated tissue. Interestingly, all such implants were observed to have high motion artifacts and frequent periods of amplifier saturation (Figure 2.9). Also, 50% of such implants had pedestal failures in parallel with failures due to poor nerve- electrode contact. Four animals (4/22; ~18%) failed due to causes which could not be classified as either of the identified failures modes in this study.

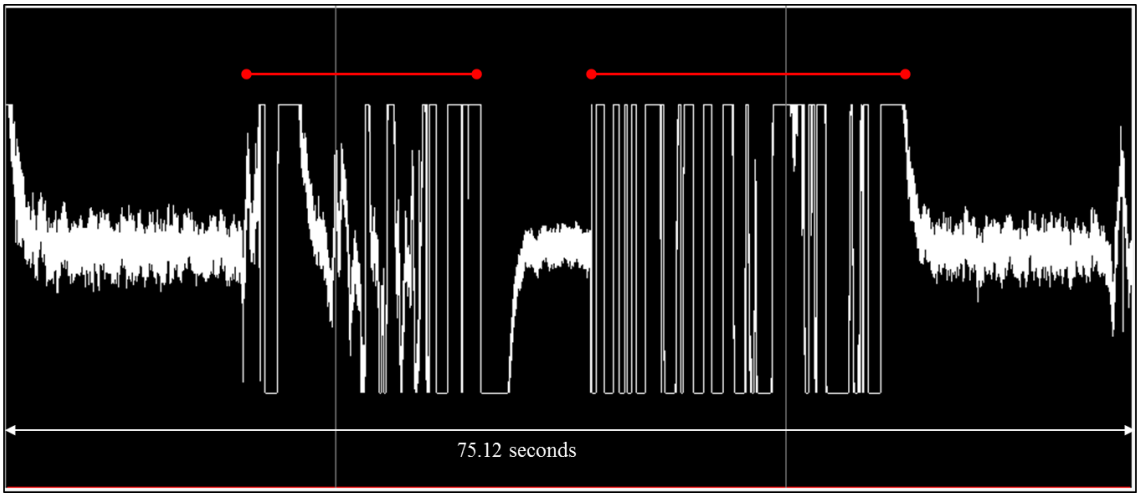

Figure 2.10 Illustration of noise due to high amplitude motion artifacts. Red lines indicate duration during which the amplitude remained saturated in ~75 second recording session.

2.4.1.2 Failures over time in SU yielding implants:

Nineteen eligible implants (19/41; ~ 46 %) were observed to yield SU activity during at least one of the attempted recording sessions at 7, 14, 21, 28, 35, 42, and 49 days post implantation over the course of the study. Two animals were terminated early at 30 day post implantation

despite any signs of failures to harvest the implanted nerve for histological evaluation. Thirteen implants (13/17; ~76%) showed pedestal expulsion between days 14 and 56. The incidence rate of this failure has been illustrated in Figure 2.10. Two animals showed SU activity until 35 days post implantation with normal background noise. These recording characteristics, however, changed considerably at the day 42 and day 56 recording sessions to displaying large amplitude saturating motion artifacts, power line interference, and absence of SU spikes. These animals showed weak pedestals that were greatly loosened due to tissue growth beneath the bone cement base making it likely that normal animal movements induced stress on the fine gold wires at the pedestal-connector assembly resulting in breakage of all or some of the wires that connect to the electrode interface. Two additional implants, (2/17) ~12 % of observed animals, that successfully displayed SUs until day 42, abruptly stopped showing any detectable spiking activity on any electrode and the reasons for such failure were not able to be identified.

The cumulative distribution of all failure modes observed in REMI implants has been summarized in Figure 2.11

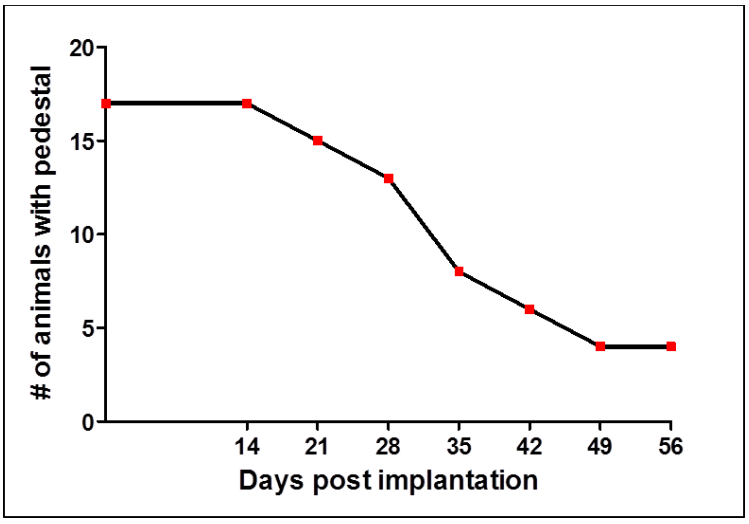

Figure 2.11 Graph depicting occurrence of mechanical failure over time in SU recording REMI implants.

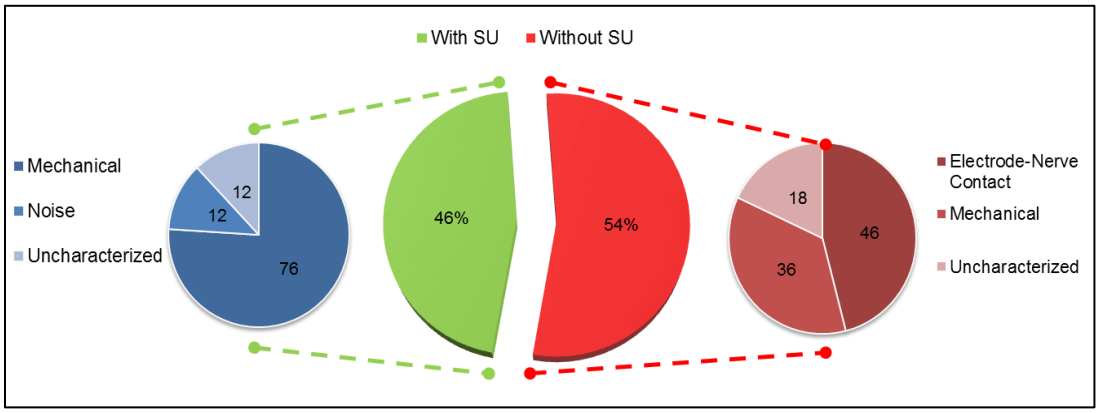

Figure 2.12 Failure distribution in REMI represented as a pie chart. (Center) Of 41 eligible implants, 19 (46%) yielded Single Units (SU, green). (Right) Exploded pie of 17 SU implants indicates failures over time due to mechanical issues in 13 (76%), increased noise contamination post day 42 in 2 implants (12%), and 2 implants (12%) with uncharacterized factors. Of 41 implants, 22 (54%) failed to yield SU (red). (Left) Exploded pie of 22 failed implants indicates 10 (46%) had poor electrode-nerve contact, 8 (36%) mechanical failures, and 4 (18%) unidentified causes.

Together, the results showed that the vast majority of the animals showed catastrophic mechanical failures related with common pedestal detachment and wire breakage. We reasoned that frequent handling of the pedestal during weekly recording sessions stressed the pedestals and that such movements could also contribute to wire breakage. To test this possibility, two additional experiments were performed.

First, weekly recordings were avoided for two animals, postponing the first recording session until 42 days. One animal suffered from pedestal loss at day 49 during the recording session, but the second animal successfully recorded SU spikes at day 49 and was sacrificed at day 50. This provided modest support to the idea that animal handling can indeed contribute to

pedestal failure. In the second approach, the attachment of the pedestal to the pelvis was postponed for 100 days in two additional animals. To that end, the connector was concealed in a protective plastic cover at the time of REMI implantation and placed in a sub-dermal pocket near the pelvis. At the 100th day mark, after surgically exposing and dissecting the cover free from fibrotic tissue, the connector was secured inside the pedestal and attached to the pelvis using bone cement. Twenty days after this procedure, we successfully recorded SU spikes in one animal, while the other had extremely high noise interferences, and no SU activity. While the number of subjects is small and a moderate 50% success rate in this approach, the result, while not conclusive, suggests that pedestal anchoring and manipulation contribute to the failing of the REMI interfaces despite relative stability of the electrode-tissue interface.

2.4.2 Quality of neural activity recorded from REMI over 120 days

2.4.2.1 Average Array Yield

The average array yield, defined as the percentage of electrodes of an implanted REMI recording SU activity from those embedded within nerve, was calculated to be in the range of 7.143% to 64.29% with 18.23 $\pm$ 12.29 % (Mean $\pm$ SD) across all observed time points. Occasional array yield values such as 78%, 92%, 100% were considered as outliers and excluded from statistical significance analysis. No statistically significant differences were determined between the medians of data at observed time points.

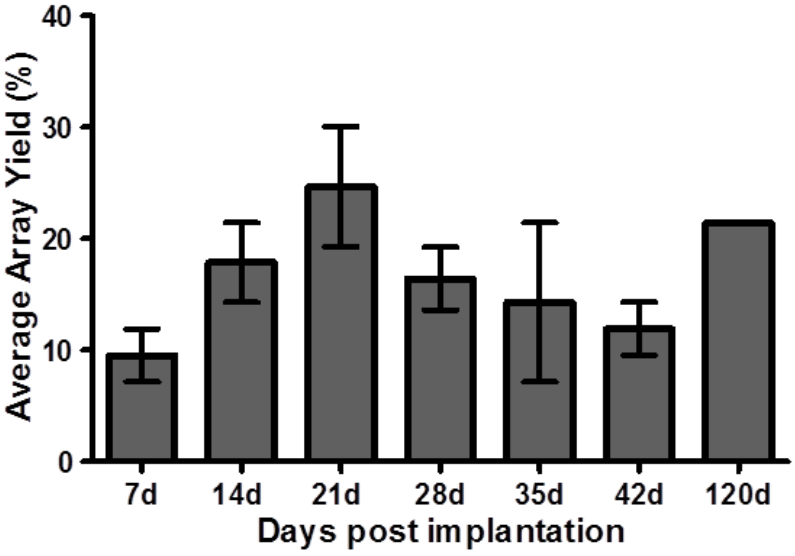

Figure 2.13 Average Array Yield from REMI implants over a 120 Day Period. Data presented as mean and SEM; n= 3, 8, 11, 9, 2, 3, and 1 implants from 7 to 120 days post implantation respectively. Kruskal-Wallis non parametric analysis and Dunn's multiple comparison test; no significance ($p = 0.53$).

2.4.2.2 Average SU per implant

Total number of SU obtained from each implanted REMI across time points of observation was in the range of 1 to 9 with 3.2 $\pm$ 2.0 (Mean $\pm$ SD). Occasionally, fifteen to seventeen SUs were obtained from one implant during early time points of regeneration; such values were considered as outliers for statistical analysis. No significant difference was observed between medians of data at observed time points; however this could be due to the lower sample size available at later time points (day 35 to 120). A bimodal distribution was seen in the average SUs per implant from recordings made during the first four weeks post implantation; specifically an initial increase from 3.0 $\pm$ 1.7 (Mean $\pm$ SD) at day 14 to 4.4 $\pm$ 2.9 (Mean $\pm$ SD) at day 21 followed by a decrease to 2.9 $\pm$ 1.8 (Mean $\pm$ SD) at day 28 with no dramatic loss of animals with

intact pedestals. Interestingly, despite losing 64% animals to mechanical failures by day 35, the average number of SU remained relatively similar from day 28 onward to longer time points.

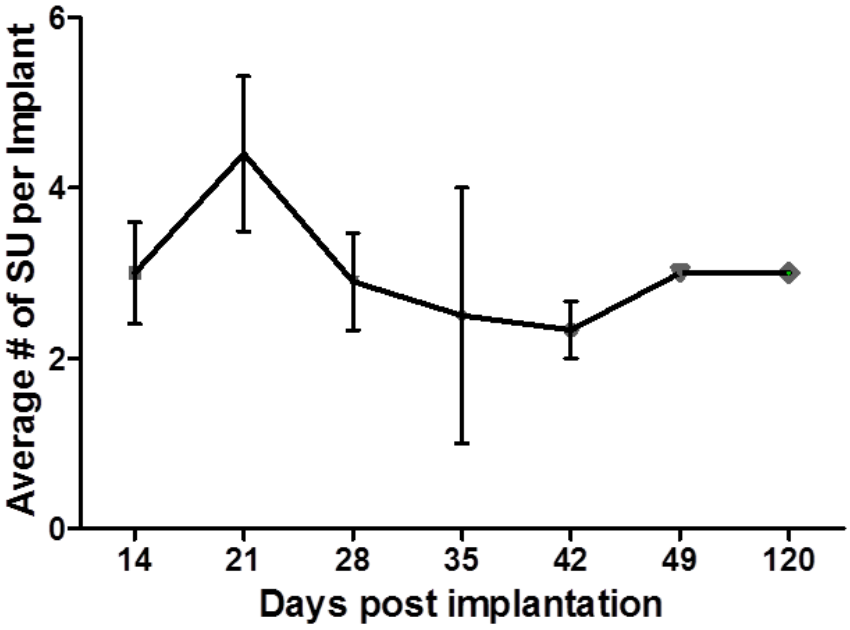

Figure 2.14 Average Number of SU acquired per REMI Implant over a 120 Day Period. Data represented as mean and SEM; n= 8, 10, 10, 2, 3, 1, and 1 implants at 14 to 120 days post implantation respectively. Kruskal-Wallis non parametric analysis and Dunn's multiple comparison test; no significance ($p = 0.8$).

2.4.2.3 Average P-P amplitude

Peak to Peak Amplitude (P-P) of Single Units observed across all time points was 100.8 $\pm$ 68.64 µV (Mean $\pm$ SD) with occasional SU of 850 µV. A decrease from the amplitudes recorded at day 7 was observed in the majority of subsequent time points. However, this is expected because at such an early time point of regeneration, the internal milieu of the tube is different from the later time points in terms of axonal growth, maturity and formation of perineural and epineural layers [173]. Also, a significant increase in amplitude was observed in the median

amplitudes from 56.84 to 102.9 µV between day 14 and 28 time points, respectively, which might be indicative of associated axonal maturation in terms of increase in diameter.

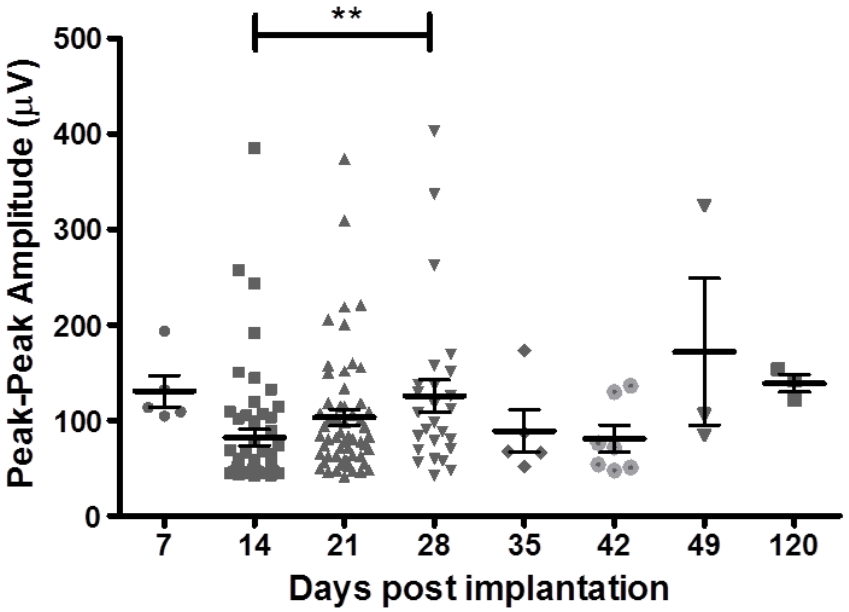

Figure 2.15 Average Peak to Peak Amplitude (P-P) of Single Units (SUs) acquired from REMI implants over a 120 day period. Individual data points of n= 5, 55, 56, 26, 35, 7, 3, and 3 total SUs are presented with mean and SEM from 7 to 120 days post implantation, respectively. Kruskal-Wallis non parametric analysis and Dunn's multiple comparison test; * indicates significant difference between day 14 and day 28 amplitudes (p = 0.0003)

2.4.2.4 Average Signal to Noise Ratio

Signal to Noise Ratio (SNR) of SU obtained from REMI was 5.01 $\pm$ 2.1 (Mean $\pm$ SD) across all time points, with occasional high SNR of 20:1 and 24:1 seen during early time points of regeneration which were considered as outliers for statistical analysis. Over time, there was no significant difference between the medians of SNR from 7 to 120 days post implantation. Thus,

despite the initial damage caused by the nerve transection associated with REMI implantation and subsequent regeneration through the conduit, the average SNR of single unit activity remained consistent which further indicates that the ongoing tissue response does not affect the recording reliability of REMI up to 120 days post implantation

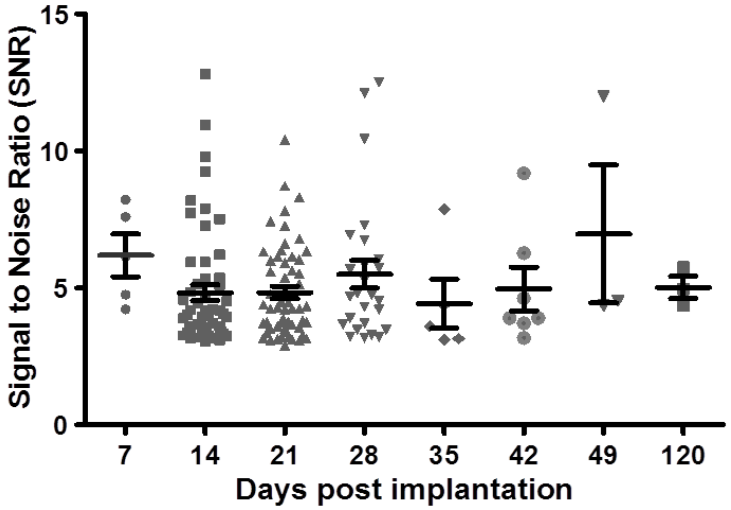

Figure 2.16 Average Signal to Noise Ratio (SNR) of Single Units (SUs) acquired from REMI implants over a 120 day period. Individual data points of n= 5, 55, 56, 26, 35, 7, 3, and 3 total SUs are presented with mean and SEM from 7 to 120 days post implantation respectively. Kruskal-Wallis non parametric analysis and Dunn's multiple comparison test; no significance (p=0.25).

2.4.3 Comparison between REMI and USEA

Thirty four animals were implanted with Utah Slanted Electrode Array (USEA) in the sciatic nerve and a pedestal enclosed with the connector was attached to the pelvis bone. Electrophysiological signals were acquired at fourteen days post implantation and animals were sacrificed at day 7 (n=2), day 14 (n=24) or day 30 (n=8) post implantation for evaluation of the

tissue electrode interface. Nine implants (9/34; 26%) displayed SU spikes at day 14 while twenty five implants (25/34; ~74%) failed to yield SU neural activity. Nine of the twenty five failed implants (9/25; 36%) suffered from mechanical failures related to pedestal expulsion or wire breakage before the day 14 recording time point. Post mortem examination revealed five animals (5/25; 20%) to have the USEA dislodged from the original implant site in the nerve to the surrounding musculature (Figure 2.16). Eleven implants (11/25; 44%) failed to display SU activity for reasons that were not identified in this study. These results are summarized in Figure 2.17. A total of 28 SU were acquired from nine implanted USEAs and evaluated for signal quality comparison with REMI.

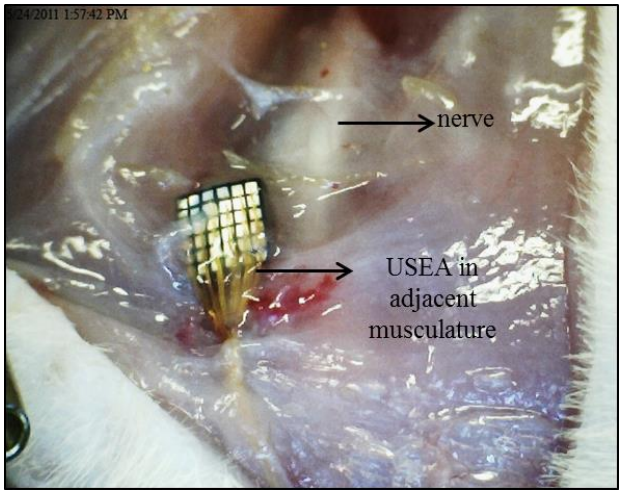

Figure 2.17 Illustration of USEA dislodged from original implantation site in sciatic nerve to adjacent musculature indicated by arrows.

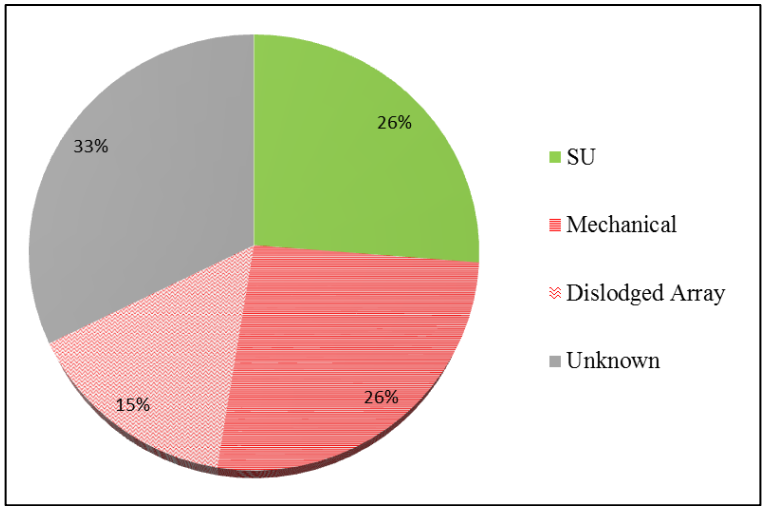

Figure 2.18 Pie Chart representation of failure distribution observed in USEA. Of 34 eligible implants, 9 (26 %) yielded Single Units (SU, green), while a lack of SU was observed in 9 (26%) due to mechanical failures, 5 (15%) due to array being dislodged from nerve, and 11 (33%) from reasons unidentified comprising a total 76% failures.

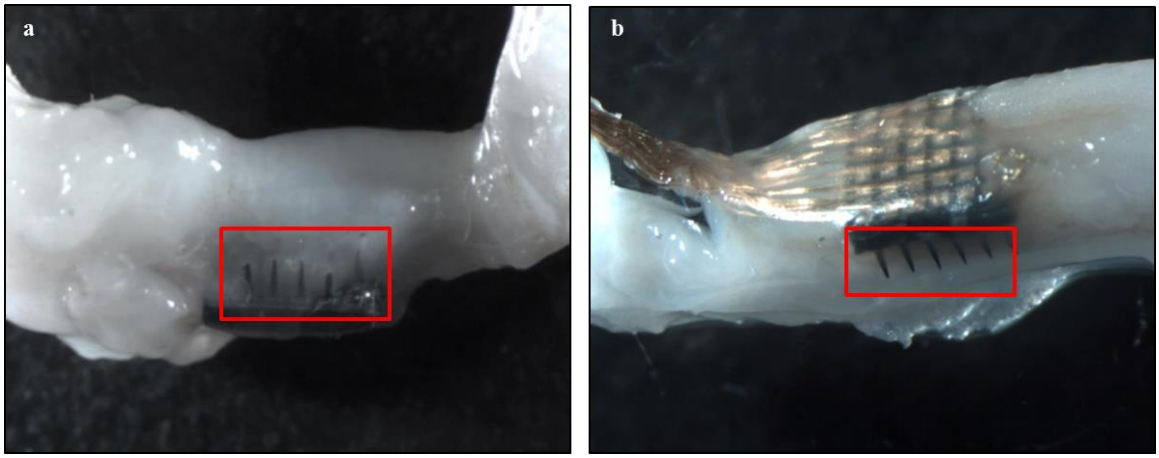

Figure 2.19 Examination of USEA explanted tissue at 15 days post implantation (a) and (b). Area in red shows typical example of electrode tips that were considered to be positioned out of nerve tissue while remaining electrode tips were well embedded.

2.4.3.1 Average USEA Array Yield

The number of electrodes with tips embedded within the nerve, upon USEA explant examination, was an average of twenty six electrodes (25.84 ± 3.8; Mean ± SD; n = 13). The average array yield, defined as the percentage of electrodes of an implanted array recording SU activity from those embedded within the nerve, was evaluated to be 8.5 ± 6.60% (Mean ± SD; n=9). In comparison, REMI implants (n=10) at day 14 had an average of 17.86 ± 10.10 % (Mean ± SD); two REMI data points (78.5 % and 92.8 %) were considered as outliers and excluded from statistical significance tests. Although REMI had increased array yield, no significant difference was observed between the median array yield of USEA (7.7%) and REMI (17.86 %) implants at day 14 post implantation.

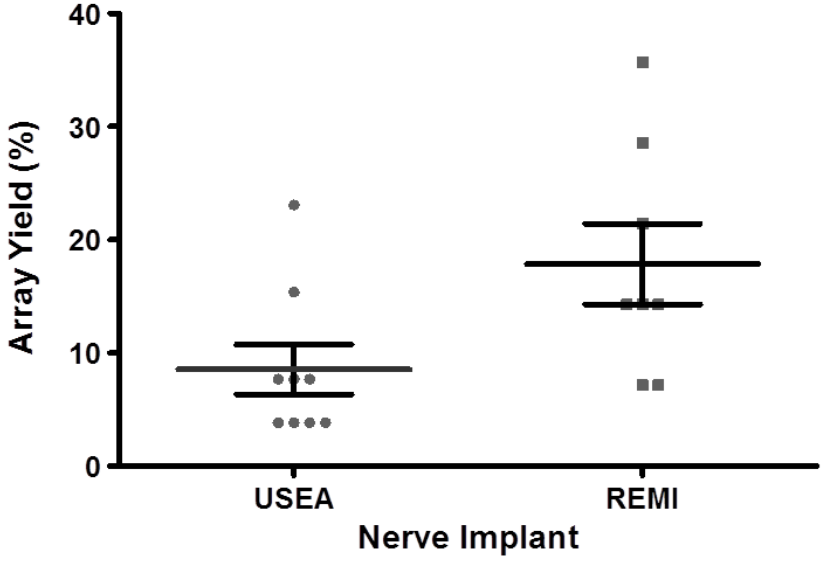

Figure 2.20 Similar Average Array Yield of SUs from USEA and REMI Implants at 14 days post implantation. Individual data points from n=9 implants (USEA) and 10 (REMI) are presented along with mean and SEM. Two tailed non parametric Mann Whitney test; no significance (p=0.0726).

2.4.3.2 Average Number of SU per USEA Implant

Total number of SU obtained from each implanted USEA was 3.1 ± 2.5 (Mean ± SD) at 14 days post implantation in comparison to 5.6 ± 5.7 (Mean ± SD) from REMI. No significant difference was observed between the median number of SU per implant i.e. 3.5 from REMI and 2.0 from USEA.

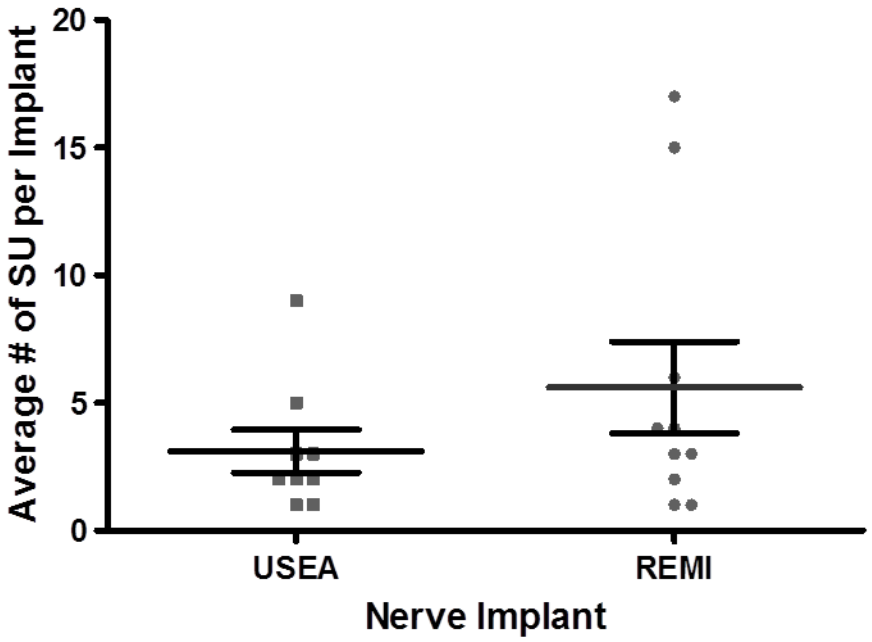

Figure 2.21 Similar Average number of SU acquired per implanted USEA and REMI at 14 days post implantation. Individual data points from n=9 implants (USEA) and 10 (REMI) are presented along with Mean and SEM. are presented along with Mean and SEM. Two tailed non parametric Mann Whitney test; no significance (p = 0.3205)

2.4.3.3 Average P-P Amplitude of USEA SU

Peak to Peak Amplitude (P-P) of Single Units acquired from USEA was 76.79 ± 50.77 µV (Mean ± SD) compared to 76.31 ± 47.50 µV (Mean ± SD) acquired from REMI at day 14. No significant difference was observed between the median values of P-P amplitude 56.35 µV and 56.38 µV from REMI and USEA respectively.

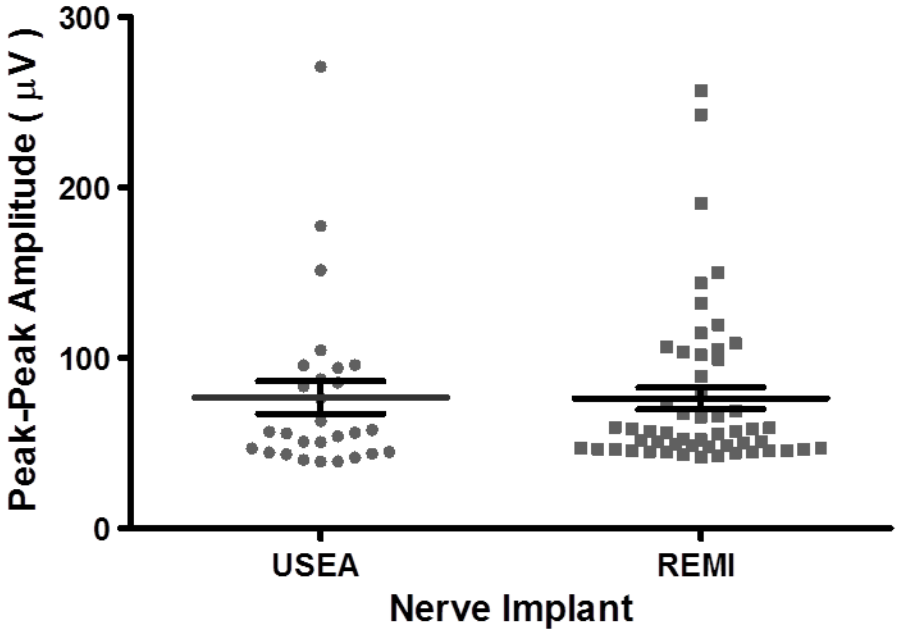

Figure 2.22 Similar Average Peak to Peak Amplitude (P-P) of SU acquired from USEA and REMI implants at 14 days post implantation. Individual data points of SUs, 28 (USEA) and 55 (REMI) are presented along with Mean and SEM. Two tailed non parametric Mann Whitney test; no significance (p = 0.57).

2.4.3.4 Average Signal to Noise Ratio (SNR) of USEA SU

Single Units acquired from USEA implants had an average SNR of 4:1 ± 1.1:1 (Mean ± SD) in comparison to 4.8:1 ± 2.2:1 (Mean ± SD) from REMI at day 14. Statistical analysis using non parametric Mann-Whitney Test confirmed a significant difference (p = 0.0329) between the medians of SU from USEA and REMI which were 3.5:1 and 3.9:1 respectively.

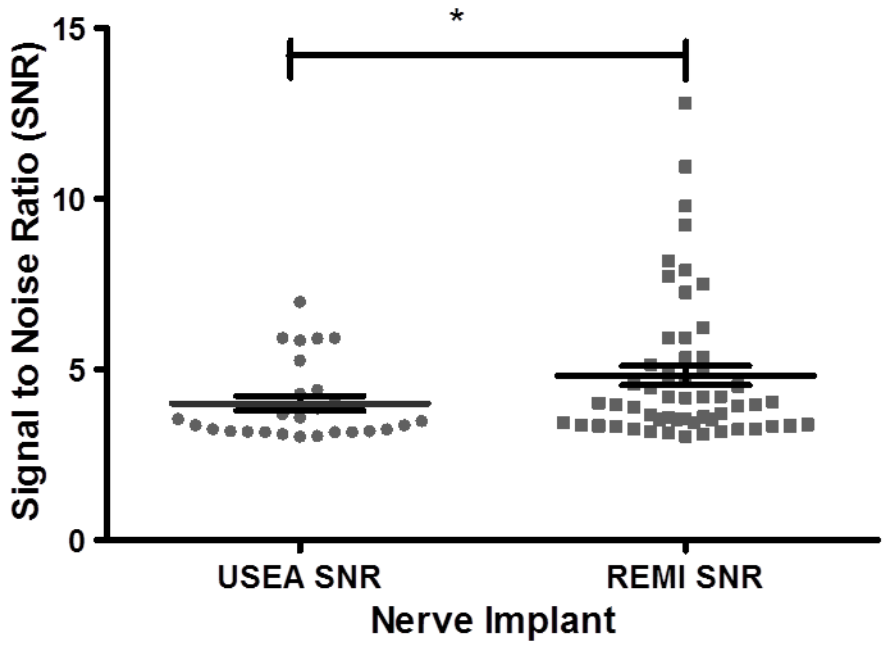

Figure 2.23 Higher Average Signal to Noise Ratio (SNR) of Single Units (SUs) acquired from USEA and REMI implants at 14 days post implantation. Individual data points of SUs, 28 (USEA) and 55 (REMI) are presented along with Mean and SEM. Two tailed non parametric Mann Whitney test; * indicates significant difference (p = 0.0329).

2.5 Discussion

This study characterized the ability of Regenerative Multi-electrode Interfaces (REMI) to record Single Unit (SU) spikes from peripheral nerves in a rat model by a 120 day longitudinal analysis of signal quality. It also reveals the common failure modes observed in REMI implants at early stages resulting in lack of SU yield, as well as gradual manifestations of failures in SU yielding REMIs at later time points. Additionally, the quality of signals recorded from REMI was compared to that of the relatively well established Utah Slanted Electrode Array (USEA).

An eventual decrease in P-P amplitude and SNR of single unit signals, occurring over a wide-ranging span of a few weeks in some cases to several months in others, has been observed in various electrode arrays used as Brain Machine Interfaces [174][175][176]. Foreign body response to implanted arrays in the form of electrode tip encapsulation by fibrotic tissue is the most commonly suggested reason for amplitude waning of intra cortical signals [82][62]. Likewise in the PNS, Lefurge et al. 1991 reported a slow significant decrease in P-P amplitude and SNR of SU recorded from LIFE electrodes implanted in cat sciatic nerves over a six month study[109]. Similarly, Branner et al. 2004 demonstrated SUs with USEA in cat sciatic nerves for the “first few days” beyond which the low SNR of signals accounted for failure [126]. Both studies attributed tissue response to implanted array interfaces, particularly the growth of connective tissue around the electrodes and increased distance from axons, as a reason for signal degradation. Also, other studies, such as those using extra neural cuff electrodes for PNI, determined causes of device failure to be lead wire breakage from becoming brittle over time or due to development of stress cracks in polyimide substrate, and partial avulsion of the nerve from the lumen of the cuff by connective tissue proliferation [91][93]. Complications arising due to tethering forces concomitant with transmission wires were also reported as a challenge in the recent variant of cuff electrodes, the Flat Interface Nerve Electrodes (FINEs) [177]. Longitudinal Intra-Fascicular Electrodes

(LIFEs) implanted in cat sciatic nerves (n=6) have been reported to fail solely from lead wire breakage [109] while details on longevity of neural signal recording from Transverse Intra-Fascicular Electrodes (TIME) has not been reported to this date. Studies on the assessment of the Utah Slanted Electrode Array (USEA) in cat peripheral nerves reported failures from lead wire issues, signal contamination from high amplitude myoelectric sources in awake animals, and placement of electrode tips in inter-fascicular space consisting of highly resistive perineurial and epineruial tissue [160][178] [128].

2.5.1 Failure Mechanisms of REMI

In this study, we successfully observed chronic spontaneous SU activity from awake, freely behaving animals in 46% of REMI implants of which 76% failed to last beyond day 49 post-implantation due to eventual wire breakage and loss of the percutaneous connector. Of the 54% of implants that completely failed to display SU spikes, acute catastrophic failures were observed in 36% cases. Together, the data showed that the main challenge for long-term REMI interfacing in the peripheral nerves was due to mechanical failures. This observation is in agreement with other published results on the recording capability of regenerative interfaces which highlight the percutaneous connecting wire breakage as the main cause of failure, specifically 40% [142], 78% [179], and close to 100 % [180]. This limitation can be obviated by wireless signal transmission technology. Aspects of this technology, which would be crucial to its integration with peripheral nerve interfaces in clinical practices, such as power consumption, delivery and dissipation within physiological tolerance, encapsulation and hermetic packaging for long term operative reliability, are being researched by several laboratories [181] [182][183]. Indeed, stable cortical recordings for over a year in non-human primates using fully implantable wireless neural interfaces have been recently demonstrated successfully [184].

Regenerative electrodes, due to their implantation method of transecting peripheral nerves, have a unique complication arising from the possibility of a poorly regenerated nerve cable through the electrode array; reported occurrences of such a failure are 16% [185] and 25 % [137]. Studies focused on the long term biocompatibility of first generation sieve design based arrays revealed possible failure from constrictive axonopathy that ensues in small diameter holes (50-100 µm) because of limited space available for regenerating axons to increase in diameter, a consequence of the maturation of nerve fibers [186][187] [188]. In this study we determined that 25% of all implanted REMIs (10/41) had more than half of the electrode tips positioned outside the nerve and completely lacked to display SU activity. This issue is not primarily a failure of the nerve to regenerate and can be resolved by reducing the heights of individual electrodes to those empirically determined to have maximal probability of being embedded within the regenerated nerve. Finally, approximately 14% of failures could not be explained and their cause remains unidentified.

2.5.2 Stable Signal Quality from REMI over a 120 day period

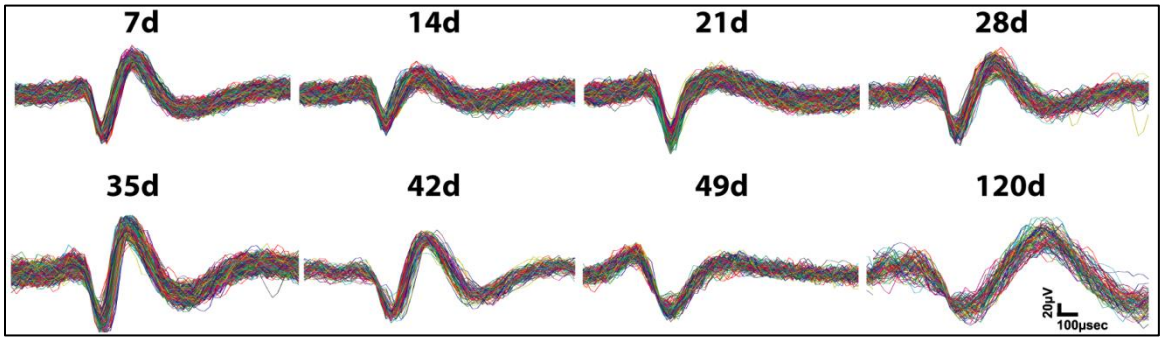

Figure 2.24 Representative Single Unit (SU) waveforms recorded from REMI at 7, 14, 21, 28, 35, 42, 49, and 120 day post implantation.

Similar to our previously reported studies, Single Unit activity was seen in REMI as early as 7 days post implantation [150]. The lack of activity before day 7 is explained by the fact that

peripheral nerve axons regenerate at an average speed of 1 to 3 mm a day; thus for an effective gap of 5 mm to be bridged between the proximal and distal nerve stumps in the REMI conduit, a duration of a week is expected [189]. The number of SU recorded per REMI implant and average array yield was determined to have a steady weekly increase from day 7 to the highest at 21 days post implantation, followed by a moderate decrease at day 28 and remaining stable thereafter. This specific decrease could be ascribed to the possibility of axonal death around the recording zone of electrodes from an increased inflammatory response, as seen in cortical implants [190]. However, the area occupied by active macrophages and axons around the electrode tips in the REMI implants was observed to be consistent throughout the entire 8 weeks of observation as reported in a separate study performed in our laboratory [191] and hence does not justify the loss of units. Additionally, immunocytochemical visualization of regenerated tissue through the REMI confirmed the presence of axons with large diameter and myelination within 100 µm vicinity of the electrode implanted sites with no observable decrease from 15 to 60 day time points (Figure 2.24). Spontaneous electrical activity in regenerating axons following nerve injury has been reported to start as early as one day, peak at 14-21 days and decrease in subsequent weeks reaching a plateau thereafter [192]. In other systems, such activity has been reported to be indicative of ongoing pain, mechano-sensitivity, and thermal allodynia present after nerve injuries [193] [194]. Alternatively, electrical impulses in developing or regenerating axons has been implicated to have a role in processes of myelination of DRG axons and optic nerves [195] [196], and in the path finding of growth cones [197]. In light of these properties of regenerating axons, the loss of spontaneously active single units after day 21 seems to be a normal physiological consequence rather than failure of the electrode interface.

Regenerative interfaces have been reported to have a specific advantage over other types of PNI as the tissue repair mechanisms seem to “anchor” the electrodes. In this study, we found evidence that partially supports this notion. Neural activity acquired from REMI was

determined to display multiple stable Single Units (SUs) without progressive decay in amplitude and SNR over the observed duration of 120 days. On the contrary, a significant increase in amplitude was observed between day 14 and day 28 which is a time period of dynamic changes occurring within the REMI conduit from a nerve tissue regeneration perspective. Peripheral nerve transection and subsequent regeneration entails extracellular matrix remodeling accompanied with a complex wound healing and inflammatory response mediated predominantly by glial macrophage cells [198]. During the process of Wallerian degeneration of the distal nerve stump after transection injury of peripheral nerves, macrophage recruitment typically starts 2-3 days after injury and peaks by 14 -21 days [199] [200]. Thus, in this study, high quality single unit activity with SNR and amplitude up to 20:1 and 850µV was obtained from REMI despite enduring maximal tissue response to its implantation. To sum up analysis of the four studied metrics, our results indicate that the quality of signals acquired from freely behaving animals implanted with REMI remained stable over a 120 day period.

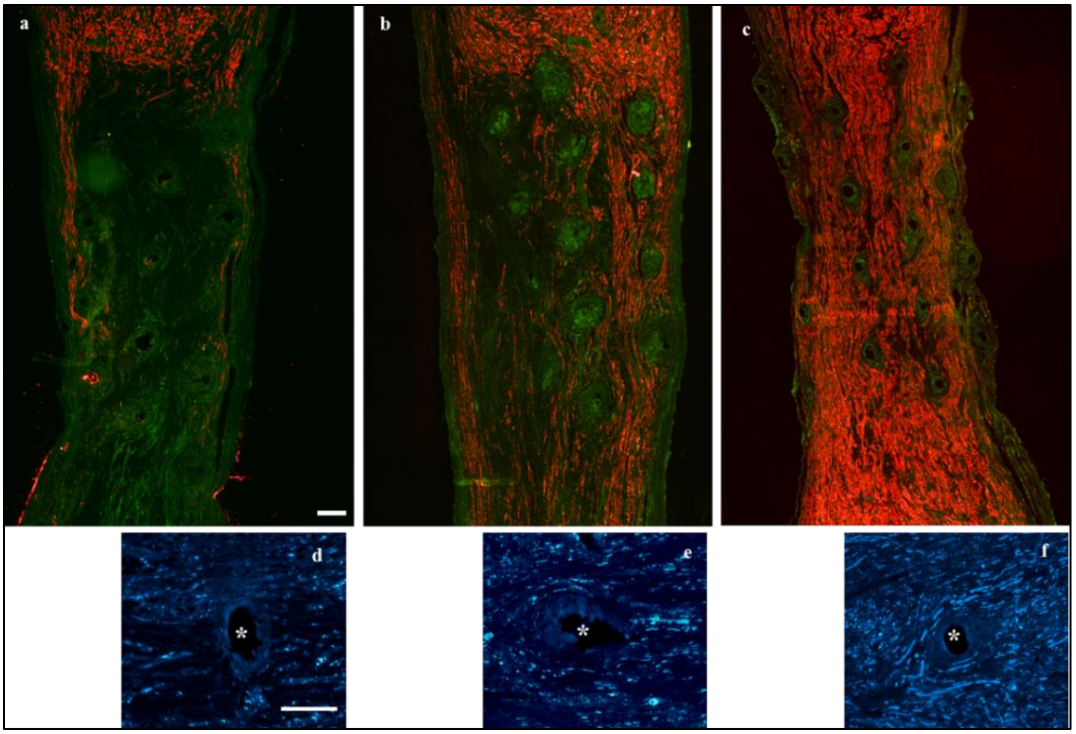

Figure 2.25 Representative Immunocytochemical visualization of regenerated axons at (a,d) 15 day (b,e) 30 day (c,f) 60 day post REMI implantation. (a-c) Immuno-labeling of myelinated axons (red) using P0 marker around electrode implanted sites (green). (d-f) Higher magnification visualization of NF200 labeled large diameter axons (blue) around an individual electrode implanted site (*). Scale bar = 100µm.

2.5.3 Superior Signal Quality from REMI compared to USEA

USEA and REMI had comparable performance for parameters of average yield and number of Single Units acquired per implant at fourteen days post implantation. However, it must be noted that the number of available electrodes in USEA was nearly twice as much as those in REMI. Average Peak to Peak amplitude of total SUs acquired from both arrays was determined to be similar which is consistent with equivalent pre-implantation impedance ranges of 100-300 kΩ corresponding to an active site area of ~ 400 μm^2 at the electrode tips (Microprobes Inc.). These

results were in agreement with amplitudes from simulated Finite Element Models (FEM) of extracellular recording from cortical neurons and dependency of signal characteristics on variables such as impedance, active site area, geometry, and recording bandwidth [201]. Experimental amplitude values of signals recorded by micro-electrodes with similar dimensions from cortical regions and peripheral nerves are in the similar range of 70-110 µV [202][58][129][134].

Interestingly, Single Units from REMI had a significantly higher average Signal to Noise Ratio than those acquired from USEA. Since mean P-P values were determined to be equivalent, it is inferred that the noise in REMI recordings was significantly lower compared to that from USEA. Dominant sources of noise in extracellular recordings include electronic noise (amplifier), thermal noise at electrode-electrolyte interface, and biological noise from undifferentiated background action potentials or other physiological signals [203][201][204]. As the same data acquisition system used in all experiments, variations due to electronic noise do not seem to account largely for noise disparity between the two interfaces. Thermal noise is reported to increase as a function of the square of the impedance and is essentially dependent on electro-chemical properties of the electrode including the resistivity at tissue interface [204][205][206]. Since the method of surgical implantation (regeneration versus insertion) was unique; it is likely that the post-implantation tissue response elicited by the electrodes in the two interfaces was dissimilar which might have led to differences in the thermal noise generated at the electrode-tissue interface. However, more detailed investigation on this aspect would be needed to validate this interpretation. Additionally, observations from online recording and offline analysis bring forth a distinct characteristic of biological noise contamination in USEA interfaces, particularly higher interferences from myoelectric sources than REMI. Such a characteristic can be explained by the fact that upon explant examination, some USEA arrays were observed to be sloppily embedded in the nerve (Figure 2.23a), perhaps due to macro-motion, making them more susceptible to

signal contamination from surrounding muscles and tissue. Contrary, better integration of electrodes with the regenerated cable, possibly enhanced by structural support from the polyurethane conduit, was observed in REMI explants (Figure 2.23b). Together these observations support the notion that the REMI forms a robust interface with peripheral nerves, yielding higher quality single units in a rodent model.

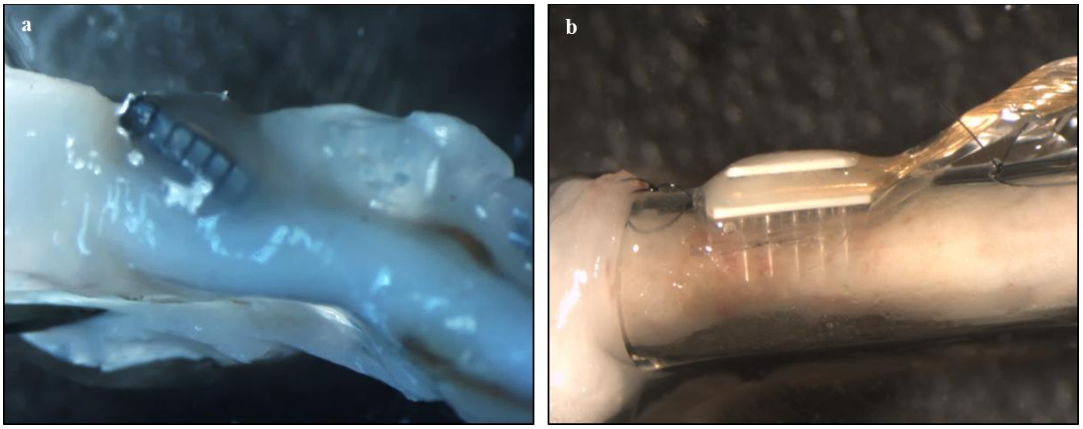

Figure 2.26 Illustration of differences in structural integrity with the sciatic nerve of (a) USEA at day 14 and (b) REMI at day 30, upon explant examination.

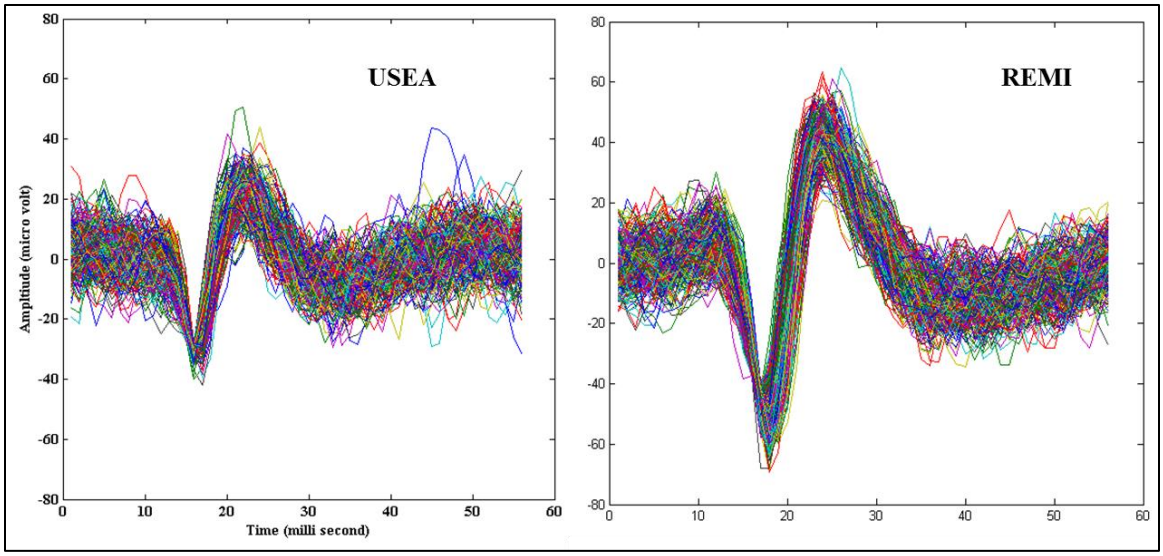

Figure 2.27 Representative Single Unit (SU) waveforms recorded from USEA (left) and REMI (right) at 14 days post implantation

2.5.4 Limitations and Additional Considerations

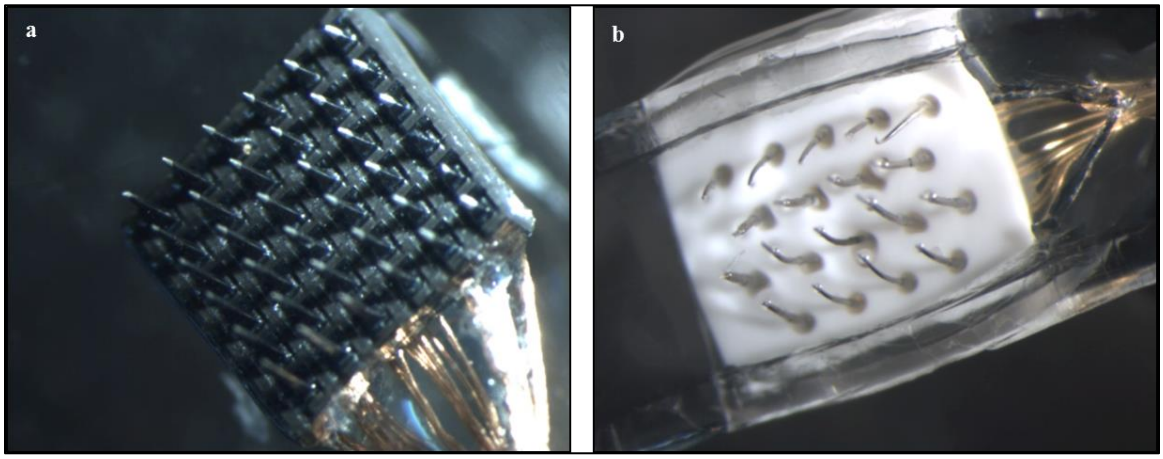

Figure 2.28 Representative photographs of (a) USEA and (b) REMI harvested and dissected free from the interfaced nerve after 30 days of implantation reveal higher structural integrity of USEA electrodes

Electrochemical Impedance Spectroscopy (EIS) has emerged as a powerful diagnostic tool to monitor changes resulting from tissue encapsulation at the electrode interface in the central nervous system [203][207]. Conversely, it can also reflect the deterioration of electrode material from delamination of the insulating layer or development of cracks in it and physical bending or breakage of electrode tips within the tissue. A recent study investigated the coupling of abiotic and biotic failures in the Pt/Ir electrodes of the Floating Micro-electrode Array (FMA) when used as a recording interface in the rat cortex [208]. They confirmed material degradation from insulation damage by pre and post Scanning Electron Microscopy examination of the electrodes and consequent continued decrease in impedance due to leakage resistance and parasitic capacitance, culminating in poor array yield and eventual functional failure. In case of peripheral nerve interfaces, such damages can be expected to occur at both the electrode-tissue interface and along the wire link to percutaneous connectors. Impedance values can also indicate the presence of an open or short circuit along the gold transmission link wires which remain concealed inside the animal body and cannot be visualized externally. While chronic EIS measurements were not obtained in this study, difference between the structural integrity of the silicon based electrodes in USEA and that of Platinum electrodes in the REMI was observed. Specifically, upon explant examination, the REMI electrodes were found to be more bent and broken than the USEA electrodes (Figure 2.27). Incorporation of EIS measurements and high resolution examination of the electrodes post implant in this study would have supplemented the investigation of failures that went unidentified in both the REMI and USEA interfaces. Additionally, it could probably clarify the distinct characteristic of the REMI electrophysiological recordings to be more susceptible than the USEA to high amplitude motion artifacts (Figure 2.8) which mostly occur due to dc offset resulting from the fluctuations in electric potentials at the electrode tissue interface. Thus, *in vivo* EIS measurements combined with wireless transmission technology can potentially institute a “time-line” of material degradation and tissue encapsulation of REMI

electrodes and its impact on the quality of single units acquired over the course of several months to years, which would be pertinent to its advancements.

Since the path of regenerating axons was not governed externally in the REMI design, it was important to determine if some specific electrodes had more success in interfacing with the axons and recording SU signals. Figure 2.29 shows that electrodes present in the extreme lateral rows (top and bottom most) and with heights of 0.7 and 0.8 mm had higher tendency to record SU, as evident by the lighter colors in the heat map depicted. This result draws attention to the inherent limitation of the REMI design where the fixed physical position of the electrodes needs to be carefully selected to ensure optimal interfacing of axons with the recording sites. Also, impact of the immobile location of reference and ground electrodes on quality of signals over time were not studied in this work but need to be considered for improvisation of future designs.

Yet another aspect of motor control by neural interfaces is the determination of the type of signal source that can remain functionally stable over long periods. Some studies have demonstrated that Multi Unit activity and Local Field Potentials (LFP) in cortical recordings remain more stable than Single Unit (SU) spikes over the course of many years [209][175]. Additionally, MU activity is acquired by simple amplitude thresholding, while SU extraction requires the process of spike sorting which is costly and inefficient for real time on-chip implementation [210]. In this study, we restricted the focus on information modality to SU activity and it is very likely that, in doing so, we under-estimated the recording ability and array yield of the REMI. It is important to acknowledge that alternatives to SU activity exist in peripheral nerves, such as those measured by LIFE electrodes[112][211] and possibly by micro-electrode based interfaces, should be taken into account for future studies to investigate the identification of information type that is more suitable and stable over years for the control of robotic prostheses.

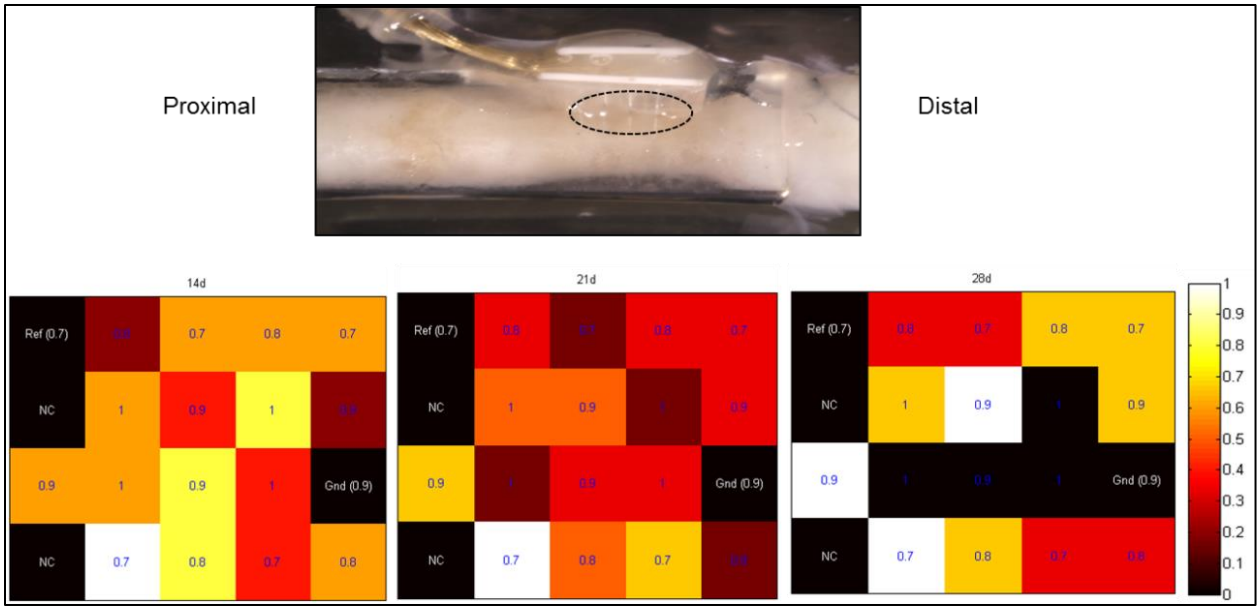

Figure 2.29 Heat map characterization of array electrodes with their heights and SU recording performance at 14, 21, and 28 days post implantation (left to right). Orientation of individual electrodes in the array as positioned from proximal (left) and distal (right) to the transection site with varying heights indicated from 0.7 to 1 mm. Color bar ranges from 0 to 1 with 1 being the highest number of SU recorded. Numbers of animals considered were 10, 11, and 10 at 14, 21, and 28 days post implantation. Ref is reference electrode, Gnd is ground electrode and NC stands for Not Connected

2.5.5 Summary

The focus of this study was to characterize the quality and reliability of signals acquired from REMI by evaluation of signal to noise ratio and peak to peak amplitude of recorded single units over time. Results determined that these parameters remained consistent, indicating that ongoing tissue response in the REMI conduit does not impede the recording ability of its electrodes, at least over the time period of 120 days. . However, the interface failed primarily due to the connector-pedestal assembly breakage. Thus, the number of single units available for quality metric assessment reduced at later time points. While this limitation does not undermine

findings of the present study (stable quality of REMI signals), it is difficult to ascertain if the single units acquired at each week belonged to the same group of axons, i.e. day to day tracking of single units was not accomplished. Variability in single units in terms of signal “non-stationarity”, seen as appearing or disappearing of units and changes in waveform shapes or amplitude, have been reported in recordings of cortical neurons. Responsible factors, in addition to the abiotic and biotic factors discussed previously, include neuronal plasticity and positional changes between electrodes and neuronal tissue due to macro/micro-motion[212][174][213]. From a neuro-prosthetic motor control perspective, such drift in signals in neural interfaces have an impact on the subsequent processes involved in generation of a control command to the end device, i.e. deciphering of movement intent using decoding algorithms which are initially trained based on the behavior (firing rates) and type of single unit. Although adaptive machine learning and daily recalibration of decoders can resolve this issue in a laboratory experimental set up, the latter is impractical and not feasible for day-to-day use in amputee patients. From a basic neuroscience standpoint, characterization of such variability can provide an insight into the dynamic physiological developments of central and peripheral neural circuitry and pathway reorganization consequent to distal muscle loss and sensory deprivation in the context of an amputation injury[214]. In the regenerative peripheral nerve interface paradigm, such as the REMI in this study, the processes of axonal regeneration and re-innervation to distal appropriate targets continue over the course of months. Electrophysiological properties of regenerating axons evolve as they mature and the electrical impulses generated by them can have distinct roles over such progression; thus providing a unique avenue to gain insight into such phenomena and yet adding to the inherent complication of neuro-plasticity from a control perspective. Nonetheless, the paradoxical pursuit of acquiring absolute stable signals from a constantly adapting, learning and changing nervous system is an important one for optimization of a potential neural interface.

Chapter 3

Comparison of Signals Acquired by Regenerative Interfacing of Rat Sciatic Nerve and its Fascicles

3.1 Abstract

In order to provide volitional control over sophisticated prosthetic arms with 22 degrees of freedom, peripheral nerve implants need to interface directly with distinct and multiple motor axons. Moreover, varied discriminable sensory percepts of small slips, texture and shape of contact objects, touch, and limb position, comparable to the human hand which is populated by an estimated 17,000 touch sensing receptors [215], need to be elicited by electrical stimulation. Hence, enabling adequate and selective interfacing with both afferent and efferent axons is recognized as an important avenue in optimization of Peripheral Nerve Interfaces. We have previously demonstrated the capacity of the Regenerative Multi-electrode Interface (REMI) to acquire spontaneous Single Unit spikes with stable signal quality from the sciatic nerve of awake and unrestrained animals[149]. However, discrimination between signal modalities has not been demonstrated due to the random interfacing of different regenerating axon types in mixed modality nerves (i.e., sciatic nerve) and the incomplete re-innervation to distal targets of regenerating axons at early time points (until day 21 post-implantation). In order to define motor and sensory signals, we implanted the REMI into the tibial and sural fascicles of sciatic nerve which have mostly axons with muscle and skin end-targets, respectively and using these naturally modality-segregated REMIs, we recorded efferent and afferent signals, 4 weeks after implantation during voluntary locomotion and tactile stimulation. This strategy allowed us to identify neural activity with distinct bursting firing pattern synchronous to stepping as well as Slowly Adapting (SA) Low Threshold Mechanoceptive signals evoked by skin sensations. Following the identification of motor and sensory signals from the REMI implants in tibial and sural fascicles, we compared such signal patterns with the recorded activity from REMI

interfacing of whole sciatic nerve. Taken together, the results indicate a higher probability to record from large diameter axons belonging to both motor and sensory modalities.

3.2 Background

Peripheral nerves are composed of heterogeneous axon types, either somatic or autonomous, and are classified based on axon diameter and myelin thickness, which in turn determine their conduction velocity and function. Such fiber types range from unmyelinated and thinly myelinated, small diameter (<5 µm) to thickly myelinated, large diameter (>10 µm) axon as shown in Table 3.1. A-alpha axons with the largest diameter (10-20 µm) are involved in motor and proprioceptive functions of limb movement, the smallest diameter A-delta and C (<5 µm) axons mostly convey sensations of pain, while the intermediate A-beta (5-12 µm) axons respond to the cutaneous mechanoceptive stimuli of touch, vibration, pressure, texture, and skin stretch [216].

Despite such fiber heterogeneity, peripheral nerves demonstrate a somatotopic organization wherein sensory fibers from specific skin areas and motor fibers going to a group of muscles remain bundled as a fascicle or within a fascicle itself [217]. The rat sciatic nerve is a mixed nerve that ramifies into tibial, peroneal, and sural fascicles around the distal third of the thigh region. In turn, the tibial nerve innervates multiple muscle targets including the ankle extensors and its synergists, i.e. Medial and Lateral Gastrocnemius, Plantaris, and Soleus as well as the posterior Tibialis, Flexor Hallucis Longis, Flexor Digitorum Longus, and intrinsic muscles of foot that are mainly related with toe and foot movements. It also contains a small sub-branch that innervates the medial aspect of the glabrous skin in the hind paw including the central and digital foot pads and toes [218][219]. Thus, the tibial fascicle carries a sizeable population of the motor fibers from

the sciatic nerve. On the other hand, the sural fascicle consists of 95% sensory axons that innervate the dorso-lateral surface of the hind leg and extreme lateral edge of the foot[220].

Table 3.1 Classification of peripheral nerve axons based on diameter, physiological function, and modality with additional information on end target or receptors and electrophysiological characteristics of Low Threshold Mechanoception (LTM), High Threshold Mechanoception (HTM), Slowly Adapting (SA), and Rapid Adapting (RA). GTO: Golgi Tendon Organ, M: Motor, S:Sensory. Fiber nomenclature based on [1]Erlanger and Gasser classification [221] and [2][222]. Adapted from [223] and [224]

Sensory and Motor Fibers[1]	Sensory Fibers[2]	Diameter (µm)	End Organ/Receptor	Function	Additional Information
A-alpha	Ia	10-20	M: extrafusal	Muscle contraction	
			S: primary intrafusal fibers	Detect changes in length and velocity of muscle stretch	Both SA and RA LTM
	Ib	10-20	S: GTO	Detect muscle and ligament tension	SA and LTM
A-beta	II	4-12	S: secondary intrafusal fibers	Detect static position muscles	
			S: Meissner's corpuscle	Touch and Pressure	RA and LTM (Mostly Glabrous Skin)
			S: Pacinian Corpuscle	Vibration, Deep Pressure	RA and LTM (Subcutaneous tissue)
			S: Merkel's Disc	Touch, Pressure	SA and LTM (hair follicles, all skin)
			S: Ruffini's endings	Skin stretch	SA and LTM (all skin)
			S: Ruffini's and Pacinian Joint Receptors	Joint Range of motion and position	RA and LTM
A-gamma		2-8	M: dynamic and static secondary fibers	Muscle spindle alignement	
A-delta and C	III and IV	1-5 and <1	S: free nerve endings (skin and joints)	Crude touch, pain, temperature	SA and HTM

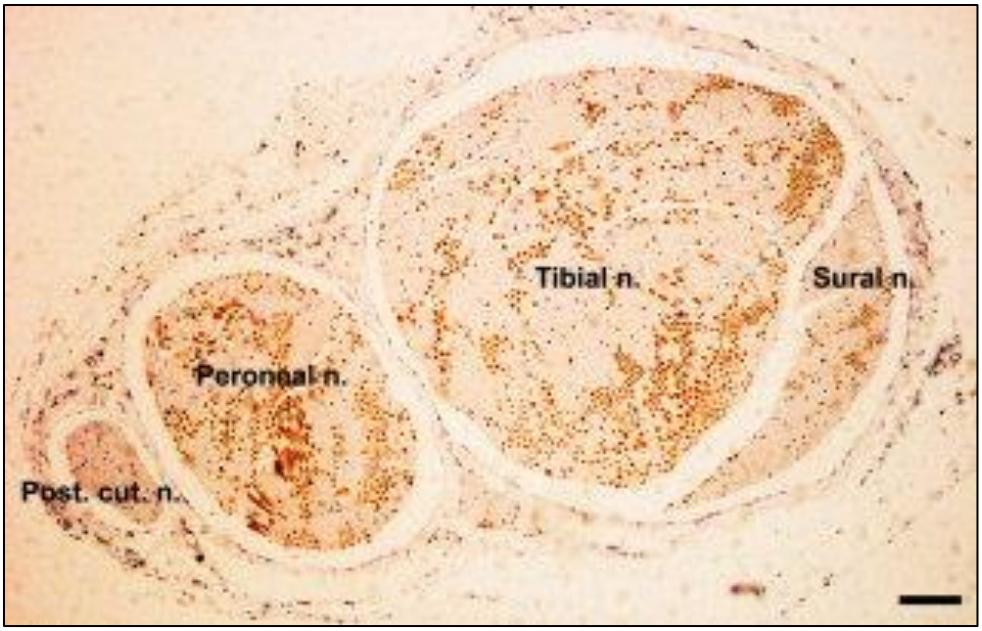

Figure 3.1 Fascicles of rat sciatic nerve at distal level depicted in a transverse section by immunohistochemical labeling of Choline Acetyltransferase (ChAT), counterstained with hematoxylin. Scale Bar = 100µm. Image taken from [218]

Residual nerve stumps remain functionally viable with intact central and peripheral pathways after years of amputation, and the feasibility to record motor signals for movement control of robotic arms with incorporation of electrical simulation mediated sensory feedback has been demonstrated using intra-fascicular electrodes [114][113]. More recently, regulation of grasping force and recognition of object shape and compliance was achieved by electrically conveyed tactile information from intra-fascicular nerve interfaces in real time conjunction with a sEMG controlled robotic hand [225]. Thus, bidirectional interfaces have the potential to provide efficient and intuitive control of robotic arms with reduced dependency on visual feedback which is crucial for its widespread acceptance in amputee patients [17]. To this end, adequate interfacing with multiple motor and distinct sensory axons in the residual amputated nerves has to be established.

Chronically transected nerves lose their regenerative capacity within months of injury and despite surgical repair, the composition of sensory and motor axons in terms of number, axon caliber, and conduction velocity are not restored to levels comparable with uninjured nerves [226][227][228]. Attributed reasons include, but not limited to, retrograde death of neurons in spinal cord [229], diminished ability of chronically denervated end targets to secrete neurotrophic factors, [230] and “accept” re-innervating axons [231]. This raises an important question for regenerative interfaces, one that relates to the effective interfacing of motor axons and sensory subtypes. Perforated sieve interfaces in rodent sciatic nerves have been reported to favor regeneration of small diameter sensory over large diameter motor axons, specifically 89% of axons regenerated distal to sieve electrode had diameters less than 5 µm after 60 days of interface implantation [143] [145]. Such hindered regrowth of large diameter axons probably attributes to the fact that neural signals acquired from sieve interfaces have largely been limited to electrically evoked responses in anesthetized animals rather than single unit spikes related to voluntary movement or sensory percepts in awake animals [142].

We have previously shown the presence of myelinated large diameter and small diameter axons in close proximity to the electrodes of the Regenerative Multi-electrode Interface (REMI) in the rat sciatic nerve [149]. However, it is currently unknown if the signals acquired from REMI in sciatic nerves of awake animals are restricted to a particular sensory or motor modality. Based on the described morphometric features and physiology of the rat sciatic nerve, we rationalized that efferent and afferent neural activity can be recorded from the tibial fascicle during locomotion and from the sural fascicle by heuristic sensory assays. Thus, the characterized neural signals recorded from these fascicles in response to varied sensory stimuli and rhythmic movement can then be compared those observed in the sciatic nerve from similar paradigms and provide insight into the modalities of interfaced regenerated axons in a mixed nerve.

3.3 Materials and Methods

3.3.1 Dual Regenerative Multi-electrode Interface (d-REMI) Implants

In order to simultaneously interface the sural and the tibial nerve, we designed a dual REMI. The basic architecture, fabrication and electrical properties of FMA electrodes in dual REMI arrays were similar to those described in Chapter 2. Here, two polyurethane conduits (Micro-Renathane, Braintree Scientific Inc., Braintree, MA; OD 3 mm, ID 1.75 mm, length 5 mm) were glued together as shown as in Figure 3.2a. Custom made Floating Micro-electrode Arrays (FMA) with 16 recording electrodes, a ground electrode, and a reference were secured within each polyurethane conduit to have a total of thirty-two recording electrodes, and two ground and reference electrodes. The range of electrode heights was 0.5 to 0.8 mm to accommodate for the smaller diameters of the fascicles. Both FMAs were wired with a 5 cm long cable to a 40 contact Zero Insertion Force (ZIF) Printed Circuit Board (PCB) based connector (Plexon Inc., Dallas, TX) as in Figure 3.1b and c. The connector was housed within a custom made Acrylonitrile Butadiene Styrene (ABS) pedestal which was attached to a polypropylene mesh (Ethicon, USA) using medical grade epoxy (Loctite).

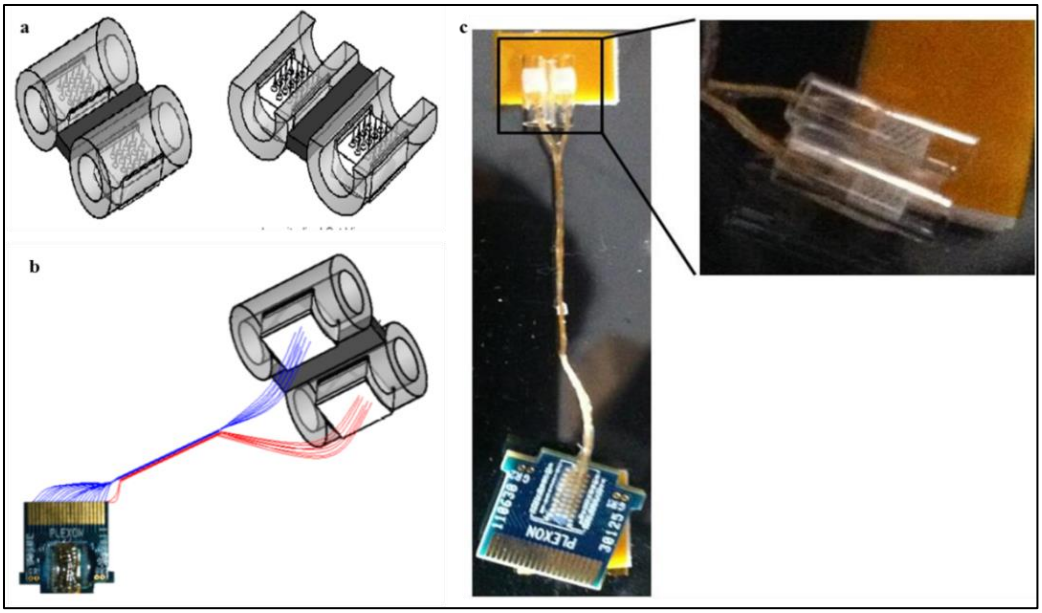

Figure 3.2 Dual Regenerative Multi-electrode Interface (REMI) for tibial and sural fascicles. Schematic of (a) dual REMIs in bottom (left) and longitudinal (right) view. (b) 40 contact ZIF board attached to dual REMIs. (c) Photograph with inset showing high magnified view of the dual REMIs

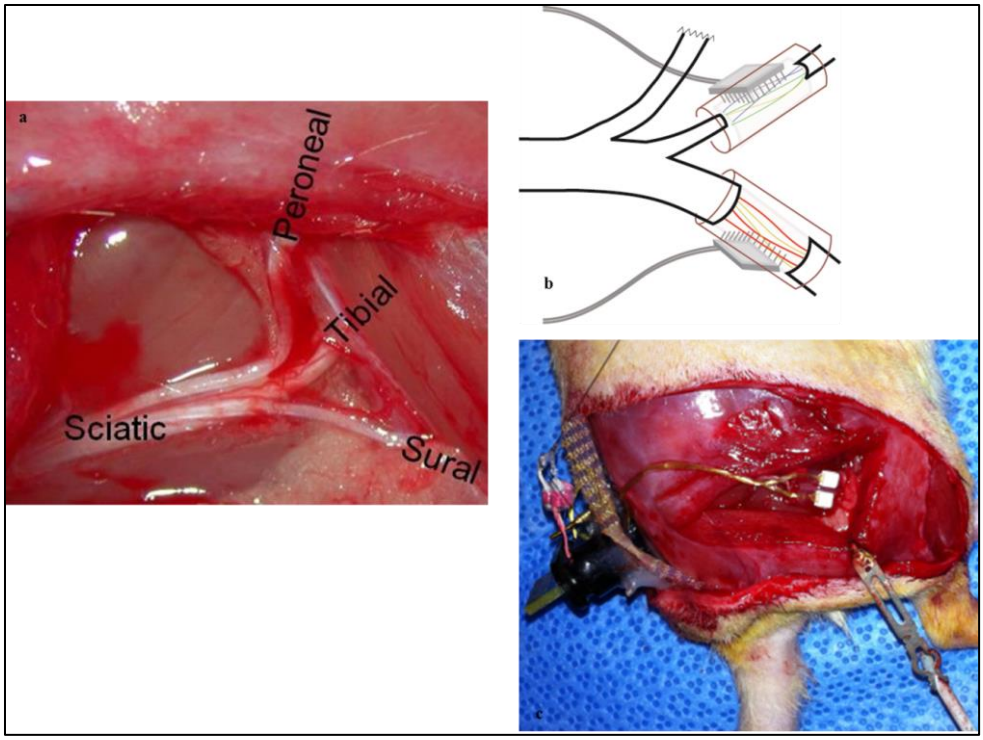

Figure 3.3 Photograph of exposed rat sciatic nerve and its peroneal, tibial, and sural fascicles (a). Schematic of dual REMI implants in tibial and sural fascicle (b). Photograph of implants with the pedestal-mesh assembly attached to pelvis (c).

3.3.2 Sural Regenerative Multi-electrode Interface (s-REMI) Implants

In addition to the d-REMI design, we modified our original REMI to provide a better fit with the sural nerve, as this fascicle is approximately 300µm in diameter. Sural REMIs consisted of a High Density (HD) FMA with sixteen recording electrodes of alternately varying heights from 0.6 to 0.7 mm height arranged in an 8-8 pattern on a 2.95 X 1.6mm ceramic base (Figure 3.4a). A 1 mm thick longitudinal window was cut along the 5 mm long polyurethane conduit (Micro-Renathane, Braintree Scientific Inc., Braintree, MA; OD 3 mm, ID 1.75 mm) and the HD-FMA was then secured within its lumen (Figure 3.4b). Using a 5 cm long cable, the array was then wired to a 18 channel connector (A8141-001, Omnetics, Minneapolis, MN) housed within a titanium pedestal which was attached to a polypropylene mesh (Ethicon, USA) using medical grade epoxy (Loctite).

3.3.3 Surgical Implantation

Five adult female Lewis rats (~220g) were implanted with dual REMI interfaces in the tibial and sural fascicles. The surgical preparation and post-operative care procedures were consistent with those described in Chapter 2. The sciatic nerve and its three terminal branches were exposed and dissected free for clear visualization (Figure 3.3a). The proximal and distal stumps of individual transected fascicles were inserted into the opposing ends of each REMI conduit and secured in place by suturing the epineurium to the conduit wall. The pedestal-mesh assembly was sutured to the pelvis musculature using 4-0 silk sutures (Ethicon, USA) (Figure 3.3b, c).

Three adult female Lewis rats (~220g) were implanted with the HD REMI in the sural fascicle while leaving the tibial and peroneal ramifications intact. Instead of transecting the sural fascicle, the epineurium was incised longitudinally and the nerve branch was manually inserted on the high density electrode array through the window made in the polyurethane conduit. (Figure 3.4 c, d). All procedures were performed in accordance with the guidelines of the Institutional Animal Care and Use Committee of the University of Texas Arlington.

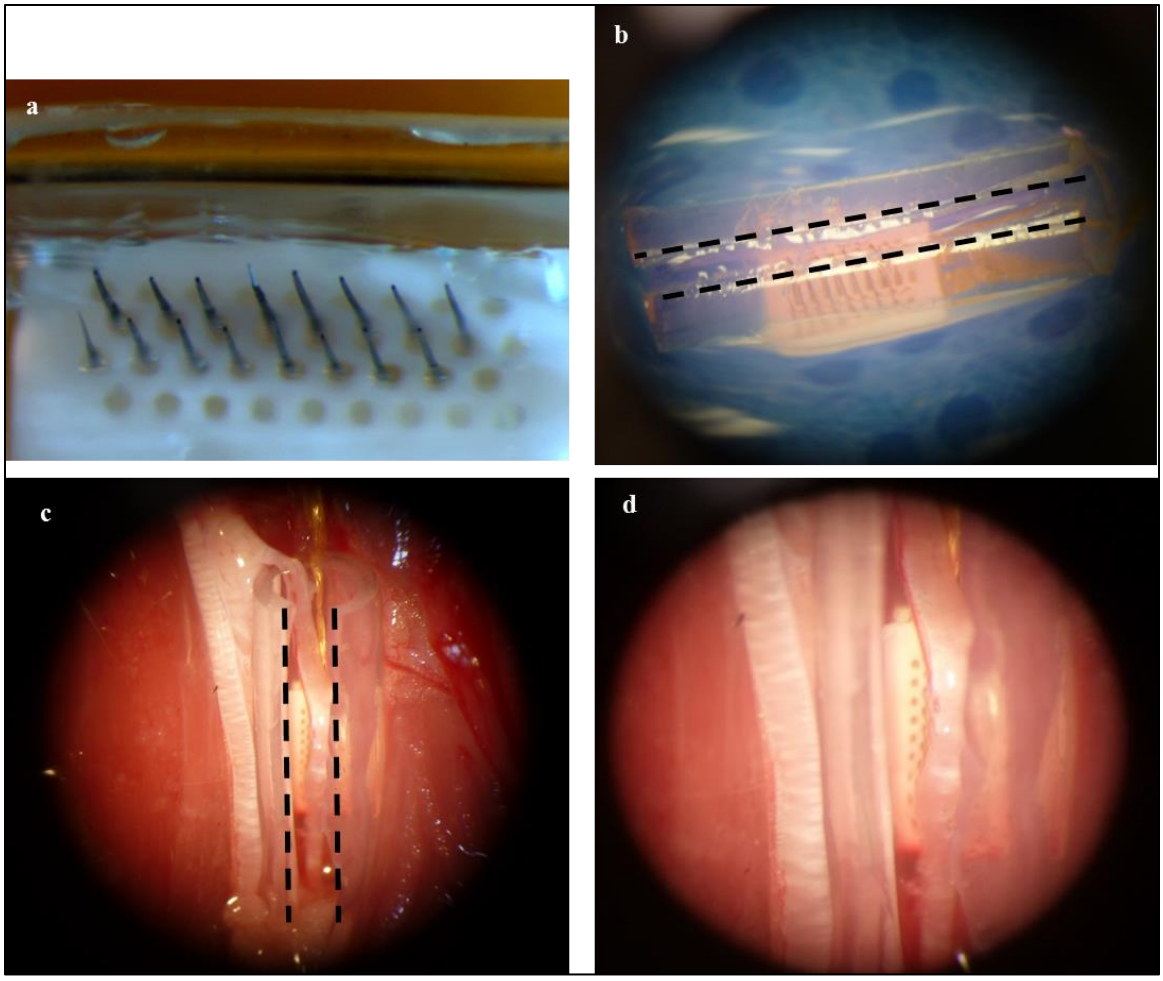

Figure 3.4 HD FMA REMI implant in the sural fascicle. Photographs of (a) High Density (HD) FMA with 18 electrodes, (b) HD-FMA secured within a 5mm long polyurethane conduit. Dotted lines indicate the 1mm thick longitudinal window, (c) Sural fascicle placed on top of HD FMA with magnified view in (d).

3.3.4 Electrophysiological Recording Paradigm and Analysis

Animals (n=5), intended for d-REMI implantation, were trained for bipedal treadmill locomotion on a robot assisted rodent treadmill (3cms^{-1}, 30 min/day) (Robomedica Inc., USA) for a month prior to surgical procedures. The overall neural signal acquisition technique, signal pre-

processing, and spike sorting techniques were similar to those described in Chapter 2. In addition, each recording session was videotaped (80 frames/sec) and synchronized with neural data using Cineplex Behavioral Research System (Plexon) as the animals performed bipedal locomotion. Heel strike and toe off events were marked manually after frame-by-frame offline inspection of the recorded video files using CinePlex Editor software (Plexon). These timestamps were then imported along with sorted Single Units into MATLAB and Neuroexplorer (Nex Technologies, Westford, MA) for further computation of Inter Spike Intervals (ISI), cross-correlograms and Peri-Stimulus Time Histograms (PSTHs). To evoke sensory signals from the s-REMI implanted hind limb, innocuous stimuli of gentle brushing on the dorso-lateral surface (Fig 3.10a) with a Q-tip, pinch using blunt forceps, deep pressure by calibrated hand held Von Frey stimulators and noxious thermal stimulation by application of ice pack and warm saline were employed [232]. Events marking the start and stop of stimulation were defined offline by visual inspection of the signal acquisition session.

Synchronized neural and behavioral video data were also acquired from a cohort implanted with REMI in the sciatic nerve (Chapter 2) at 3 weeks post- implantation. Animals were subjected to thermal and mechanical stimulation (n=11), and quadrupedal locomotion (n=10) on a 15” walkway (~ 4 steps). Thermal stimulation involved the heating of plantar surface of the foot with an infra-red beam (temperature 0-55°C) using Hargreaves Apparatus (Ugo Basile, Italy) until voluntarily paw withdrawal, indicative of experienced pain and discomfort. Mechanical stimulation included application of gradually increasing force (0.5g steps within 20s up to a maximum of 50g) with a 0.5mm diameter nylon filament using Von Frey aesthesiometer.

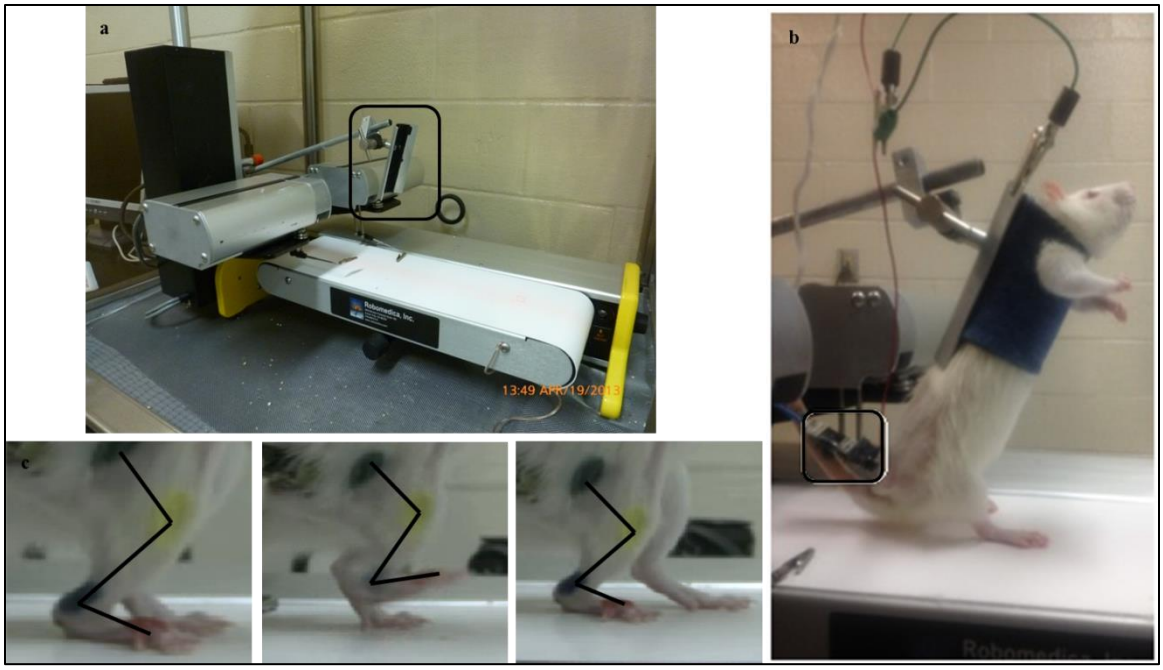

Figure 3.5 Bipedal locomotion recording paradigm. Photographs of (a) Robotic rodent treadmill, black box indicates body weight support structure. (b) Dual REMI implanted rat during a typical recording session, black box shows “headstage” and cable interfacing with data acquisition system. (c) Stance-swing-stance phases of a typical gait cycle.

3.4 Results

3.4.1 Dual REMI Interfacing of Tibial and Sural Fascicles

Electrophysiological signals were acquired weekly after 30 days of d-REMI implantation and 3 out of 5 interfaced animals successfully displayed SU activity from tibial fascicle while two failed from unidentified causes. One of the three successful implants suffered from high amplitude motion artifacts and hence was not suitable for recording of neural signals during locomotion. Electrodes implanted in the sural fascicle of all five animals failed to provide any neural activity, and upon explant examination, it was confirmed that the diameter of the regenerated sural nerve

was too small (100-250 µm) to be interfaced adequately with the electrodes (Figure 3.6). This motivated the redesign of the REMI and the use of HD-FMAs in subsequent experiments.

3.4.1.1 Electrophysiological signals from tibial fascicle

Using the d-REMI in tibial nerve, we observed single unit spikes with a bursting firing pattern, revealed by brief Inter Spike Interval (ISI) in the 30-70 milliseconds range, in two animals during bipedal locomotion at 37, 45, and 56 days post implantation (Figure 3.6). Each recording session typically consisted of 30 gait cycles with each cycle duration of 1.48 $\pm$ 0.65 seconds (mean $\pm$ SD). These bursting units were observed to occur synchronous to stepping, mostly during the swing phase defined as the period between the heel strike and toe off events (Figure 3.7). In one rat, a total of four SUs, with units additional to the bursts, were observed on the same and other electrodes. Specificity of these SUs to locomotion was confirmed by the silencing or change to a tonic firing pattern when the animal was standing with the treadmill turned off (Figure 3.8).

Figure 3.8c shows the presence of the specific bursting units on Ch1 and Ch2b, in addition to SUs with larger ISI (70-100 milliseconds) on Ch2a and Ch3, which were also synchronous with the rhythmic stepping during locomotion at 45 days post implantation. The larger ISI units had different activation timing and occurred in alternating phases with respect to each other. Cross-correlograms obtained between the binned (5ms bin width) spike trains each of the Ch2a and Ch3 units and the bursting Ch2b SUs (Figure 3.9) showed that the Ch2a unit occurred 17.5 ms after, while the Ch3 unit occurred 7.5ms prior, to the bursting unit which indicates that the spikes in these units carried information from distinct axons and were mutually exclusive with undetectable signal overlap.

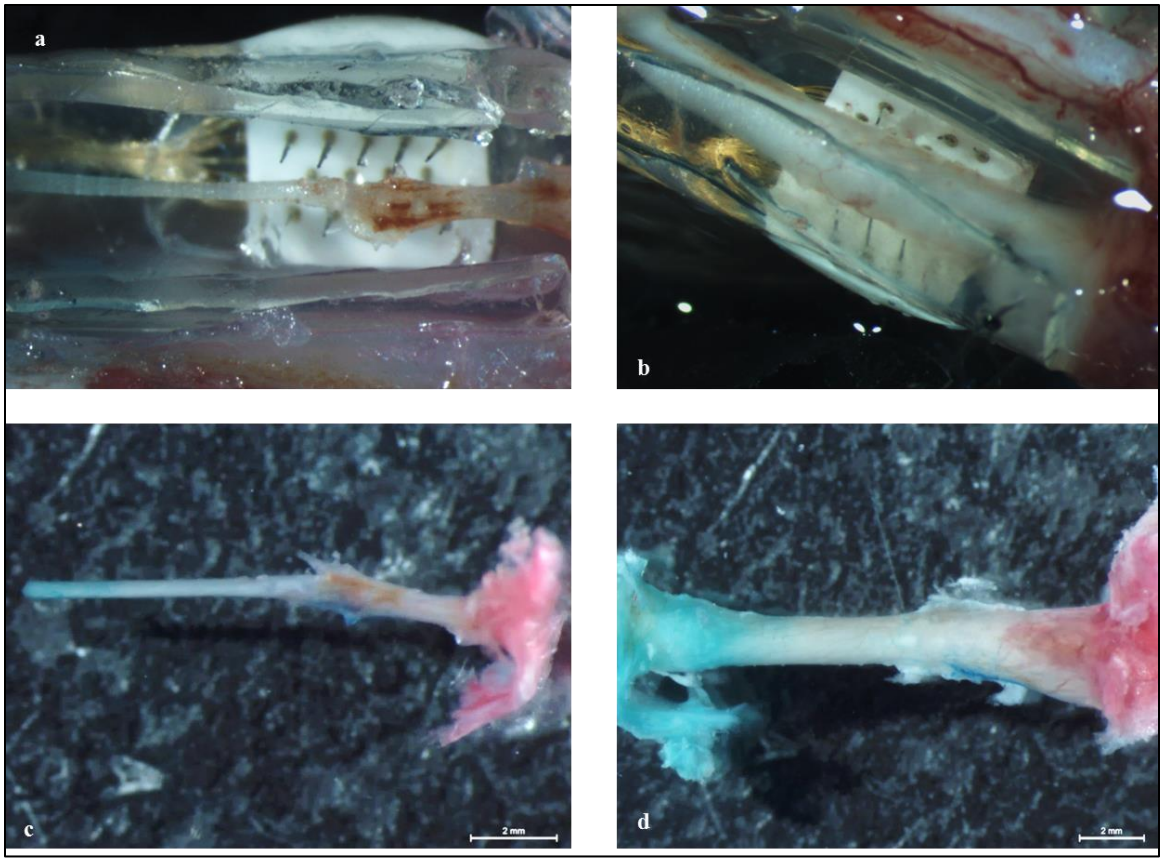

Figure 3.6 Dual REMI explant tissue examination. Photographs of regenerated sural and tibial fascicles (a,b) through the FMA electrodes and (c,d) dissected free from connective tissue after array removal; segments proximal and distal to the implanted conduit marked in blue and red colors, respectively. Scale bar = 2 mm.

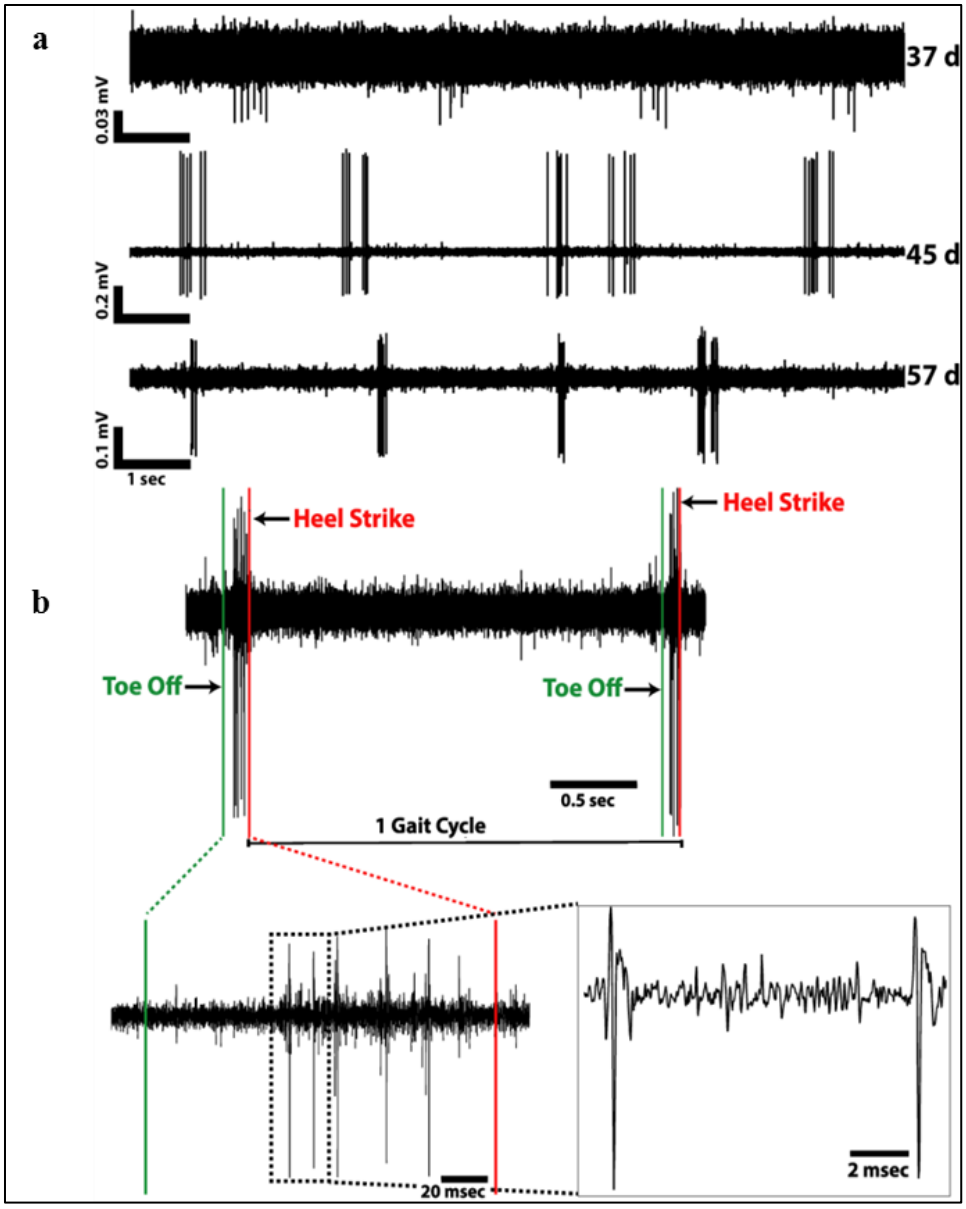

Figure 3.7 Tibial nerve activity during bipedal locomotion. (a) Bursting neural spikes observed during treadmill walking at 37, 45, and 57 days post implantation. (b) Neural activity during one representative gait cycle at 57 day with inset (left) showing time magnified view of signals from toe off (green) to heel strike (red) and individual action potential spikes within a burst (right).

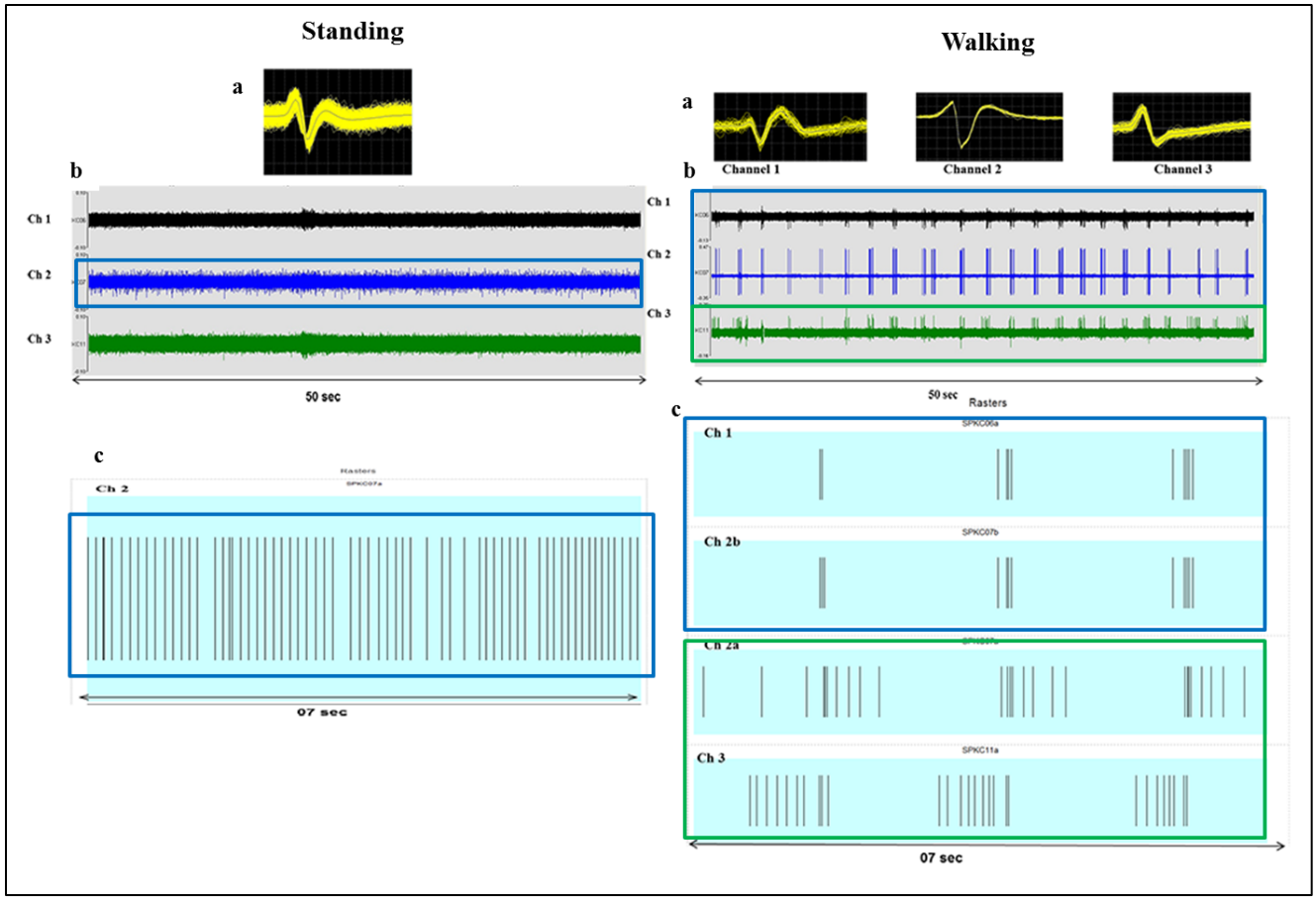

Figure 3.8 Differences in tibial neural activity during standing (left) and walking (right) on treadmill. Representative (a) spike sorted SU waveforms (b) Continuous time domain view of neural signals acquired on three different electrodes (c) Raster plots of SU recording electrode channels shows tonic firing pattern (blue box) during standing which changed to bursting units (right, blue box) in addition to other burst-like SU (green box) during walking.

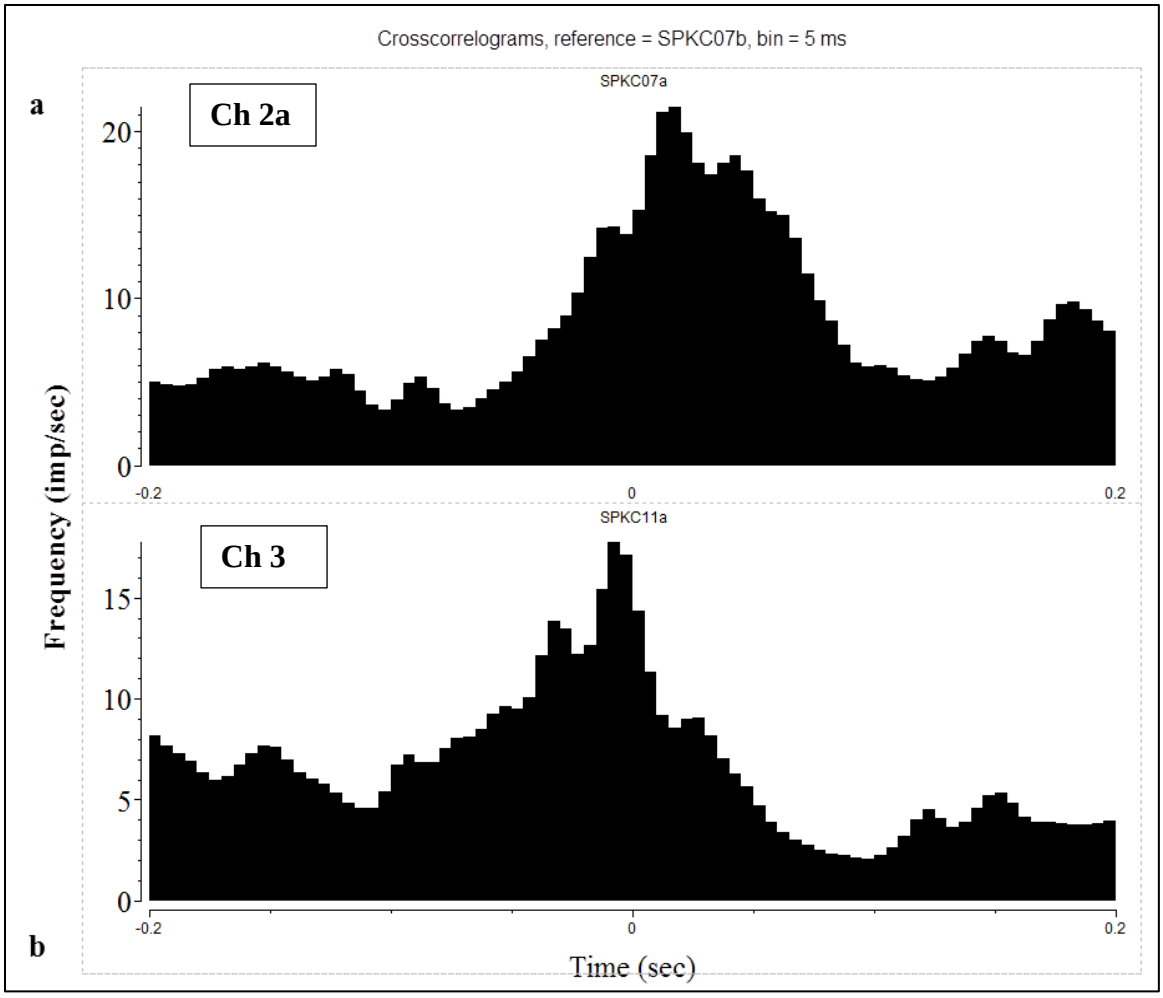

Figure 3.9 Cross-correlograms of larger burst-like SUs show peaks in (a) Ch2a with positive lag of 17.5ms (b) Ch3 with negative lag of 7.5ms with respect to bursting Ch2b unit.

3.4.2 HD-REMI Interfacing of the sural fascicle

The two animals interfaced with the HD-REMI in the sural fascicle were terminated early due to surgical complications. The remaining one implanted animal showed successful recordings with SU spikes on one electrode present consistently from day 13 to 61 days post implantation. The receptive properties of this unit were defined by subjecting the sural nerve innervated dermatome to various stimuli. While no responses were evoked to noxious thermal stimulation or deep pressure by Von Frey fibers, gentle brushing of the dorso-lateral surface Figure 3.10a

elicited SU spikes. Some of these recording sessions were videotaped and used to study offline the firing properties of the evoked single unit in correlation to the stimuli application. Figure 3.10b shows the representative spike raster plot at 31 and 54 days post implantation. This activity disappeared at 73 days post implantation indicating implant failure. Post-mortem examination of the entire REMI-connector assembly confirmed one of the fine gold wires in the cable linking the FMA to the percutaneous connector to be broken (Figure 3.11a,b).

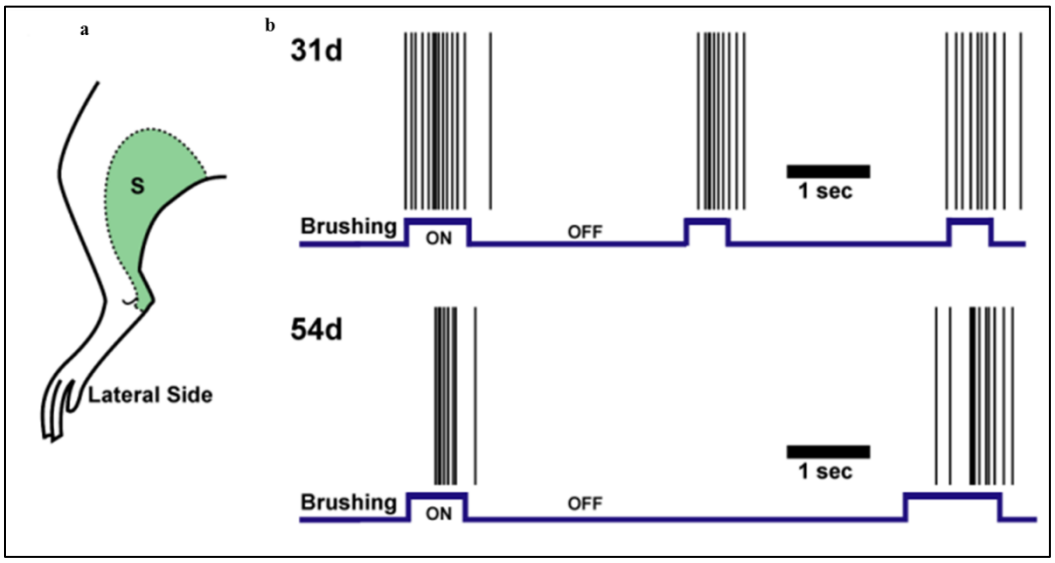

Figure 3.10 Sensory action potentials from sural fascicle. (a) Schematic showing the area (green) of hind limb subjected to brushing stimuli. (b) Representative raster plot of single unit spikes in response to brushing (blue) at day 31 (top row) and day 54 (bottom)

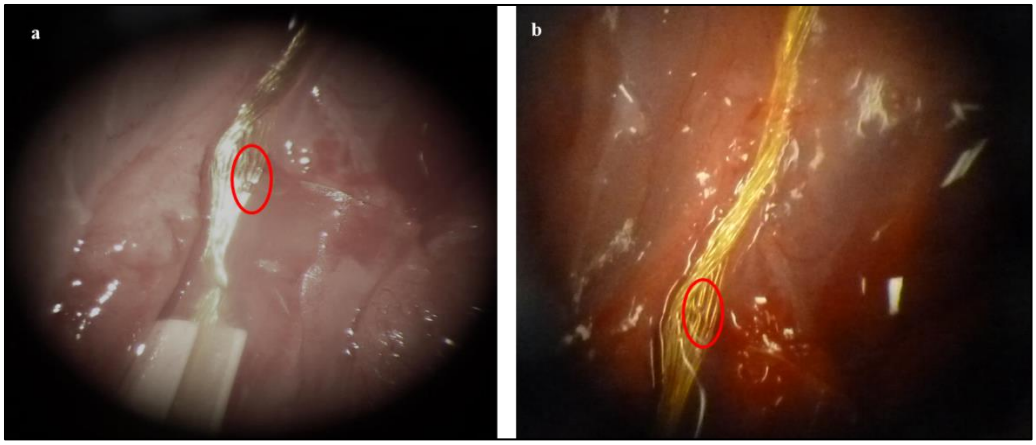

Figure 3.11 Representative photographs depicting wire breakage along the gold cable linking the FMA in REMI to percutaneous connector (a,b).

3.4.3 Signal Comparison between Sciatic Nerve and its Fascicles

At the observed time points (21, 28, 42 day), ten of the eleven animals (91%, 10/11) implanted with the REMI in the sciatic nerve did not display SUs in response to noxious thermal stimulation while five implants (45%, 5/11) responded to Von Frey mechanical stimulation, with increased activity in correlation with the paw withdrawal or paw licking behavior. The Peri-Stimulus Time Histogram in Figure3.12 shows a representative example where the single unit on one electrode continuously fired action potential spikes without any significant modulation by subjected stimulations, while the second electrode was activated only by mechanoception with increased firing rate during paw withdrawal behavior.

Three out of the ten animals subjected to quadrepedal locomotion with REMI implanted in sciatic nerve were not eligible for analysis of single units due to extensive motion artifacts during walking. Seven implants successfully displayed Single Units during quadrepedal locomotion of which five implants (5/7; 71%) exhibited bursting firing pattern similar to those observed in tibial fascicle during bipedal treadmill walking (Figure 3.13a).

One additional animal implanted with the REMI in the sciatic nerve was subjected, under adequate anesthesia, to consecutive gentle brushing of the dorso lateral surface of the foot (near the ankle) and the toes at 47 days post implantation. Evoked action potential spikes, recorded on one electrode, in response to innocuous brushing were sorted into two distinct Single Units. These SUs were determined to be differentially activated; where one unit responded to the ankle receptive field (Figure 3.14 a) and remained silent during toe stimulations. Conversely, the second unit was activated only during stimulation of toes and remained silent while the ankle area was brushed (Figure 3.14 b).

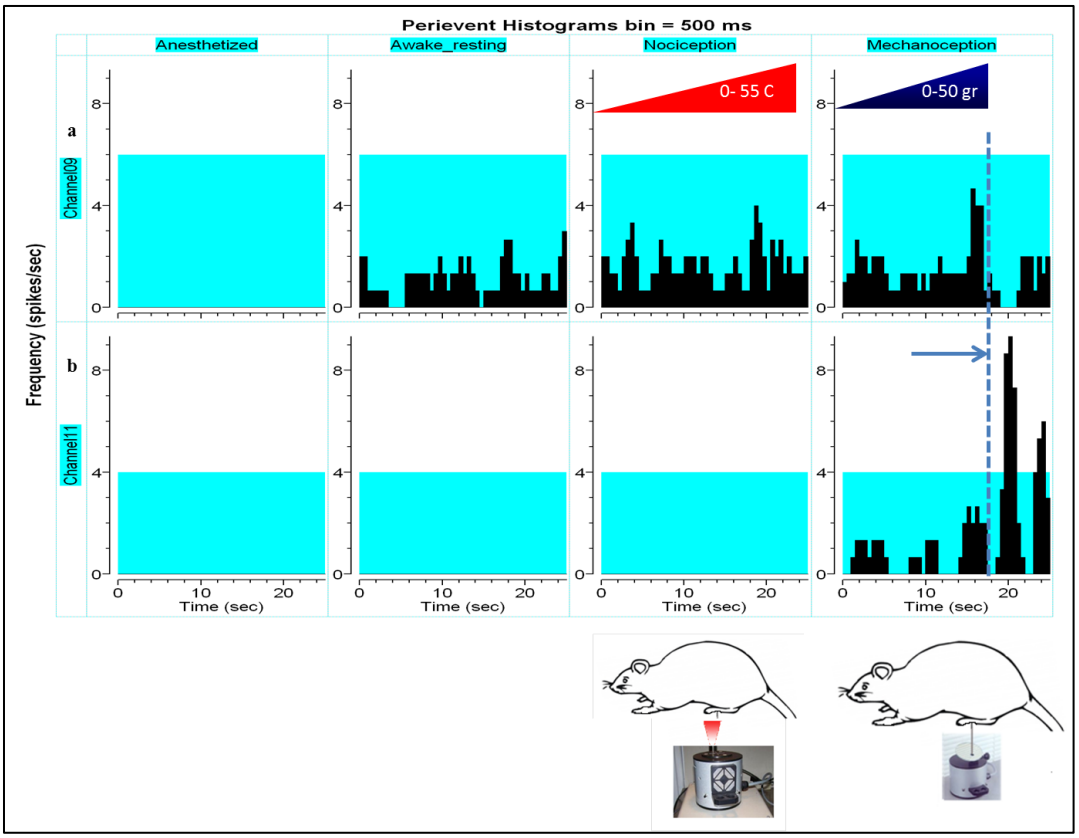

Figure 3.12 Peri-Stimulus Time Histograms (PSTH) of Single Unit (SU) spikes on two electrodes (top and bottom) of REMI when animal was (left to right) anesthetized, wake, thermally stimulated and mechanical stimulated. Blue dotted line indicates the time instant when paw and stimuli were withdrawn.

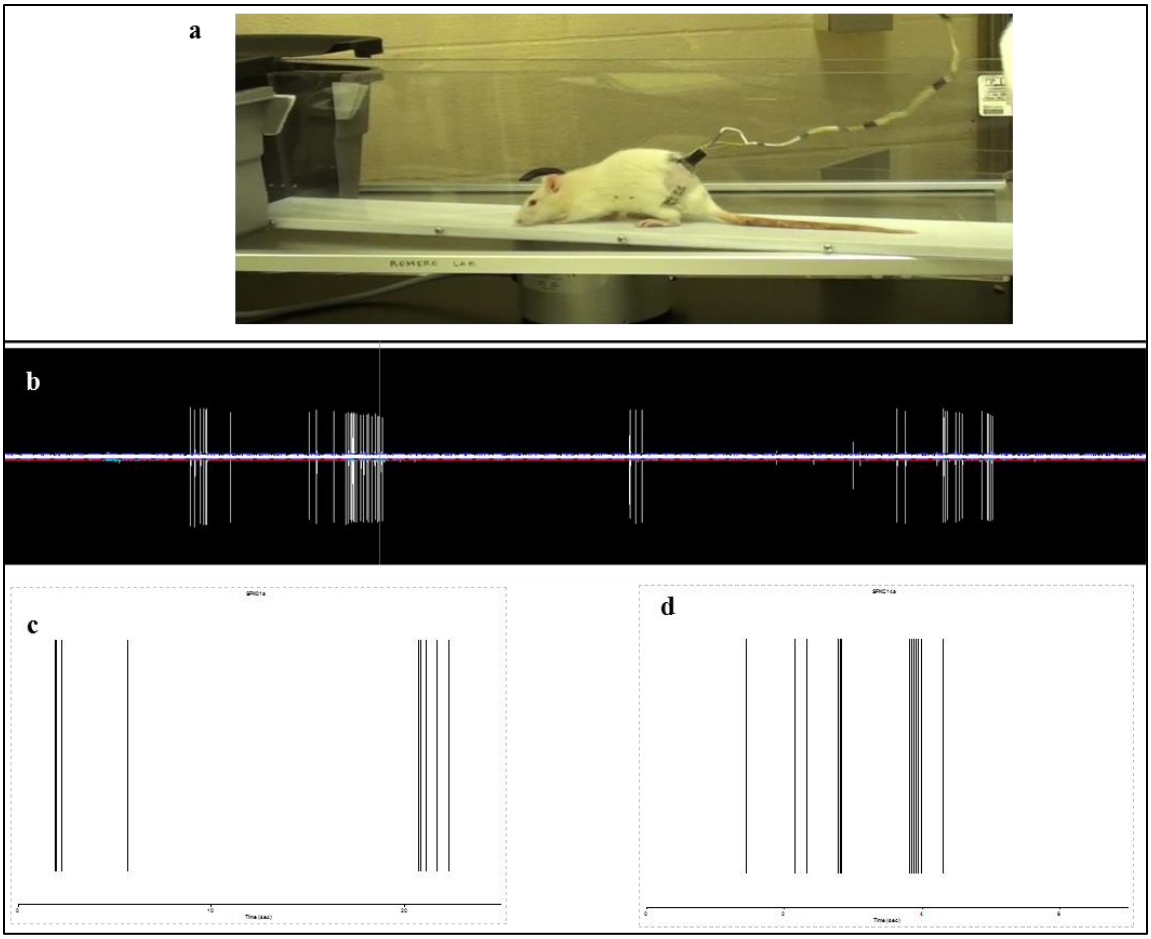

Figure 3.13 Neural activity from REMI in sciatic nerve during quadrepedal locomotion. (a) Photograph of walkway. Representative (b) time domain view of continuous signals acquired with action potentials of bursting firing pattern (c,d) Representative raster plot of bursts from two implanted animals.

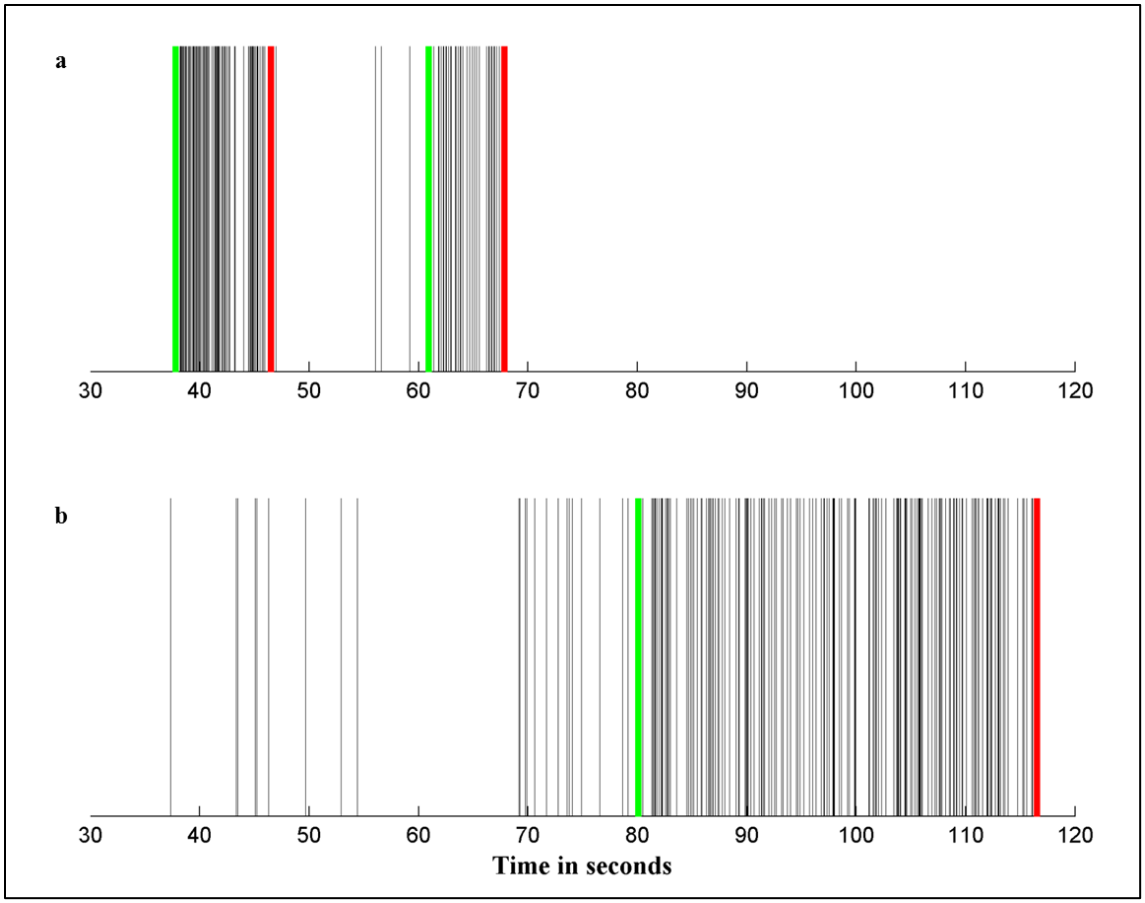

Figure 3.14 Evoked distinct sensory signals from REMI in sciatic nerve. Raster plots of (a) A Single Unit (SU) during brushing of ankle area and (b) Second SU during brushing of toes. Duration of stimulation is indicated by green (start) and red (end) vertical lines.

3.5 Discussion

3.5.1 Signal comparison between Sciatic-REMI and Tibial-REMI during locomotion

Regenerative Multi-electrode Interfacing of the tibial fascicle of rat sciatic nerve successfully recorded multiple Single Units (SUs) during bipedal treadmill locomotion. As seen in Figure 3.7c and 3.8, three out of the four SUs available at day 45 were distinct in terms of available information content and hence have the potential to provide independent control signals for one to two Degree Of Freedom movements.

Differences in firing pattern of action potential spikes, specifically tonic all through standing position that changed to phasic or bursting firing upon initiation of walking mode, were observed. Motor units in skeletal muscles are known to differ in their contractile properties which are determined by their usage. For example, motor units involved in rapid and rare movements are more prone to get quickly fatigued while those contributing to the maintenance of posture fatigue slowly and yet others exhibit a mix of both properties; also recognized as Fast Fatigue (FF), Slow Fatigue (S), and Fatigue Resistant (FR) type, respectively. These properties of motor units are the interplay between the parent motor neuron and the innervated muscle fiber types which are further categorized into Type I (Slow Oxidative), Type IIa (Fast Oxidative), and Type IIb (Fast Glycolytic FG). It is well established from other reported works that the soleus muscle in rats is constituted with the highest percentage of SO fibers [233] and electrical discharges from its corresponding motor units display a tonic firing pattern, i.e. action potentials with regular inter spike interval [234]. The gastrocnemius medialis and plantaris muscles are reported to have an approximately similar distribution of FO and FG fibers which can be extrapolated from other studies to have phasic discharges of motor unit electrical activity [233][234]. Based on these observations, the tonic activity from the tibial nerve during standing (baseline) position seems likely to have been acquired from axons innervating the soleus muscle, which is active for posture

maintenance in such behavior. Conversely, the SU spikes with phasic or bursting firing pattern were probably acquired from axons innervating the Gastrocnemius or Plantaris which are involved in plantar flexion function and activated mostly during stance phase. The possibility of the specific bursting SU to be derived from sensory axons of the tibial fascicle that innervate the glabrous skin in the plantar surface (central region) of the hind paw [219] can be rejected based on the evidence that these spikes were acquired predominantly in the swing phase when the plantar surface of the skin is not in continued contact with the treadmill. Thus, in this study, the likelihood of the SUs observed in tibial fascicle to have its source of origin or termination in muscle end-targets is high. These recorded signals could be a) efferent, i.e. from motor axons to contract the innervated muscle or b) afferent, i.e. from sensory axons with receptors in muscle spindles or Golgi Tendon Organs transmitting information about the position, velocity or tension generated in the innervated muscles. While proprioceptive signals were not distinguished from motor commands in this study, only motor signals can be expected in amputee preparations that lack distal target muscle organs. Similar to the signals acquired from tibial fascicle, 71% of animals implanted with REMI in sciatic nerves showed the characteristic burst type firing of spikes in some of the SUs recorded during quadrupedal locomotion (Figure 3.13).

3.5.2 Signal comparison between Sciatic-REMI and Sural-REMI

In contrast to the successful implantation of REMI in the tibial fascicle, interfacing of the sural fascicle in a regenerative paradigm failed due to the small size of this fascicle. This result underlies an important limitation in interfacing of small fascicles. However, fascicular sizes in human amputees are expected to be significantly larger, mitigating some of the concerns associated with this result. Importantly, using a modified insertion approach, sensory afferent activity evoked by tactile stimuli was recorded. This neural activity was observed in response to innocuous brushing along the dorso-lateral surface of the hind limb i.e. the receptive field of sural fascicle. Also, no SU activity was obtained in response to noxious thermal stimulation, pinching,

and deep pressure application suggesting that the electrode interfaced axons belonged to the Low Threshold Mechanoceptors (LTM) as opposed to the High Threshold Mechanoceptors that respond to harmful stimuli. Since these electrical discharges were observed to be sustained throughout the entire duration of tactile stimulation and silenced on stimulus withdrawal, it can be inferred to be of the Slowly Adapting (SA) type [235]. Such activity was also recorded from the sciatic nerve with two distinct Single Units from the cutaneous receptive fields of sural and tibial fascicles, respectively. The fact that these SUs were recorded in response to mechanical stimulation in anesthetized preparations confirms their purely sensory nature. Although, 90% animals with REMI in sciatic nerves did not show any evoked thermoceptive neural activity, moderate 45% animals showed SU activity evoked by Von Frey stimulation, with almost 100 % displaying an increase with paw withdrawal behavior, suggesting them to have mechanoceptive nature.

Thus, taking into account all the electrophysiological signals acquired, we confirmed the ability of the REMI to interface with pure sensory axons of the sciatic nerve and sural fascicle in the regenerative and insertion paradigm, respectively. Conversely, successful regenerative interfacing with the sensory and motor axons of sciatic nerve and tibial fascicle that innervate hind limb muscles involved in locomotion was also confirmed.

3.5.3 Sampling Bias of REMI recording from peripheral nerves

Majority of the REMI implants in cutaneous (sural) and mixed modality nerves (sciatic) failed to record evoked activity in response to noxious thermal stimulation in both anesthetized and wake conditions while 45% responded to mechanical stimuli. Pure sensory signals of cutaneous origin have Low Threshold Mechanoceptive receptors and are innervated by afferent A-beta axons which mostly have medium-to-large diameters of 4-12µm (refer Table3.1). Terminal free nerve endings in the skin that convey sensations of pain and temperature have high

thresholds of activation and are innervated by afferent axons with < 5µm diameter, belonging to the A-delta and C subtype. Thus these results indicate that the ability of REMI electrodes to record signals from medium-large diameter axons was higher than small diameter axons.

Majority of the tibial and sciatic implants (~70-100%) recorded single unit activity, with higher propensity for bursts, during locomotion behavior indicating their dominant role in motor control or proprioception. Muscle spindles or Golgi Tendon Organs (GTO) act as strain and force transducers conveying proprioceptive information (limb state and position) to the spinal cord and cortex, and are innervated by primarily A-alpha and A-beta afferent axons. Muscle efferent or motor axons, of A-alpha subtype with a diameter range of 10-20µm, transmit electrical commands (action potentials) from motor cortex or Central Pattern Generators (CPGs) in the spinal cord to extrafusal fibers in order to generate associated limb movement, upon induced muscle contraction. Thus, whether proprioceptive or motor in origin, the bursting SUs acquired from tibial and sciatic nerves are inferred to have been recorded from large diameter axons.

To summarize, findings of this chapter draw attention to the presence of a sampling bias in Regenerative Multi-electrode Interfacing of peripheral nerves towards axons of high caliber i.e. medium-to-large diameter axons involved in movement and mechanoception. This is explained by the power relationship between the circumference of the axons and the amplitude and conduction velocity of signals recorded from them, which has been established by computer modelling and experimental studies [236][237][238]. In fact, small caliber axons (A-delta and C) generate signals of extremely low amplitude evidenced by a consistent small peak in recordings of Compound Nerve Action Potentials across many species [239]. Furthermore, these interpretations of the observed sampling bias in REMI signals are in concurrence with extracellular micro-electrode recordings in cortical and spinal cord neurons that also favor action potentials from cell bodies with large diameters [240][241][232]. Researchers at the University of

Pittsburgh have also reported a similar bias toward recruitment of large diameter (A-alpha) proprioceptive afferents (muscle spindles and GTO) and medium diameter (A-beta) cutaneous afferents by micro-stimulation using electrode arrays in the Dorsal Root Ganglion (DRG) [242] [243][244]. From a neuro-prosthetic motor control perspective, such a sampling bias in the potential of REMI recording is rather beneficial, due to the higher affinity towards large-to-medium axons which mostly belong to the motor/proprioceptive and mechanoceptive sub-types, thereby making it easier to obtain movement-related information with limited contamination from small sensory and sympathetic axons.

Chapter 4

Identification of Functional Efferent Motor Activity in Regenerative Peripheral Nerve Interfaces

4.1 Abstract

Movement related efferent activity can either be motor commands from axons of ventral motor neurons or proprioceptive signals from muscle spindles and Golgi tendon organs. In this study, we discriminated between motor and proprioceptive efferent signals from the spiking activity of a mixed population of sensory and motor axons recorded by regenerative interfacing of tibial nerve which innervate ankle extensors. Electrophysiological signals synchronized with kinematic data were acquired during active bipedal treadmill locomotion at 4 and 5 weeks post REMI implantation into the tibial nerve and fine wire electrodes placed in the Gastrocnemius (GM) and Tibialis Anterior (TA) muscles. Offline Peri-Stimulus Time Histograms (PSTHs) and cross correlation analysis of the neural and EMG recordings revealed that SU activity with a characteristic bursting firing pattern occured during mid and terminal swing phases of the gait cycle, specifically 115 milliseconds after maximal TA contraction and 100-200 milliseconds before heel strike or onset of GM activation. Characteristics of such SU bursts were not altered by Botulinum Toxin-A (BTX) induced GM muscle paralysis eliminating the possibility of signals to be associated with proprioceptive feedback during active movement which was further confirmed by the lack of evoked afferent activity by passive dorsi and plantar flexion. The mean frequency range of these bursting units (15-20Hz) is consistent with the reported firing frequency of motor axons and a significant stable correlation with signals from ankle flexor muscle validates its physiological function in the studied locomotion behavior.

4.2 Background

Peripheral neural interfaces require identification of motor efferent activity from which intent of limb movement can be decoded to generate command signals that can be translated to desired movements of the prosthetic hand. To accomplish this task, acquiring high quality signals from functionally distinct motor axons is imperative. The feasibility of recording some motor information from nerve stumps of residual nerves by Longitudinal Intra fascicular Electrodes (LIFE) to perform few grasping movements in robotic hands has been demonstrated [116]. However, these early studies report the difficulty of identifying pure motor signals due to the interferences from large amplitude activity of adjacent muscles and employ complex signal processing techniques to uncover the neural activity. In addition, the firing rates or the number of electrical impulses discharged per second by activated motor axons is low in the range of 5 – 40 Hz compared to that of sensory axons which, depending on the stimulus intensity, can reach 100-300 Hz [245]. Thus, the possibility of detecting multiple discrete motor signals from peripheral nerves is very low. Furthermore, specific interfacing of motor axons is intrinsically difficult in most peripheral nerves as they are present in a very small proportion compared to the entire axon population. In the rat sciatic nerve only 6% of the approximately 27000 axons at the trochanter level are myelinated alpha motor axons; the rest are myelinated (23%) and unmyelinated (48%) afferent axons, and 23% unmyelinated sympathetic axons [246]. This limitation is further exacerbated by the reported 50% decline in number of motor neurons after chronic peripheral nerve axotomy [189][247][248]. Thus, the availability of motor axons seems to be limited for interfacing with the REMI; hence this study was designed to test whether pure motor signals can be effectively recorded. In Chapter 3, we described the acquisition of efferent SU spikes with a distinct bursting firing pattern from REMI interfacing of the rat tibial nerve. The primary objective of this study is to determine whether these bursting units, obtained during bipedal locomotion, belong to motor or sensory modalities. We reasoned that motor signals could be eliminated by

passive limb stretching whereas pharmacological denervation by Botox of distal target muscles would restrict proprioceptive activation leaving the motor activity unchanged. In addition, the extent and stability of correlation with distal muscle activity was evaluated to ascertain the potential functional use of the recorded bursting SU spikes.

4.3 Materials and Methods

4.3.1 Pedestal Fabrication

In order to simultaneously record from hind limb muscles and the nerve we designed a new pedestal using AutoCAD (Autodesk Inc, USA) to house and 18 channel neural connector and 6 channel EMG connector (A8141-001 and A79109-001, Omnetics, Minneapolis, MN) (Figure 4.1a). Custom made Acrylonitrile Butadiene Styrene (ABS) pedestals were Computer Numerical Control (CNC) machine manufactured by ProtoLabs (Maple Plain, MN) (Figure 4.1b). The connectors were secured in the fabricated pedestal with medical grade epoxy (Loctite).

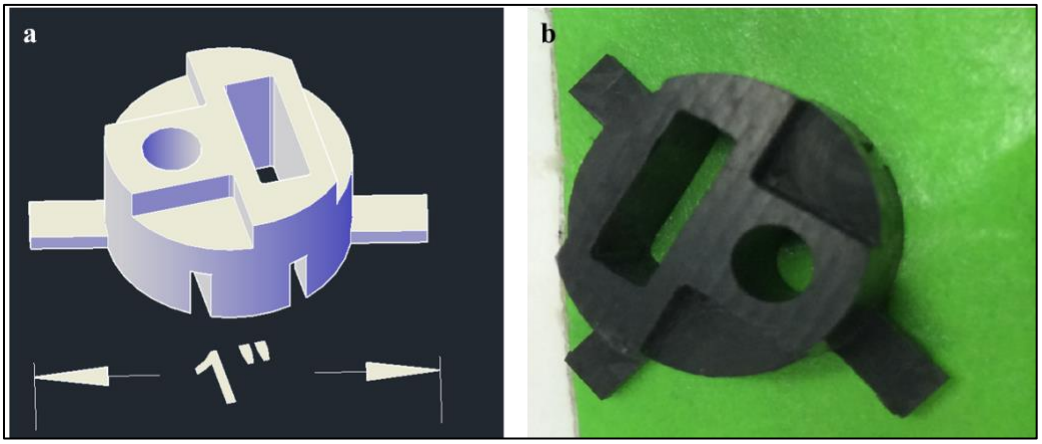

Figure 4.1 Pedestal for neural and EMG connectors (a) 3D model in Auto Cad (b) CNC machined ABS pedestal

4.3.2 Regenerative Multi-electrode Interface (REMI) and Electromyogram (EMG) Implants

The basic architecture, fabrication and electrical properties of FMA electrodes in the REMIs were similar to those described in Chapter 2. In order to accommodate for the comparatively smaller diameter of the tibial fascicle than the whole sciatic nerve, custom made High Density (HD) FMAs with eighteen Pt electrodes of alternating heights from 0.5 to 0.8 mm and arranged in a 5-4-5-4 pattern with an inter-electrode spacing of 250 µm on a 1.95 mm X 1.6 mm ceramic base were used. The REMI was wired to an 18 channel Omnetics connector with a 6 cm long cable. Five teflon coated stainless steel wires (AS 631/632, Cooner Wire, Chatsworth, CA) served as two pairs of electromyogram (EMG) electrodes and an additional ground wire. Individual wires were crimped to interconnect pins (32 AWG, Harwin Plc, England) and then soldered to the pins of the Omnetics connector. An amphenol pin connected to the additional ground wire was held in a polypropylene mesh (Ethicon, USA) which in turn was attached to the pedestal using medical grade epoxy (Loctite).

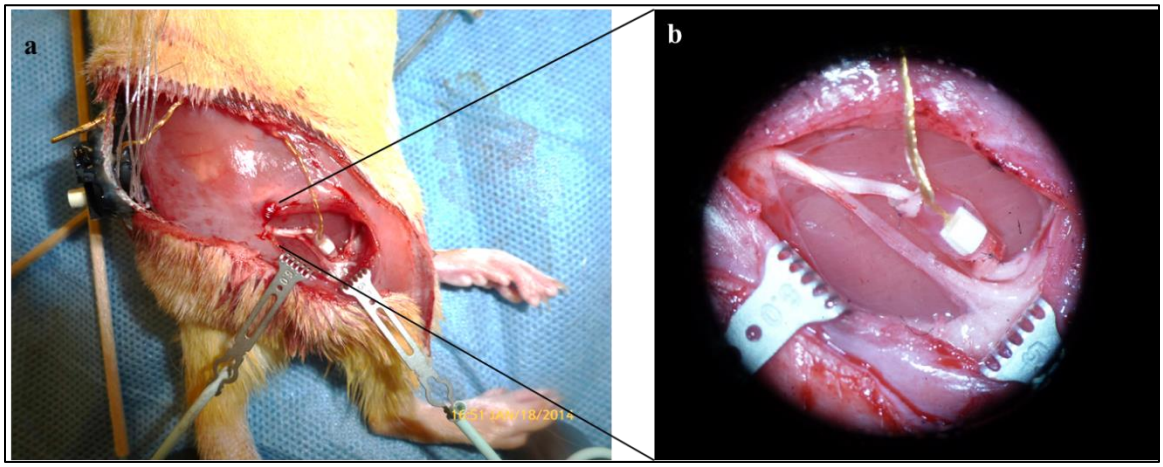

Figure 4.2 Surgical Implantation of REMI in tibial fascicle. (a) Representative photograph of implanted pedestal and REMI implanted tibial fascicle with (b) inset showing a magnified view.

4.3.3 Surgical Implantation

Four adult female Lewis rats (~220g) were implanted with the REMI interface in the tibial fascicles with overall procedures consistent as described in Chapters 2 and 3, except that only tibial fascicle was transected for REMI implantation leaving other fascicles intact. Additionally, all animals were implanted with bipolar EMG electrodes in the Gastrocnemius Medialis (GM) and Tibialis Anterior (TA) muscles. Implantation of intramuscular electrodes were adapted from procedures described in [249] and [250]. Specifically, a pair of stainless steel wires was tied together in a knot and at ~3-5 mm distance from the knot ~ 1mm of insulation was removed from individual wires. These wires were routed through two 21G needles that were crimped into a hook shape and inserted into the muscle belly with an inter electrode spacing of ~1-3mm. Needles were retracted from the muscle after implantation of wires which were tied in knots at the distal end and further attached to the underlying fascia using 4-0 silk sutures (Ethicon, USA). Individual muscles were stimulated via the implanted wire electrodes using an isolated pulse stimulator (A-M systems#2100, Sequim, WA) until a visible dorsi and plantar flexion was elicited which verified correct placement of electrodes in the TA and GM muscles, respectively. The ground wires were placed subcutaneously in the pelvis region after removing 1-2 cm of insulation. The pedestal-mesh assembly was secured to the pelvis musculature using 4-0 silk sutures (Ethicon, USA). All procedures were performed in accordance with the guidelines of the Institutional Animal Care and Use Committee of the University of Texas Arlington.

4.3.4 Synchronized Electroneurogram (ENG) and Electromyogram (EMG) Acquisition

Before surgical implantation of EMG and ENG interfaces, four animals were trained for bipedal walking (3cms-1, 30 min/day, and 30 days) using a robotic rodent treadmill (Robomedica Inc., USA). Neural recording procedures and involved amplifier specifications were consistent with those described in Chapter 2 with the additional incorporation of Common Average

Referencing (CAR) during data acquisition (Plexon) to digitally subtract and reduce common noise on all channels (e.g. EMG, motion artifacts). EMG signals were collected using a custom made probe and a differential amplifier in a bandwidth of 1-1000 Hz and 1000X gain (Model 1700, A-M systems, Sequim, WA). Synchronized ENG, EMG and kinematic signals were recorded using Omniplex and Cineplex data acquisition systems during locomotion from the third to sixth week post implantation. Heel strike and toe off events were marked manually offline after frame by frame inspection of the recorded video files using Cine Plex Editor Software (Plexon).

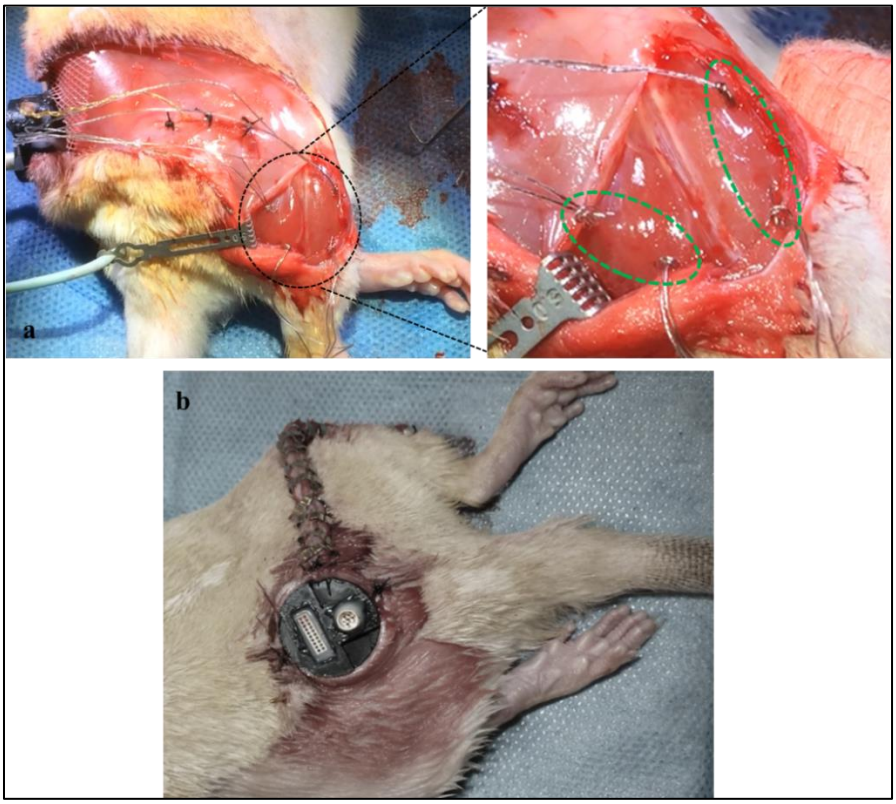

Figure 4.3 Surgical Implantation of fine wire (EMG) electrodes in Medial Gastrocnemius (left) and Tibialis Anterior (right) with magnified view in inset, green dotted circle outlines the insertion of wires in the muscle belly (a) Representative photograph of neural and EMG connector-pedestal assembly secured to the pelvis musculature (b).

4.3.5 Passive Stretching

Under adequate anesthesia (2% isoflurane), animals were subjected to passive dorsi and plantar flexion of the electrode implanted hind limb foot using a custom-built device [251] in which manually operated stepper motor controlled linear actuators (Zaber Technologies, Canada) propel a clamp along two stationary rails. Cycles of plantar flexion and dorsi flexion of the foot were employed to passively activate the muscle spindles afferent axons in the involved Gastrocnemius Medialis (GM) and Tibialis Anterior (TA) and its synergists respectively. Synchronized video, neural and EMG signals were acquired during passive stretching of the hind limb foot along the ankle joint.

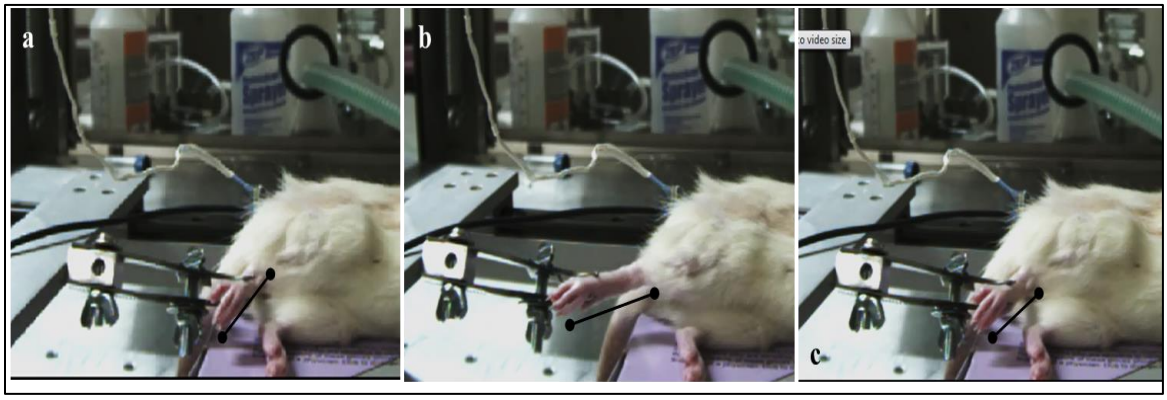

Figure 4.4 Photographs depicting a typical recording session during (a) baseline position (b) passive plantar flexion (c) return to baseline position

4.3.6 Botulinum Toxin-A Injection

One animal was injected with Botulinum Toxin-A (BOTOX, Allergan Inc., Irvine, CA) forty days after surgical implantation of EMG and neural electrodes to induce a neuro-muscular block. After adequate anesthesia, the hind limbs were shaved and sterilized using 70% ethanol and Povidine solution. Similar to techniques and dosage described in [252], the Gastrocnemius

Medialis was injected intramuscularly with 5 units of reconstituted BOTOX in 0.1 mL saline using 28G insulin needles.

4.3.7 Terminal Compound Muscle Action Potential (CMAP)

Compound Muscle Action Potentials (CMAPs) were measured from the GM and TA muscles before sacrificing the animals, using the data acquisition system described in Section 4.3.4. Under adequate anesthesia, the sciatic nerve was exposed proximal to the site of REMI implantation in the tibial fascicle. After dissecting free from connective tissue and underlying fascia, the sciatic nerve was placed on a bipolar hook electrode (FHC, Bowdoin, ME), with paraffin film underneath and isolated in mineral oil bath. The nerve was then stimulated with biphasic pulses of 20 µs pulse width and 2Hz frequency (isolated pulse stimulator, A-M systems#2100). The minimum voltage required to elicit a visible twitch in the distal muscles was defined as the threshold level and CMAPs were acquired in response to twice the threshold level stimulation. The recorded signals were then exported to MATLAB for further processing and extraction of CMAPs. Briefly, signals were filtered at 10 Hz (4 pole Low cut Butterworth) to remove baseline wandering and other low frequency components. Waveforms were extracted in windows of 65ms (50 ms post and 15 ms prior to stimulus), overlapped and averaged to form a composite waveform of CMAP.

4.3.8 Offline Signal Processing

Signal pre-processing, spike extraction and sorting procedures are described in Chapter 2. After detection of Single Unit (SU) spikes, the individual time stamps along with wide band EMG and ENG data were exported to MATLAB. Procedures to obtain EMG envelop and firing rate estimate were adapted from [34] and [253][77], respectively.

4.3.8.1 EMG Envelope Detection

EMG signals were down sampled by a factor of 10 and digitally filtered offline in a 10-800 Hz bandwidth using a combination of low and high cut 4 pole Butterworth filters, followed by signal rectification using “abs” function in MATLAB. High amplitude motion artifacts were removed by a visually determined threshold and resulting signals were then low pass filtered at 5Hz to yield an EMG envelope (Figure 4.6).

4.3.8.2 Estimation of SU spike Firing Rate

The overall procedure used to obtain a continuous firing rate estimate is depicted in Figure 4.5. First, a spike train variable was created in a binary fashion with spike occurrences defined as “ones” and non-occurrences as “zeroes” in a collection of time stamps from the entire recording duration (Figure 4.5a). A Gaussian window of 200ms (Figure 4.5b) was then convolved with the spike train to yield a continuous instantaneous firing rate estimate signal (Figure 4.5c).This signal was low pass filtered (5Hz) and further down sampled to 4 KHz to match the EMG signal.

Cross correlation between the EMG envelope and spike firing rate estimate signals was computed using “xcorr” MATLAB function. Peri Stimulus Time Histograms, representing firing rates averaged over multiple trials, were constructed using an available neural analysis tool box (MLIB, Maik Stüttgen). Briefly, neural signals in 3000ms time segments were aligned with the onset of heel strike events (1500ms pre and post) that repeated N+1 times during N gait cycles (period between one Heel Strike to a consecutive Heel Strike (HS) event) in a recording session. The observation time segments were further divided in equal bins (50ms each), the number of spikes in each bin counted and represented as a histogram of spikes relative to the Heel Strike trigger event.

Bursts were detected automatically by a commonly used Poisson-surprise method [254] based built-in algorithms available in NeuroExplorer (Nex Technologies, Westford, MA) software package along with computations of average number and firing frequency of spikes within burst. Inter Spike Interval Histograms (ISIH) and auto-correlograms of single unit spike trains were also computed to determine the characteristic profiles of bursting single units. ISIH were constructed by a logarithmic transformation of the Inter Spike Intervals segmented into equally sized bins (each 0.001s) within a range of 0.0001 to 100 seconds where the right hand side of the "ith" bin within a decade interval is defined according to [255] as below:

$ISI_i = ISI_{ds} \times 10^{i/D}$ where ds = start of decade interval and D=10 bins per decade.

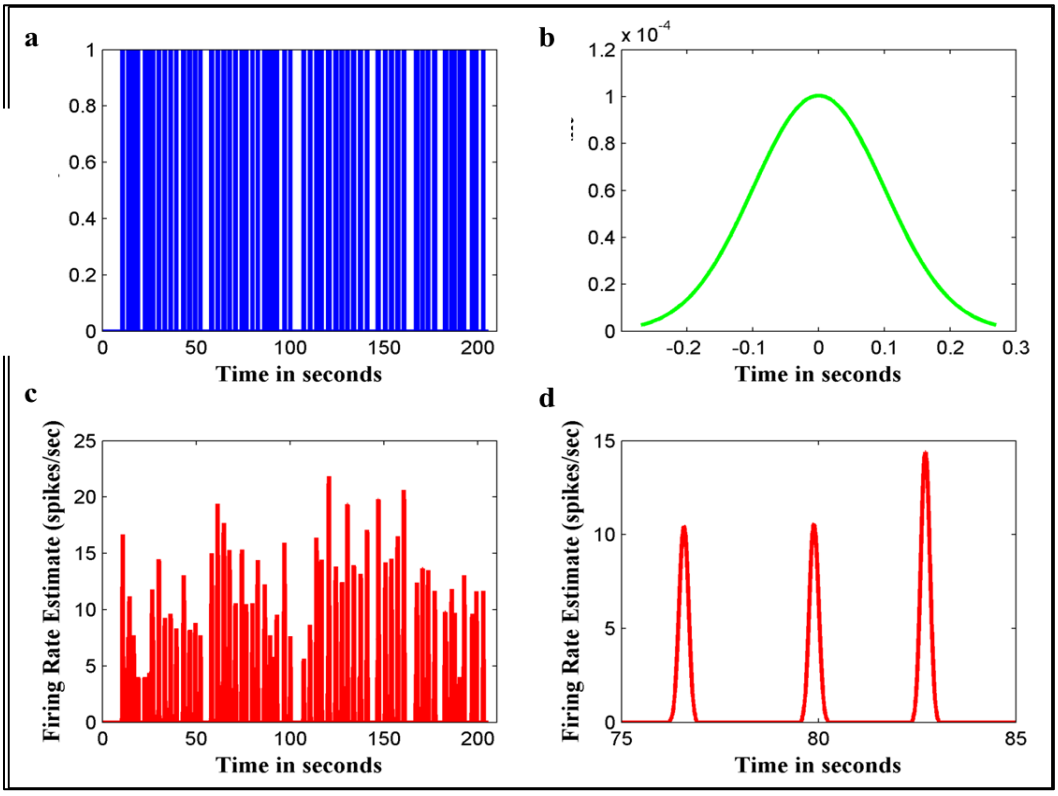

Figure 4.5 Steps involved in computation of firing rate estimate (a) Spike train generation (b) Gaussian window of 200 ms (c) Firing rate estimated by convolution of (a) and (b) with a time domain zoomed view of 10 sec (d)

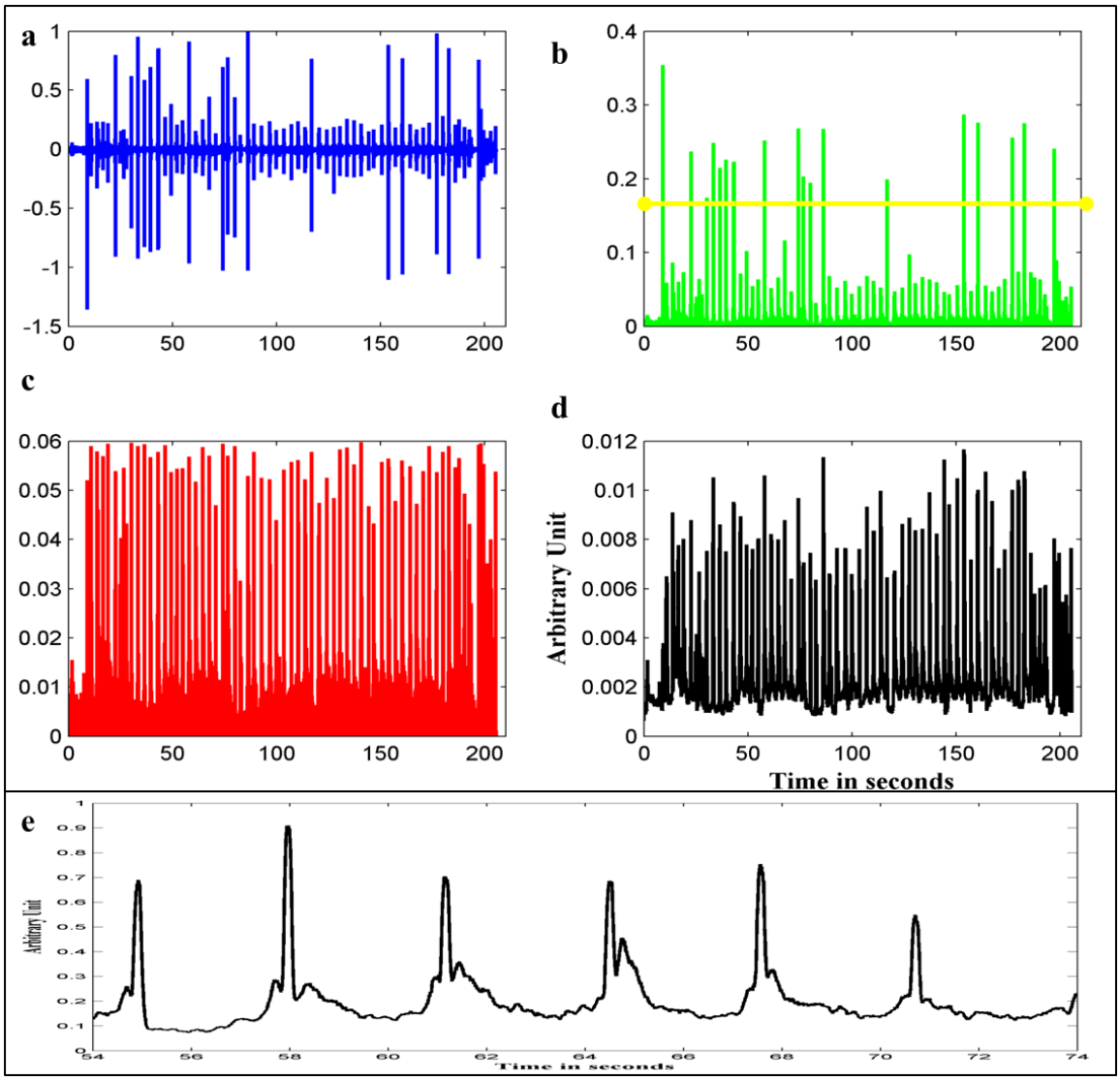

Figure 4.6 Steps involved in computation of EMG envelope (a) Representative EMG signals acquired in a 200s session (b) Rectified signals and yellow line indicates artifact threshold level (c) Rectified signals after artifact removal (d) Low pass filtered EMG envelope with time domain zoomed view in (e).

4.4 Results

Three out of four animals implanted with REMI in tibial fascicle of sciatic nerve recorded SU spikes starting 2 weeks post implantation. However, in two of these animals, the amphenol pin connected to a ground wire detached from the pelvis resulting in increased noise contamination from movement generated artifacts. These animals were excluded from further analysis due to compromised quality of recorded signals. Thus, one animal was successfully tested for neural and EMG signals during locomotion and passive stretching from 3 to 6 weeks of implantation. Two channels denoted as Ch09 and Ch10 yielded SU spikes starting 3 weeks and remained consistent until 45 days post implantation. These SUs were observed displayed the characteristic bursting firing pattern during recording sessions of bipedal treadmill locomotion from 35 to 45 days post implantation.

4.4.1 Characterization of electrophysiological signals during bipedal locomotion

Single Unit neural spikes and electromyographic signals from Gastrocnemius Medialis (GM) and Tibialis Anterior (TA) were acquired during bipedal treadmill locomotion in synchrony with video captured data. A typical recording session consisted of at least 30 gait cycles with each cycle duration of 3.5 $\pm$ 1.12 seconds (mean $\pm$ standard deviation) and divided into stance phase (period between one Heel Strike (HS) to Heel Off (HO) event) of 2.8 + 1.1 seconds (mean $\pm$ standard deviation) and swing phase (period between HO to HS) averaging 374 $\pm$ 145 milliseconds (mean $\pm$ standard deviation). Figure 4.7 shows representative signals from the tibial fascicle and GM and TA muscles in one gait cycle at 40 days post implantation. Visualization of EMG signals confirmed the alternating activation of TA and GM muscles in the swing and stance phase respectively. Signals from TA muscle were stronger than GM, as evident by strong bursts in TA EMG signal during swing phase compared to tonic firing of GM during stance (Figure 4.7 c,d). This result is indicative of the incomplete re-innervation of the denervated GM muscle by 40

days of regeneration as opposed to the TA muscle with intact peroneal fascicle innervation. Ch09 and Ch10 displayed identical bursts with an average of 5.5 ± 1.65 spikes/second and firing frequency of 15.85 ± 4.91 Hz (mean ± standard deviation).

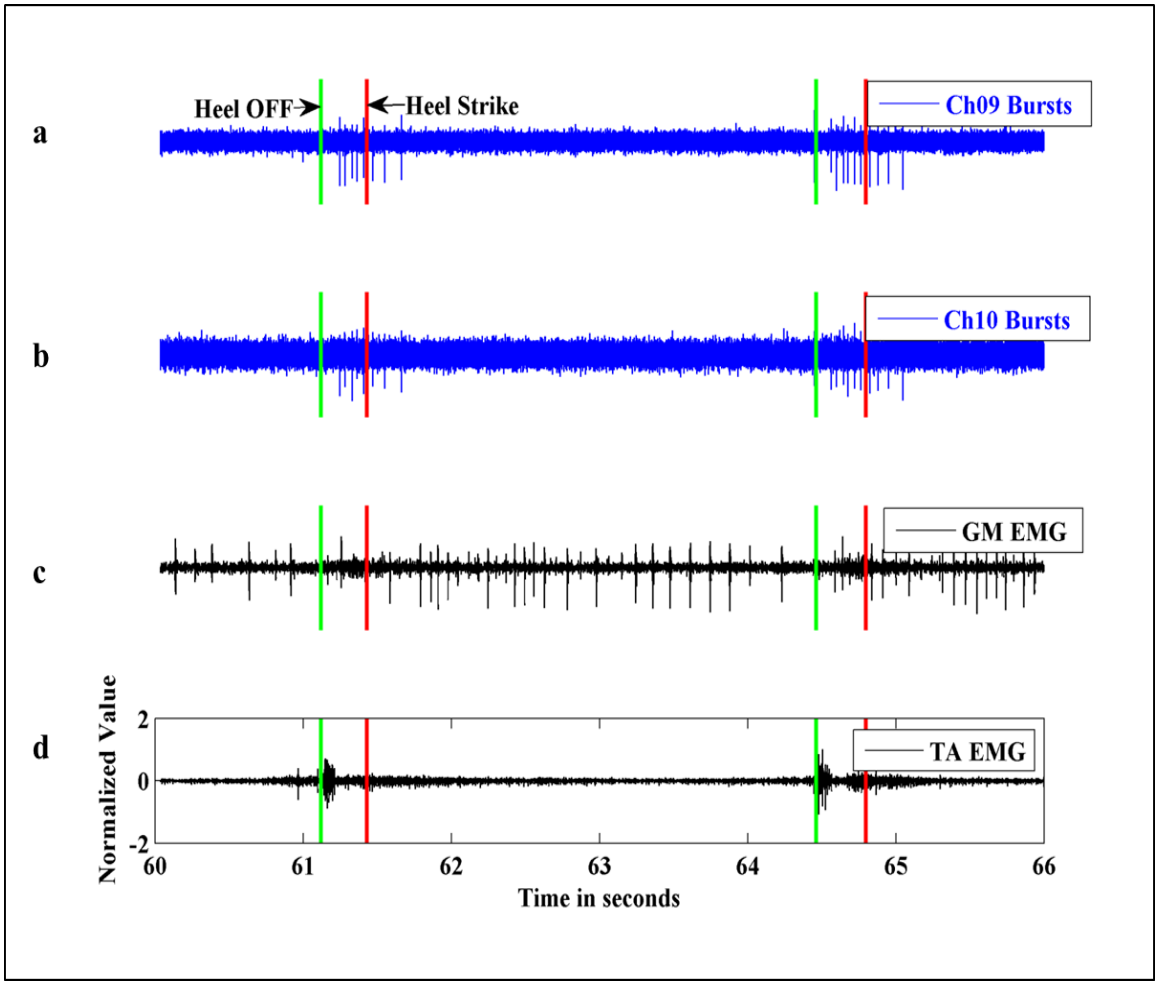

Figure 4.7 Representative signals from tibial fascicle (a,b) and GM and TA muscles (c,d) in one gait cycle at 40 days post implantation. Red and Green lines indicate time stamps of Heel Strike and Heel Off events. X and Y axis consistent through plots (a,d).

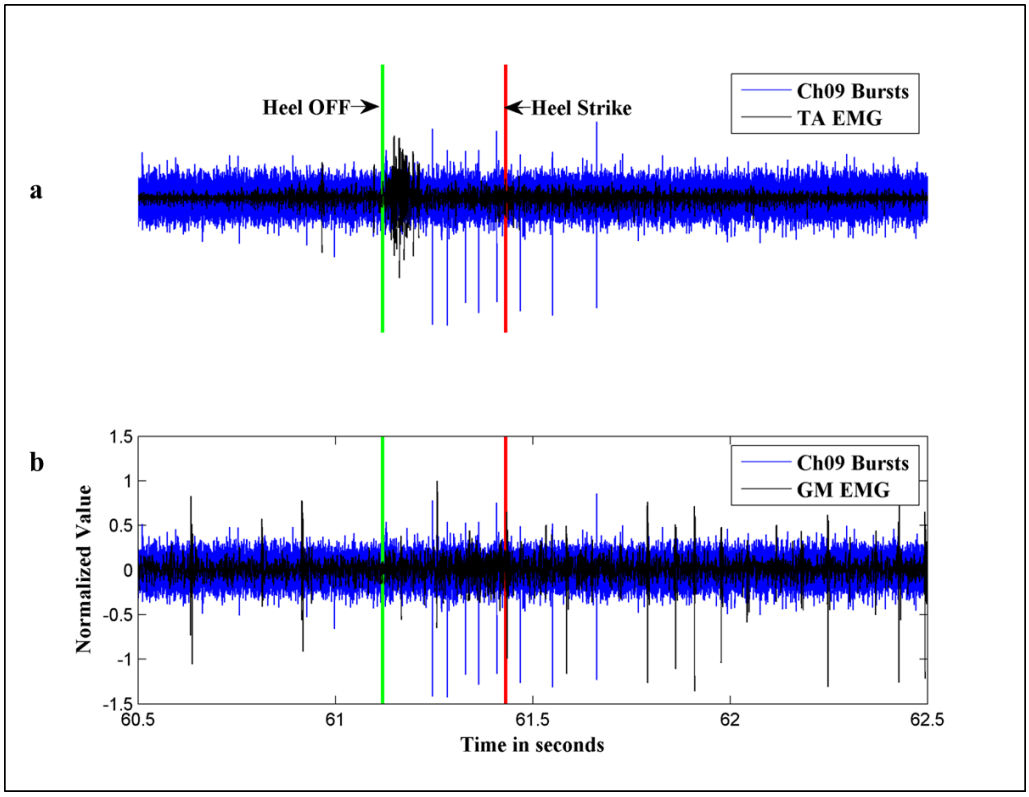

Figure 4.8 Representation of Ch09 neural signals overlapped with TA (a) and GM (b) EMG during swing phase of a gait cycle. X and Y axis consistent through plots (a,b).

Observation of SU spikes with respect to EMG signals within individual gait cycles revealed the onset of spike firing to be after maximal TA muscle contraction (Figure 4.8a) in the mid to late swing phase and continuing into initial stance phase for a few milliseconds. Also, most of the spikes within the burst occurred before GM contraction (Figure 4.8b). PSTH analysis confirmed the firing rate of spikes to peak before end of swing phase within 200 milliseconds relative to the Heel Strike event (Figure 4.9a). Cross correlation measured between Ch09 spike firing rate estimate and EMG envelope of TA muscle determined the precise lag between the two signals to be 115 milliseconds with a correlation coefficient of 0.59 (Figure 4.9 b).

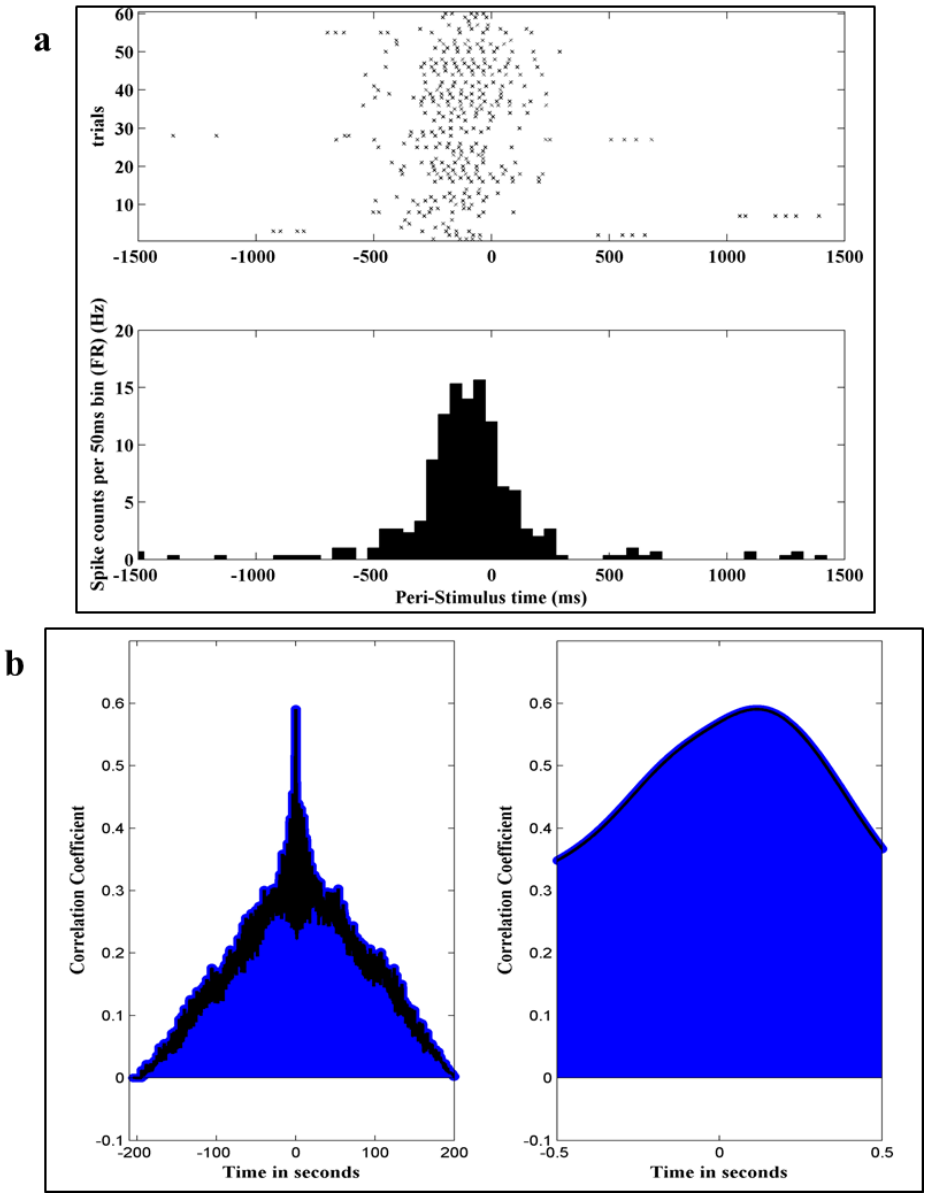

Figure 4.9 Representative Peri Stimulus Time Histogram of Ch09 spikes relative to Heel Strike events centered at 0 ms (a) and Cross correlation analysis between firing rate estimate of bursts and TA EMG envelope (b, left) over a recording session of 59 gait cycles. (b, right) shows a time domain magnified view revealing a peak at lag of 0.115 seconds.

4.4.2 Electrophysiological signals during passive stretching

In the animal that displayed locomotion specific SU bursts, sensory muscle afferents were repeatedly stimulated by passive dorsi and plantar flexion of the foot using controlled linear actuators as well as manual movements over as many as 30 trials at 21, 22, and 37 days post implantation. However, none of the sixteen recording electrodes of REMI in the tibial fascicle displayed SU spikes correlated with passive movements. The argument that the lack of burst spikes could be from effects of anesthesia resulting in electrical activity suppression is negated by the fact that sensory cutaneous signals could be recorded from other electrodes of the same array in response to brushing stimuli. Additionally, two other implanted animals which displayed neural activity during the first three weeks of implantation were tested similarly with lack of evoked neural responses to passive stretching of hind limb.

4.4.3 Verification of Botox induced paralysis

Two uninjured animals were injected with Botulinum Toxin-A (BTX) in GM to verify the successful induction of neuro-muscular block by our injection technique and dosage. Terminal Compound Muscle Action Potentials (CMAP) were measured at 3 days post injection in one animal, since the effect of BTX in GM muscles of rats has been reported to peak by 3 – 7 days post injection [10]. Figure 4.10a shows the electrically evoked CMAPs recorded from GM and TA muscles in one control animal with early-latency or M-wave response from direct recruitment of motor axons at 2.5 milliseconds and a medium-latency or H-wave response elicited by activation of group Ia (primary muscle afferents,) fibers mediated monosynaptic reflex at 6 milliseconds [7]. A 50% reduction in the amplitude of the M-wave of GM muscle was seen from 0.184 mV (peak to peak) to 0.05 mV at three days post BTX injection with a dramatic (~85%) attenuation of H-wave to 0.02 mV from an initial 0.14 mV, clearly confirming muscle paralysis and restriction of muscle afferent activation. To further confirm the effect of BTX induced neuro-muscular block, EMG

signals from TA and GM muscle activation were acquired during bipedal treadmill locomotion in a second control animal at 5 days post BTX injection. Figure 4.11 shows a reduction in amplitude of time normalized average EMG profiles from day 0 i.e. before injection (n=23 gait cycles) to 5 days post injection (n=13 gait cycles) specifically 8mV to 4mV (50 %) for TA and 5.8mV to 0.9mV (~85%) for GM muscles.

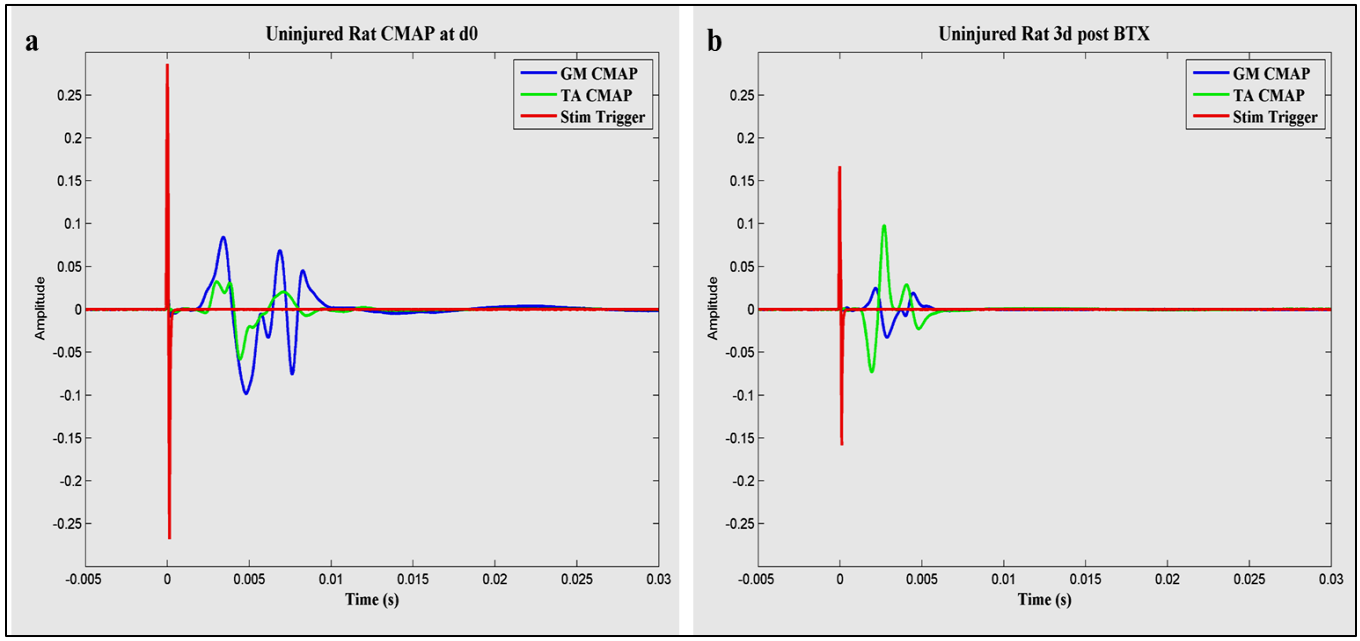

Figure 4.10 Confirmation of BTX induced neuro-muscular block by terminal CMAP measurements from TA and GM muscles evoked by stimulation of (a) 1.2V for uninjured rat at day 0 and (b) 1.5V at day 3 post-injection. (a,b) X-axis represents time in seconds and Y-axis amplitude in millivolts. Waveforms depict stimulus artifact (red), GM CMAP (blue), and TA CMAP (green).

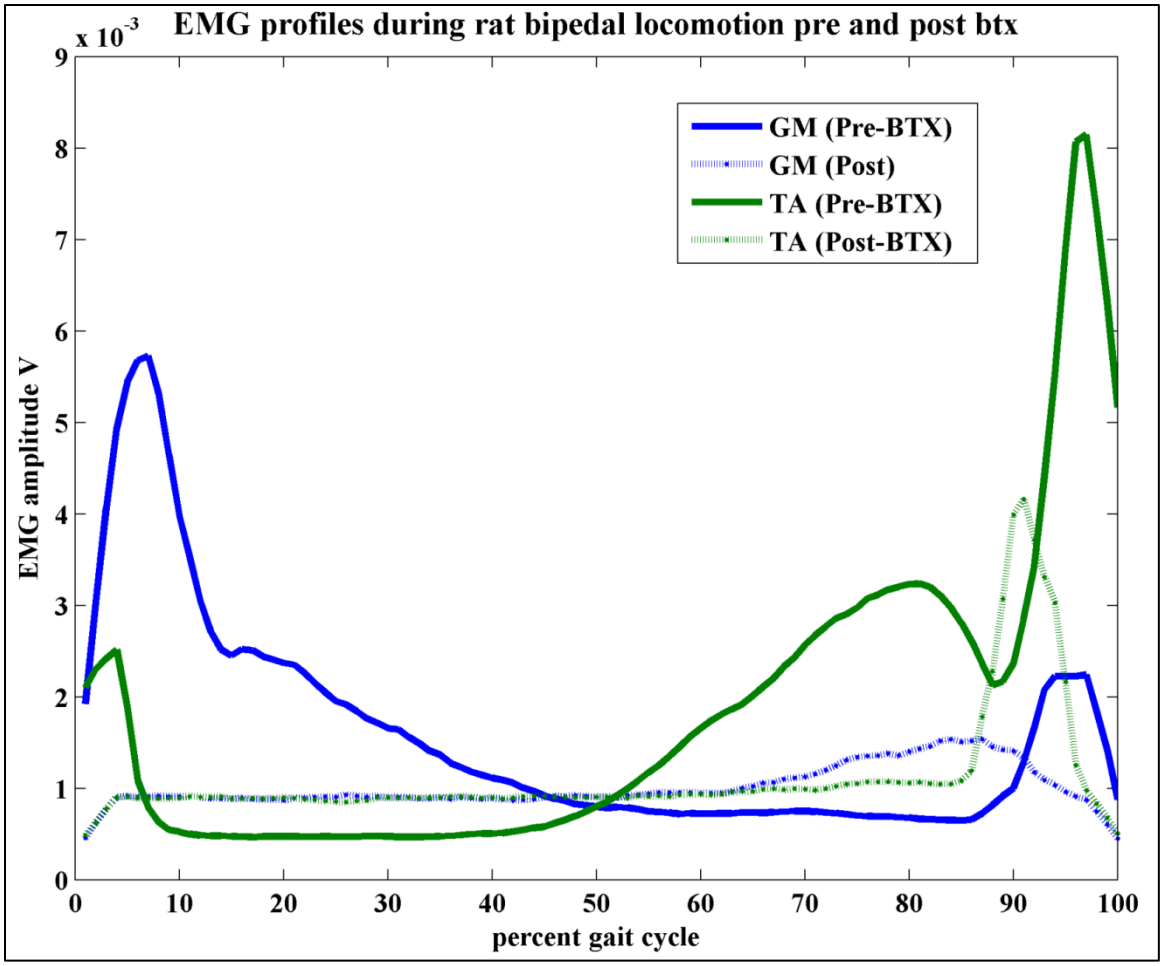

Figure 4.11 Time normalized average EMG profiles during bipedal treadmill locomotion from TA and GM muscles pre and post BTX injection confirm the induction of muscle paralysis.

4.4.4 Characterization of locomotion specific SU bursts post Botox induced paralysis

Botulinum Toxin-A (BTX) was injected in the Gastrocnemius Medialis muscle of the rat that successfully displayed SU spike bursts at 40 days post implantation to induce a neuromuscular block in order to restrict the activation of this muscle and thus attenuate proprioceptive sensory afferent activation. Electrophysiological (neural and emg) signals were acquired during bipedal treadmill locomotion at 5 days post injection. Although signals from TA muscles were relatively comparable to those observed before BTX injection, strength of GM muscle contraction had

highly reduced after induced muscle paralysis and EMG signal from it could not be detected. Neural signals displayed consistent presence of SU spike bursts on Ch09 and Ch10 REMI electrodes in tibial fascicle. ISI Histograms and auto-correlograms of neural spikes obtained from both channels showed similar profiles before and after BTX injection in Figure 4.12 and 4.13. ISIH showed bidmodal distribution profiles which have been reported to be characteristic of spikes firing in a bursting pattern [15] with the first peak at ~0.0316 sec in the histogram reflecting the approximate ISI of spikes within burst and the inter-burst interval indicated by the second peak at ~1.6 sec (Figure 4.12). Auto-correlograms of neural spikes in Ch09 and Ch10 also revealed an approximate lag of 40 milliseconds between individual spikes confirming that firing property of spikes obtained from both the channels were not affected by BTX injection (Figure 4.13). The number of spikes within detected bursts and their firing frequency were calculated for 36, 37, and 40 days post implantation and determined to remain stable across the observed time points (Figure 4.14 a,b). Values of such parameters were determined to remain unchanged at five days post BTX injection in comparison with those prior to injection at 40 days post REMI implantation (Figure 4.14 c,d). Figure 4.15 shows terminal CMAPs obtained at 82 days post REMI implantation in the animal treated with BTX at day 40 which further confirmed the lack of any GM muscle activation after induced muscle paralysis evident by absence of EMG signal opposed to EMG signals obtained from a control REMI implanted animal (not treated with BTX). Thus, taken together Botox induced neuro-muscular block in Gastrocnemius Medialis had no significant changes to the bipedal locomotion specific SU spike bursts obtained from REMI interfacing of tibial fascicle.

4.4.5 Stability of Correlation between REMI acquired neural signals and target muscle activity

To determine the strength and reliability of potential functional “use” of the SU bursts derived from regenerative interfacing of tibial fascicle, coefficients of cross-correlation measured between the spike firing rate and the EMG signal envelope of electrical activity in one of its major

end target muscle, the Gastrocnemius Medialis was initially proposed. However, we observed the strength of recorded EMG signals from GM to be extremely low despite 1000X amplification. This could be attributed most likely to muscle atrophy due to its denervation following tibial nerve transection and incomplete recovery by the observed time points and therefore we computed cross correlation measures with EMG envelope of the intact antagonistic muscle, i.e. Tibialis Anterior. Figure 4.16 shows the stability of computed Pearson's correlation coefficients in a range of 0.44 to 0.55 over a 10 day observation period. Statistical comparison across days could not be evaluated for this result due to the low sample size.

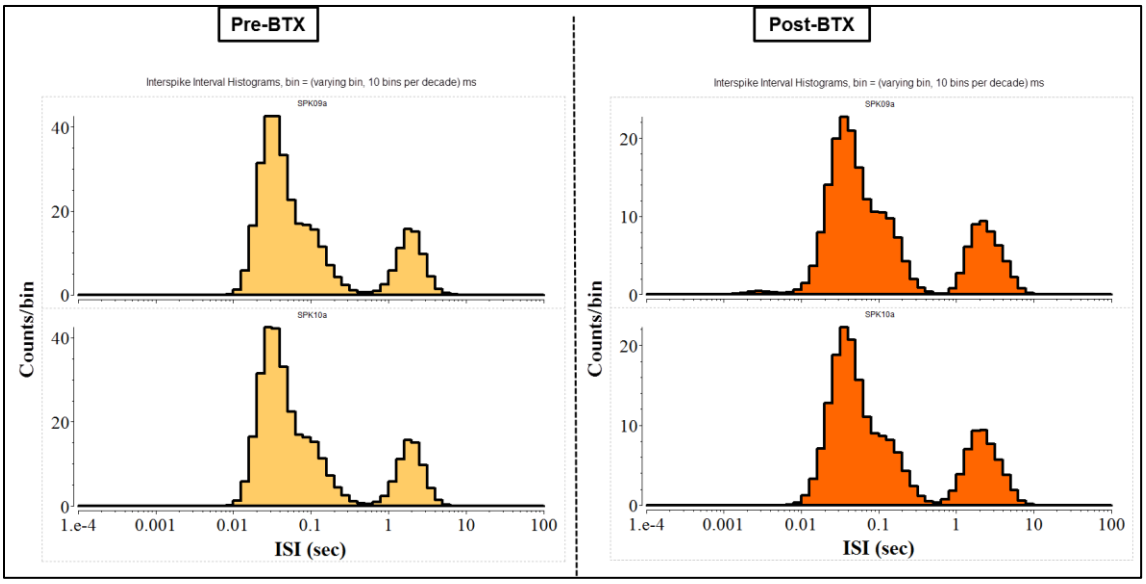

Figure 4.12 Inter Spike Interval Histograms (ISIH) with logarithmic transformation of Ch 09 (top row) and Ch 10 (bottom row) SU spikes from tibial REMI before (left) and after (right) Botox injection in GM muscle

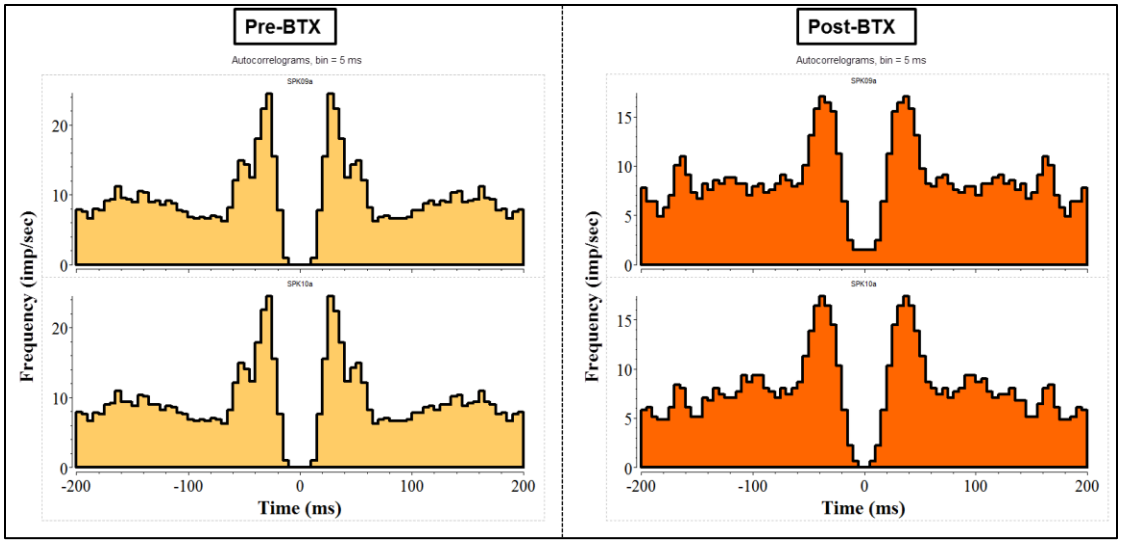

Figure 4.13 Auto-correlograms of SU spikes from tibial REMI in Ch 09 (top row) and Ch 10 (bottom row) before (left) and after (right) Botox injection in GM muscle

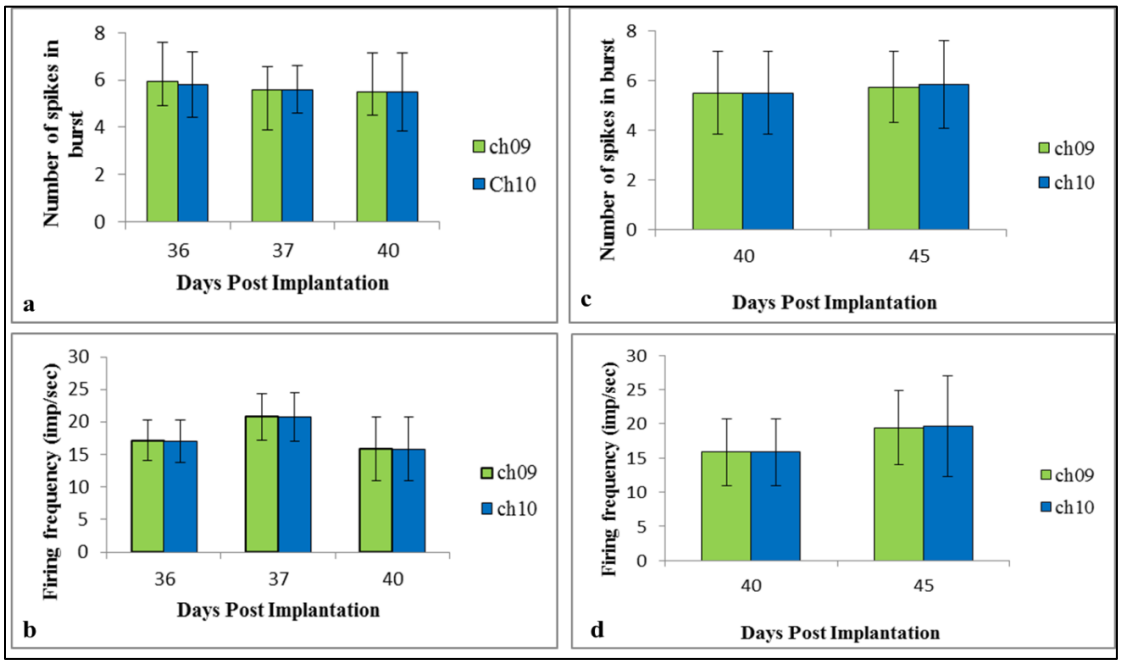

Figure 4.14 Characteristics of SU spike bursts before and 5 days after Botox induced GM muscle paralysis. (a,b) Average number and firing rate of spikes in burst from Channel 09 and 10 at day 36, 37, and 40 days post REMI implantation in tibial fascicle and before BTX treatment. Comparison of average number and firing rates before (40d) and after (45d) five days post BTX injection (c,d). Data presented as mean $\pm$ standard deviation.

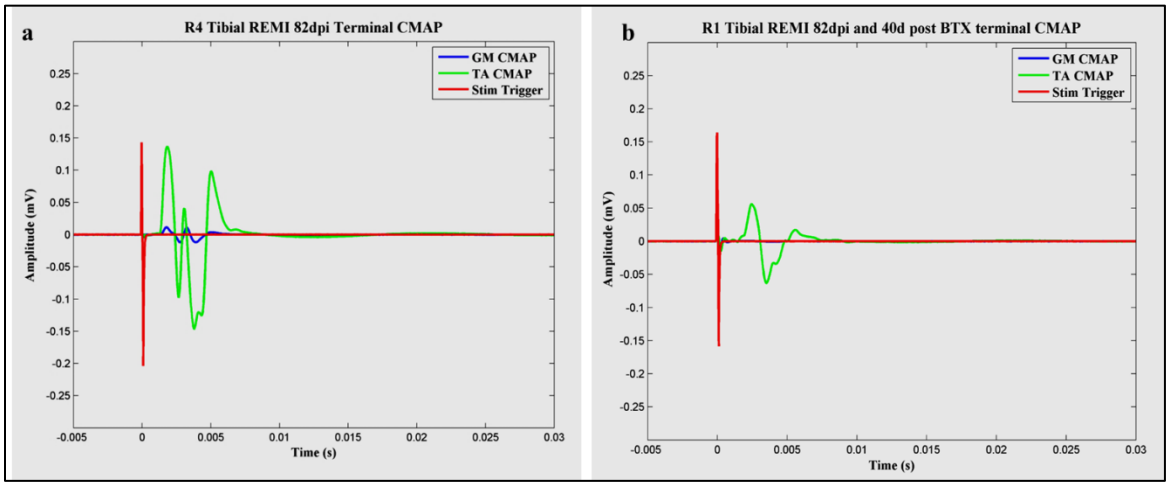

Figure 4.15 Comparison of terminal CMAPs from GM and TA muscles from animals with REMI in tibial fascicle at 82 days post implantation evoked by electrical stimulation of (a) 0.95V and without BTX treatment and (b) 1.5V at 42 days post BTX injection. X-axis represents time in seconds and Y-axis amplitude in millivolts. Waveforms depict stimulus artifact (red), GM CMAP (blue), and TA CMAP (green).

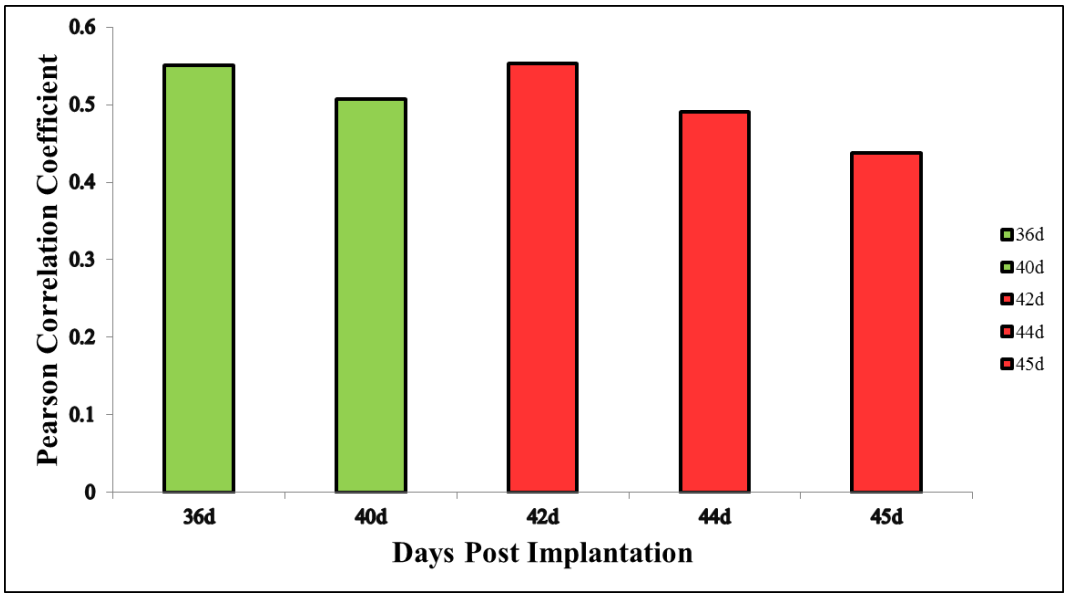

Figure 4.16 Coefficients of cross correlation measured between firing rate estimated from neural spikes and TA EMG envelope at day 36, 40 (pre-BTX), 42, 44, and 45 (post-BTX) post implantation from one animal implanted with REMI in tibial fascicle.

4.5 Discussion

In this study, we distinguished from motor and sensory fibers interfaced with the REMI implant in the tibial nerve, the efferent motor SU spikes that displayed the expected bursting firing pattern synchronous to stepping during bipedal locomotion. This identification was verified over the course of involved experiments by the lack of evoked afferent neural activity in response to passive stretching of implanted hind limb foot and consistent activity despite induction of neuromuscular block in distal target muscles. Additionally, the estimated firing rate had a significant and stable correlation with the distal muscle activity providing evidence of a physiological “functional linkage” with the executed movement in this paradigm.

4.5.1 Identification of efferent nature of SU spike bursts from REMI in tibial fascicle

Locomotion in all animal species is a complex form of voluntary movement that is requires the activity of neural circuits in the spinal cord, known as Central Pattern Generators (CPGs) which can govern motor aspects of locomotion even in the absence of sensory feedback [256]. Conversely, proprioceptive sensory information on muscle displacement, velocity, and tension obtained by muscle spindles and Golgi Tendon Organs along with feedback from skin afferents convey this feedback information to the CPGs to control their motor output through mono/polysynaptic reflexes and cutaneous reflexes [257]. In this study, we obtained consistent SU spike activity on two electrodes of REMI in tibial fascicle of one rat from three to six weeks post implantation with a characteristic bursting firing pattern during bipedal treadmill locomotion. These spikes were observed to occur in the mid to terminal swing phase after maximal contraction of Tibialis Anterior muscle and before initiation of stance phase, i.e. heel strike event. A plausible explanation for such activation timing of the recorded spikes could be attributed to the reciprocal excitation of spinal cord motor neurons that innervate ankle extensors (GM) during the inverse myotatic reflex initiated by the Golgi Tendon (Ib afferent) in the ankle flexors (TA) which

are most active in swing phase of gait cycle. The phenomenon of inverse myotatic reflexes generated by agonist-antagonist pair of muscles is well understood. Briefly, contraction of a muscle such as ankle flexor TA in this study leads to the generation of tension in the muscle that activates the Golgi Tendon Ib afferents axons which innervate in the spinal cord and synapse onto inhibitory and excitatory interneurons. The inhibitory neurons in turn synapses onto the alpha motor neuron of the homonymous muscle (TA) restricting its further contraction while the excitatory interneuron connects with alpha moto-neurons innervating an antagonistic muscle (GM in this case) so that the its contraction is initiated while the agonist relaxes [258]. This reciprocal excitation in myotatic reflexes have been known to mediate the alternating extension and flexion in agonist and antagonist muscles resulting in smooth progression-like movements of opposing limbs such as in walking [259]. Thus, the recorded SU bursts from tibial fascicle during mid to terminal swing phase are more likely to be motor in nature with a role in “pre-activating” the Gastrocnemius Medialis muscle or its synergists for stance phase of the gait cycle.

The efferent nature of specific bursting neural SUs in question of this study was verified by its continued persistence even after five days post BTX injection in the Gastrocnemius Medialis muscle. BTX when injected into skeletal muscles, diffuses into the nerve endings and through proteolytic events leads to cleavage of synaptosomal-associated protein (SNAP-25) inhibiting the release of Acetylcholine neurotransmitter at the neuro-muscular junction and thus prevents muscle contraction [260][261]. Thus, we rationalized that BTX induced neuromuscular block in the GM muscle would attenuate proprioceptive feedback from muscle spindles and GTO due to chemical denervation of the muscle [262] [263], eliminating spikes generated by muscle afferents in the recorded SU activity from tibial fascicle. However, no significant changes in the characteristics (firing rates, number of spikes, and ISI) were observed in the bursts recorded during bipedal locomotion before and after BTX induced neuro muscular blockade of ankle extensor muscle. Failure to evoke similar bursting SU spikes during passive activation of muscle

spindles by simulated plantar and dorsi flexion of foot in the same anesthetized animal further confirmed the possibility of the burst spikes recorded solely during active limb movements to be of motor origin. The fact that the observed firing rates (15-20 Hz) acquired in this study were similar to those reported in human peroneal nerves [245] also corroborates the conclusion of efferent nature of SU spike bursts recorded by REMI interfacing of tibial fascicle.

The identification of efferent motor activity in peripheral nerves with this specific bursting firing pattern of 30-70ms inter spike interval can be potentially used to develop criteria for online algorithms to distinguish motor signals from sensory during real time control procedures of robotic prostheses. Additionally, such characteristic firing pattern can be used to develop informed artificial stimulation paradigms, based on their intrinsic electrophysiological properties, rather than the currently employed “blind” parameters to enhance regeneration of injured peripheral nerves.

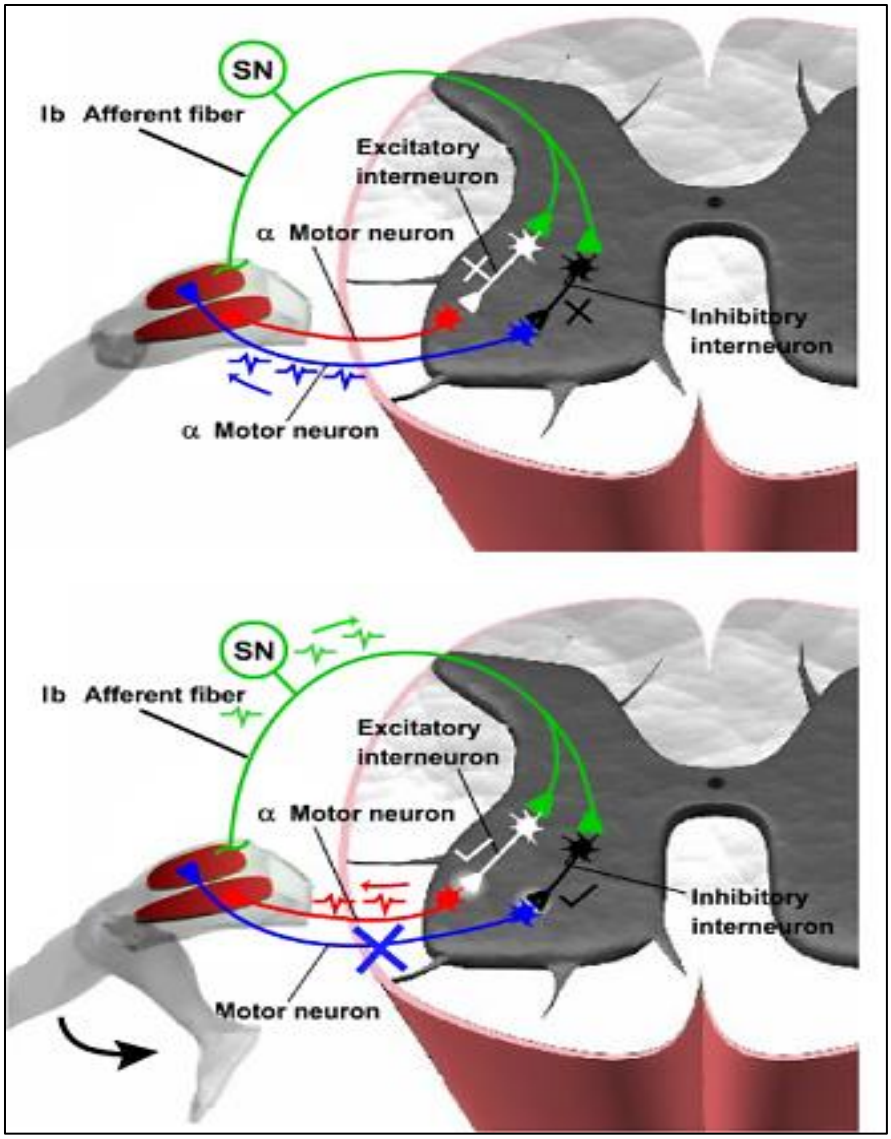

Figure 4.17 Inverse Myotatic Reflex as a possible explanation for precise timing of REMI recorded efferent SU spike bursts (after TA contraction and before GM activation): (A) Contraction of flexor muscle (e.g. TA) by motor axon firing (blue) results in (B) activation of Golgi Tendon (Ib afferent) axons signaling muscle tension to the spinal cord where it synapses onto an inhibitory (black) and an excitatory interneuron (white). The latter stops the homonymous (TA) muscle from further contraction while the excitatory interneuron activates simultaneously the antagonist flexor muscle (GM) by motor axon firing (red) - likely the type of spikes recorded by REMI in tibial fascicle

4.5.2 Stable Correlation between REMI acquired neural signals with distal muscle activity.

Demonstration of functional utility of recorded signals by extraction of motor intent related information and generation of commands to execute the desired movement is at the cornerstone of neural interface development for control of robotic prostheses. The existence of a direct correlation between electrical discharges in the motor cortex and limb movement established by the pioneering work of Edward Evarts [60]and Eberhard Fetz [264] in the 1960s and 1970s has led to the evolution of current Brain Machine Interfaces which can feasibly use the cortical electrical activity of paraplegic patients to provide volitional control over robotic hands in clinical trials. Similarly, pinch and palmar grasp movement of robotic hands by Longitudinal Intra-Fascicular Electrodes in peripheral nerves of upper limb amputee patients [116], and more recently real-time decoding of leg position from Dorsal Root Ganglion (DRG) sensory neurons in animal models have been reported [265]. Although encouraging, most of the BMI and PNI studies are reported to have limited prosthetic movement due to success in decoding of only few kinematic parameters, i.e. velocity and trajectory from acquired neural signals. Dexterous control over the versatile range of movements and manipulations, which are indigenous to the human hand, such as differential force exertion based on physical characteristics of objects (delicate versus heavy) by limb stiffening through muscle co-contractions are yet to be translated in neural interface driven prostheses[78][266]. Such force or tension related information concerning the dynamics of involved muscles, commonly termed as movement kinetics, can be extracted from the motor and sensory axons of interfaced peripheral nerves on the premise of a one to one correspondence between the motor axon and the muscle fibers it innervates[134]. In this study, we demonstrated the existence of a significant correlation between the identified efferent motor SU spikes and activity of distal muscle associated with the movement of stepping during locomotion. This correlation was determined to remain stable over a 10 day observation period despite the generally stochastic and noisy nature of EMG signals [267], which further substantiates the notion that functionally relevant and reliable motor signals can be derived from

our regenerative peripheral nerve interface. Although modulation of muscle activity and its effect on spike firing rate induced by load changes in associated limbs during different movements or behaviors was beyond the scope of this feasibility testing study, its incorporation in future studies can provide insight into the possibility of extracting information related to torque and strength of muscle activation, encoded in motor signals from REMI interfaced nerves. Additionally, the results described here encourage further studies evaluating the use of spiking activity derived from regenerative nerve interfaces to predict offline and in real-time the muscle activity and limb kinematics for execution of movement in a potential prosthetic device.

References

[1] K. Ziegler-Graham, E. J. MacKenzie, P. L. Ephraim, T. G. Travison, and R. Brookmeyer, “Estimating the prevalence of limb loss in the United States: 2005 to 2050.,” *Arch. Phys. Med. Rehabil.*, vol. 89, no. 3, pp. 422–9, Mar. 2008.

[2] E. J. Ligthelm and S. C. D. Wright, “Lived experience of persons with an amputation of the upper limb,” *Int. J. Orthop. Trauma Nurs.*, vol. 18, no. 2, pp. 99–106, May 2014.

[3] A. L. Dougherty, C. R. Mohrle, M. R. Galarneau, S. I. Woodruff, J. L. Dye, and K. H. Quinn, “Battlefield extremity injuries in Operation Iraqi Freedom.,” *Injury*, vol. 40, no. 7, pp. 772–7, Jul. 2009.

[4] C. Behrend, W. Reizner, J. A. Marchessault, and W. C. Hammert, “Update on advances in upper extremity prosthetics.,” *J. Hand Surg. Am.*, vol. 36, no. 10, pp. 1711–7, Oct. 2011.

[5] D. J. Tennent, J. C. Wenke, J. C. Rivera, and C. A. Krueger, “Characterisation and outcomes of upper extremity amputations.,” *Injury*, vol. 45, no. 6, pp. 965–9, Jun. 2014.

[6] P. Hernigou, “Ambroise Paré IV: The early history of artificial limbs (from robotic to prostheses).,” *Int. Orthop.*, vol. 37, no. 6, pp. 1195–7, Jun. 2013.

[7] M. P. McLoughlin, “DARPA Revolutionizing Prosthetics 2009,” Jan. 2009.

[8] D. S. Childress, “Powered Limb Prostheses: Their Clinical Significance,” *IEEE Trans. Biomed. Eng.*, vol. BME-20, no. 3, pp. 200–207, May 1973.

[9] T. Dillingham, “Rehabilitation of the upper limb amputee,” *Rehabil. Inj. Combat.*, pp. 33–77, 1998.

[10] C. Toledo, L. Leija, R. Munoz, A. Vera, and A. Ramirez, “Upper limb prostheses for amputations above elbow: A review,” in *2009 Pan American Health Care Exchanges*, 2009, pp. 104–108.

[11] E. a Biddiss and T. T. Chau, “Upper limb prosthesis use and abandonment: a survey of the last 25 years.,” *Prosthet. Orthot. Int.*, vol. 31, no. 3, pp. 236–57, Sep. 2007.

[12] L. Resnik, M. R. Meucci, S. Lieberman-Klinger, C. Fantini, D. L. Kelty, R. Disla, and N. Sasson, “Advanced Upper Limb Prosthetic Devices: Implications for Upper Limb Prosthetic Rehabilitation,” *Archives of Physical Medicine and Rehabilitation*, vol. 93, no. 4. pp. 710–717, 2012.

[13] L. V McFarland, S. L. Hubbard Winkler, A. W. Heinemann, M. Jones, and A. Esquenazi, “Unilateral upper-limb loss: satisfaction and prosthetic-device use in veterans and servicemembers from Vietnam and OIF/OEF conflicts.,” *J. Rehabil. Res. Dev.*, vol. 47, no. 4, pp. 299–316, Jan. 2010.

[14] C. Pylatiuk, S. Schulz, and L. Döderlein, “Results of an Internet survey of myoelectric prosthetic hand users.,” *Prosthet. Orthot. Int.*, vol. 31, no. 4, pp. 362–70, Dec. 2007.

[15] C. A. Krueger, J. C. Wenke, M. S. Cho, and J. R. Hsu, “Common factors and outcome in late upper extremity amputations after military injury.,” *J. Orthop. Trauma*, vol. 28, no. 4, pp. 227–31, Apr. 2014.

[16] E. Biddiss and T. Chau, “Upper-limb prosthetics: critical factors in device abandonment.,” *Am. J. Phys. Med. Rehabil.*, vol. 86, no. 12, pp. 977–87, Dec. 2007.

[17] E. Biddiss, D. Beaton, and T. Chau, “Consumer design priorities for upper limb prosthetics,” *Disabil. Rehabil. Assist. Technol.*, vol. 2, no. 6, pp. 346–357, Jan. 2007.

[18] D. Atkins, “Epidemiologic overview of individuals with upper-limb loss and their reported research priorities,” *JPO J. Prosthetics …*, 1996.

[19] R. F. ff Weir, P. R. Troyk, G. A. DeMichele, D. A. Kerns, J. F. Schorsch, and H. Maas, “Implantable myoelectric sensors (IMESs) for intramuscular electromyogram recording.,” *IEEE Trans. Biomed. Eng.*, vol. 56, no. 1, pp. 159–71, Jan. 2009.

[20] S. Micera, J. Carpaneto, and S. Raspopovic, “Control of hand prostheses using peripheral information.,” *IEEE Rev. Biomed. Eng.*, vol. 3, pp. 48–68, Jan. 2010.

[21] A. E. Schultz and T. a Kuiken, “Neural interfaces for control of upper limb prostheses: the state of the art and future possibilities.,” *PM R*, vol. 3, no. 1, pp. 55–67, Jan. 2011.

[22] T. A. Kuiken, G. A. Dumanian, R. D. Lipschutz, L. A. Miller, and K. A. Stubblefield, “The use of targeted muscle reinnervation for improved myoelectric prosthesis control in a bilateral shoulder disarticulation amputee.,” *Prosthet. Orthot. Int.*, vol. 28, no. 3, pp. 245–53, Dec. 2004.

[23] L. a Miller, R. D. Lipschutz, K. a Stubblefield, B. a Lock, H. Huang, T. W. Williams, R. F. Weir, and T. a Kuiken, “Control of a six degree of freedom prosthetic arm after targeted muscle reinnervation surgery.,” *Arch. Phys. Med. Rehabil.*, vol. 89, no. 11, pp. 2057–65, Nov. 2008.

[24] P. D. Marasco, A. E. Schultz, and T. a Kuiken, “Sensory capacity of reinnervated skin after redirection of amputated upper limb nerves to the chest.,” *Brain*, vol. 132, no. Pt 6, pp. 1441–8, Jun. 2009.

[25] T. a Kuiken, L. a Miller, R. D. Lipschutz, B. a Lock, K. Stubblefield, P. D. Marasco, P. Zhou, and G. a Dumanian, “Targeted reinnervation for enhanced prosthetic arm function in a woman with a proximal amputation: a case study.,” *Lancet*, vol. 369, no. 9559, pp. 371–80, Mar. 2007.

[26] K. A. Stubblefield, L. A. Miller, R. D. Lipschutz, and T. A. Kuiken, “Occupational therapy protocol for amputees with targeted muscle reinnervation.,” *J. Rehabil. Res. Dev.*, vol. 46, no. 4, pp. 481–8, Jan. 2009.

[27] A. D. Roche, H. Rehbaum, D. Farina, and O. C. Aszmann, “Prosthetic Myoelectric Control Strategies: A Clinical Perspective,” *Curr. Surg. Reports*, vol. 2, no. 3, p. 44, Jan. 2014.

[28] T. A. Kuiken, G. Li, B. A. Lock, R. D. Lipschutz, L. A. Miller, K. A. Stubblefield, and K. B. Englehart, “Targeted muscle reinnervation for real-time myoelectric control of multifunction artificial arms.,” *JAMA*, vol. 301, no. 6, pp. 619–28, Feb. 2009.

[29] P. R. Troyk, G. A. DeMichele, D. A. Kerns, and R. F. Weir, “IMES: an implantable myoelectric sensor.,” *Conf. Proc. IEEE Eng. Med. Biol. Soc.*, vol. 2007, pp. 1730–3, Jan. 2007.

[30] J. J. Baker, D. Yatsenko, J. F. Schorsch, G. A. DeMichele, P. R. Troyk, D. T. Hutchinson, R. F. ff Weir, G. Clark, and B. Greger, “Decoding individuated finger flexions with Implantable MyoElectric Sensors.,” *Conf. Proc. IEEE Eng. Med. Biol. Soc.*, vol. 2008, pp. 193–6, Jan. 2008.

[31] J. J. Baker, E. Scheme, K. Englehart, D. T. Hutchinson, and B. Greger, “Continuous detection and decoding of dexterous finger flexions with implantable myoelectric sensors.,” *IEEE Trans. Neural Syst. Rehabil. Eng.*, vol. 18, no. 4, pp. 424–32, Aug. 2010.

[32] D. R. Merrill, J. Lockhart, P. R. Troyk, R. F. Weir, and D. L. Hankin, “Development of an implantable myoelectric sensor for advanced prosthesis control.,” *Artif. Organs*, vol. 35, no. 3, pp. 249–52, Mar. 2011.

[33] C. Cipriani, J. Segil, J. Birdwell, and R. Weir, “Dexterous control of a prosthetic hand using fine-wire intramuscular electrodes in targeted extrinsic muscles.,” *IEEE Trans. Neural Syst. Rehabil. Eng.*, vol. PP, no. 99, p. 1, Jan. 2014.

[34] M. Zecca, S. Micera, M. C. Carrozza, and P. Dario, “Control of multifunctional prosthetic hands by processing the electromyographic signal.,” *Crit. Rev. Biomed. Eng.*, vol. 30, no. 4–6, pp. 459–85, Jan. 2002.

[35] E. Scheme and K. Englehart, “Electromyogram pattern recognition for control of powered upper-limb prostheses: state of the art and challenges for clinical use.,” *J. Rehabil. Res. Dev.*, vol. 48, no. 6, pp. 643–59, Jan. 2011.

[36] B. Hudgins, P. Parker, and R. N. Scott, “A new strategy for multifunction myoelectric control.,” *IEEE Trans. Biomed. Eng.*, vol. 40, no. 1, pp. 82–94, Jan. 1993.

[37] J.-U. Chu, I. Moon, and M.-S. Mun, “A real-time EMG pattern recognition system based on linear-nonlinear feature projection for a multifunction myoelectric hand.,” *IEEE Trans. Biomed. Eng.*, vol. 53, no. 11, pp. 2232–9, Nov. 2006.

[38] P. Zhou, M. M. Lowery, K. B. Englehart, H. Huang, G. Li, L. Hargrove, J. P. A. Dewald, and T. A. Kuiken, “Decoding a new neural machine interface for control of artificial limbs.,” *J. Neurophysiol.*, vol. 98, no. 5, pp. 2974–82, Nov. 2007.

[39] P. Pilarski and M. Dawson, “Adaptive artificial limbs: a real-time approach to prediction and anticipation,” *Robot. …*, no. March 2013, pp. 53–64, 2013.

[40] R. Quian Quiroga and S. Panzeri, “Extracting information from neuronal populations: information theory and decoding approaches.,” *Nat. Rev. Neurosci.*, vol. 10, no. 3, pp. 173–85, Mar. 2009.

[41] J. P. Donoghue, “Bridging the brain to the world: a perspective on neural interface systems.,” *Neuron*, vol. 60, no. 3, pp. 511–21, Nov. 2008.

[42] J. C. Sanchez and J. C. Principe, *Brain–Machine Interface Engineering*, vol. 2, no. 1. 2007, pp. 1–234.

[43] B. C. Lega, M. D. Serruya, and K. A. Zaghloul, “Brain-machine interfaces: electrophysiological challenges and limitations.,” *Crit. Rev. Biomed. Eng.*, vol. 39, no. 1, pp. 5–28, Jan. 2011.

[44] G. A. Ojemann, I. Fried, and E. Lettich, “Electrocorticographic (ECoG) correlates of language. I. Desynchronization in temporal language cortex during object naming.,” *Electroencephalogr. Clin. Neurophysiol.*, vol. 73, no. 5, pp. 453–63, Nov. 1989.

[45] N. Nakasatp, M. F. Levesque, D. S. Barth, C. Baumgartner, R. L. Rogers, and W. W. Sutherling, “Comparisons of MEG, EEG, and ECoG source localization in neocortical partial epilepsy in humans,” *Electroencephalogr. Clin. Neurophysiol.*, vol. 91, no. 3, pp. 171–178, Sep. 1994.

[46] G. Schalk, K. J. Miller, N. R. Anderson, J. A. Wilson, M. D. Smyth, J. G. Ojemann, D. W. Moran, J. R. Wolpaw, and E. C. Leuthardt, “Two-dimensional movement control using electrocorticographic signals in humans.,” *J. Neural Eng.*, vol. 5, no. 1, pp. 75–84, Mar. 2008.

[47] C. Toro, C. Cox, G. Friehs, C. Ojakangas, R. Maxwell, J. R. Gates, R. J. Gumnit, and T. J. Ebner, “8-12 Hz rhythmic oscillations in human motor cortex during two-dimensional arm movements: evidence for representation of kinematic parameters.,” *Electroencephalogr. Clin. Neurophysiol.*, vol. 93, no. 5, pp. 390–403, Oct. 1994.

[48] S. Micera, X. Navarro, J. Carpaneto, L. Citi, O. Tonet, P. M. Rossini, M. C. Carrozza, K. P. Hoffmann, M. Vivó, K. Yoshida, and P. Dario, “On the use of longitudinal intrafascicular peripheral interfaces for the control of cybernetic hand prostheses in amputees.,” *IEEE Trans. Neural Syst. Rehabil. Eng.*, vol. 16, no. 5, pp. 453–72, Oct. 2008.

[49] J. D. GREEN, “A Simple Microelectrode for recording from the Central Nervous System,” *Nature*, vol. 182, no. 4640, pp. 962–962, Oct. 1958.

[50] D. H. Hubel, “Tungsten Microelectrode for Recording from Single Units.,” *Science*, vol. 125, no. 3247, pp. 549–50, Mar. 1957.

[51] F. STRUMWASSER, “Long-Term Recording from Single Neurons in Brain of Unrestrained Mammals,” *Science (80-.).*, vol. 127, no. 3296, pp. 469–470, Feb. 1958.

[52] M. Salcman and M. J. Bak, “Design, Fabrication, and In Vivo Behavior of Chronic Recording Intracortical Microelectrodes,” *IEEE Trans. Biomed. Eng.*, vol. BME-20, no. 4, pp. 253–260, Jul. 1973.

[53] M. Salcman and M. J. Bak, “A new chronic recording intracortical microelectrode,” *Med. Biol. Eng.*, vol. 14, no. 1, pp. 42–50, Jan. 1976.

[54] P. K. Campbell, K. E. Jones, R. J. Huber, K. W. Horch, and R. A. Normann, “A silicon-based, three-dimensional neural interface: manufacturing processes for an intracortical electrode array.,” *IEEE Trans. Biomed. Eng.*, vol. 38, no. 8, pp. 758–68, Aug. 1991.

[55] A. C. Hoogerwerf and K. D. Wise, “A three-dimensional microelectrode array for chronic neural recording.,” *IEEE Trans. Biomed. Eng.*, vol. 41, no. 12, pp. 1136–46, Dec. 1994.

[56] J. F. Hetke, J. L. Lund, K. Najafi, K. D. Wise, and D. J. Anderson, “Silicon ribbon cables for chronically implantable microelectrode arrays.,” *IEEE Trans. Biomed. Eng.*, vol. 41, no. 4, pp. 314–21, Apr. 1994.

[57] M. A. L. Nicolelis, D. Dimitrov, J. M. Carmena, R. Crist, G. Lehew, J. D. Kralik, and S. P. Wise, “Chronic, multisite, multielectrode recordings in macaque monkeys.,” *Proc. Natl. Acad. Sci. U. S. A.*, vol. 100, no. 19, pp. 11041–6, Sep. 2003.

[58] R. J. Vetter, J. C. Williams, J. F. Hetke, E. a Nunamaker, and D. R. Kipke, “Chronic neural recording using silicon-substrate microelectrode arrays implanted in cerebral cortex.,” *IEEE Trans. Biomed. Eng.*, vol. 51, no. 6, pp. 896–904, Jun. 2004.

[59] S. Suner, M. R. Fellows, C. Vargas-Irwin, G. K. Nakata, and J. P. Donoghue, “Reliability of signals from a chronically implanted, silicon-based electrode array in non-human primate primary motor cortex.,” *IEEE Trans. Neural Syst. Rehabil. Eng.*, vol. 13, no. 4, pp. 524–41, Dec. 2005.

[60] E. V. Evarts, “Relation of pyramidal tract activity to force exerted during voluntary movement,” *J Neurophysiol*, vol. 31, no. 1, pp. 14–27, Jan. 1968.

[61] E. E. Fetz and D. V Finocchio, “Correlations between activity of motor cortex cells and arm muscles during operantly conditioned response patterns.,” *Exp. brain Res.*, vol. 23, no. 3, pp. 217–40, Sep. 1975.

[62] A. B. Schwartz, “Cortical neural prosthetics.,” *Annu. Rev. Neurosci.*, vol. 27, pp. 487–507, Jan. 2004.

[63] A. P. Georgopoulos, A. B. Schwartz, and R. E. Kettner, “Neuronal population coding of movement direction.,” *Science*, vol. 233, no. 4771, pp. 1416–9, Sep. 1986.

[64] M. A. Wilson and B. L. McNaughton, “Dynamics of the hippocampal ensemble code for space.,” *Science*, vol. 261, no. 5124, pp. 1055–8, Aug. 1993.

[65] E. M. Maynard, N. G. Hatsopoulos, C. L. Ojakangas, B. D. Acuna, J. N. Sanes, R. A. Normann, and J. P. Donoghue, “Neuronal interactions improve cortical population coding of movement direction.,” *J. Neurosci.*, vol. 19, no. 18, pp. 8083–93, Sep. 1999.

[66] N. G. Hatsopoulos, C. L. Ojakangas, L. Paninski, and J. P. Donoghue, “Information about movement direction obtained from synchronous activity of motor cortical neurons.,” *Proc. Natl. Acad. Sci. U. S. A.*, vol. 95, no. 26, pp. 15706–11, Dec. 1998.

[67] J. K. Chapin, K. a Moxon, R. S. Markowitz, and M. a Nicolelis, “Real-time control of a robot arm using simultaneously recorded neurons in the motor cortex.,” *Nat. Neurosci.*, vol. 2, no. 7, pp. 664–70, Jul. 1999.

[68] J. Wessberg, C. R. Stambaugh, J. D. Kralik, P. D. Beck, M. Laubach, J. K. Chapin, J. Kim, S. J. Biggs, M. a Srinivasan, and M. a Nicolelis, “Real-time prediction of hand trajectory by ensembles of cortical neurons in primates.,” *Nature*, vol. 408, no. 6810, pp. 361–5, Nov. 2000.

[69] M. D. Serruya, N. G. Hatsopoulos, L. Paninski, M. R. Fellows, and J. P. Donoghue, “Instant neural control of a movement signal.,” *Nature*, vol. 416, no. 6877, pp. 141–2, Mar. 2002.

[70] D. M. Taylor, S. I. H. Tillery, and A. B. Schwartz, “Direct cortical control of 3D neuroprosthetic devices.,” *Science*, vol. 296, no. 5574, pp. 1829–32, Jun. 2002.

[71] L. R. Hochberg, M. D. Serruya, G. M. Friehs, J. A. Mukand, M. Saleh, A. H. Caplan, A. Branner, D. Chen, R. D. Penn, and J. P. Donoghue, “Neuronal ensemble control of prosthetic devices by a human with tetraplegia.,” *Nature*, vol. 442, no. 7099, pp. 164–71, Jul. 2006.

[72] S.-P. Kim, J. D. Simeral, L. R. Hochberg, J. P. Donoghue, and M. J. Black, “Neural control of computer cursor velocity by decoding motor cortical spiking activity in humans with tetraplegia.,” *J. Neural Eng.*, vol. 5, no. 4, pp. 455–76, Dec. 2008.

[73] J. M. Carmena, M. A. Lebedev, R. E. Crist, J. E. O’Doherty, D. M. Santucci, D. F. Dimitrov, P. G. Patil, C. S. Henriquez, and M. A. L. Nicolelis, “Learning to control a brain-machine interface for reaching and grasping by primates.,” *PLoS Biol.*, vol. 1, no. 2, p. E42, Nov. 2003.

[74] M. Velliste, S. Perel, M. C. Spalding, A. S. Whitford, and A. B. Schwartz, “Cortical control of a prosthetic arm for self-feeding.,” *Nature*, vol. 453, no. 7198, pp. 1098–101, Jun. 2008.

[75] G. a Tabot, J. F. Dammann, J. a Berg, F. V Tenore, J. L. Boback, R. J. Vogelstein, and S. J. Bensmaia, “Restoring the sense of touch with a prosthetic hand through a brain interface.,” *Proc. Natl. Acad. Sci. U. S. A.*, pp. 2–7, Oct. 2013.

[76] L. R. Hochberg, D. Bacher, B. Jarosiewicz, N. Y. Masse, J. D. Simeral, J. Vogel, S. Haddadin, J. Liu, S. S. Cash, P. van der Smagt, and J. P. Donoghue, “Reach and grasp by people with tetraplegia using a neurally controlled robotic arm.,” *Nature*, vol. 485, no. 7398, pp. 372–5, May 2012.

[77] J. L. Collinger, B. Wodlinger, J. E. Downey, W. Wang, E. C. Tyler-Kabara, D. J. Weber, A. J. C. McMorland, M. Velliste, M. L. Boninger, and A. B. Schwartz, “High-performance neuroprosthetic control by an individual with tetraplegia.,” *Lancet*, vol. 381, no. 9866, pp. 557–64, Mar. 2013.

[78] M. A. Lebedev and M. A. L. Nicolelis, “Brain-machine interfaces: past, present and future.,” *Trends Neurosci.*, vol. 29, no. 9, pp. 536–46, Sep. 2006.

[79] J. C. Barrese, N. Rao, K. Paroo, C. Triebwasser, C. Vargas-Irwin, L. Franquemont, and J. P. Donoghue, “Failure mode analysis of silicon-based intracortical microelectrode arrays in non-human primates.,” *J. Neural Eng.*, vol. 10, no. 6, p. 066014, Dec. 2013.

[80] D. H. Szarowski, M. D. Andersen, S. Retterer, A. J. Spence, M. Isaacson, H. G. Craighead, J. N. Turner, and W. Shain, “Brain responses to micro-machined silicon devices.,” *Brain Res.*, vol. 983, no. 1–2, pp. 23–35, Sep. 2003.

[81] R. Biran, D. Martin, and P. Tresco, “The brain tissue response to implanted silicon microelectrode arrays is increased when the device is tethered to the skull,” *J. Biomed. …*, 2007.

[82] V. S. Polikov, P. A. Tresco, and W. M. Reichert, “Response of brain tissue to chronically implanted neural electrodes.,” *J. Neurosci. Methods*, vol. 148, no. 1, pp. 1–18, Oct. 2005.

[83] W. M. Grill and J. T. Mortimer, “Electrical properties of implant encapsulation tissue.,” *Ann. Biomed. Eng.*, vol. 22, no. 1, pp. 23–33, 1994.

[84] R. Biran, D. C. Martin, and P. A. Tresco, “Neuronal cell loss accompanies the brain tissue response to chronically implanted silicon microelectrode arrays.,” *Exp. Neurol.*, vol. 195, no. 1, pp. 115–26, Sep. 2005.

[85] D. J. Weber, R. Friesen, and L. E. Miller, “Interfacing the somatosensory system to restore touch and proprioception: essential considerations.,” *J. Mot. Behav.*, vol. 44, no. 6, pp. 403–18, Jan. 2012.

[86] B. Rosén, H. H. Ehrsson, C. Antfolk, C. Cipriani, F. Sebelius, and G. Lundborg, “Referral of sensation to an advanced humanoid robotic hand prosthesis.,” *Scand. J. Plast. Reconstr. Surg. Hand Surg.*, vol. 43, no. 5, pp. 260–6, Jan. 2009.

[87] L. Schmalzl, A. Kalckert, C. Ragnö, and H. H. Ehrsson, “Neural correlates of the rubber hand illusion in amputees: a report of two cases.,” *Neurocase*, vol. 20, no. 4, pp. 407–20, Aug. 2014.

[88] W. Jensen, S. Micera, X. Navarro, T. Stieglitz, D. Guiraud, J. L. Divoux, P. M. Rossini, and K. Yoshida, “Development of an implantable transverse intrafascicular multichannel electrode (TIME) system for relieving phantom limb pain.,” *Conf. Proc. IEEE Eng. Med. Biol. Soc.*, vol. 2010, pp. 6214–7, Jan. 2010.

[89] T. Boretius, K. Yoshida, J. Badia, K. Harreby, a. Kundu, X. Navarro, W. Jensen, and T. Stieglitz, “A transverse intrafascicular multichannel electrode (TIME) to treat phantom limb

pain — Towards human clinical trials," *2012 4th IEEE RAS EMBS Int. Conf. Biomed. Robot. Biomechatronics*, pp. 282–287, Jun. 2012.

[90] J. Valle and X. Navarro, *Interfaces with the Peripheral Nerve for the Control of Neuroprostheses*, 1st ed., vol. 109. Elsevier Inc., 2013, pp. 63–83.

[91] G. E. Loeb and R. a Peck, "Cuff electrodes for chronic stimulation and recording of peripheral nerve activity.," *J. Neurosci. Methods*, vol. 64, no. 1, pp. 95–103, Jan. 1996.

[92] D. Ceballos, A. Valero, and E. Valderrama, "Polyimide cuff electrodes for peripheral nerve stimulation," *J. Neurosci. …*, vol. 98, pp. 105–118, 2000.

[93] R. Stein, T. Nichols, and J. Jhamandas, "Stable long-term recordings from cat peripheral nerves," *Brain Res.*, vol. 128, pp. 21–38, 1977.

[94] J. a Hoffer and G. E. Loeb, "Implantable electrical and mechanical interfaces with nerve and muscle.," *Ann. Biomed. Eng.*, vol. 8, no. 4–6, pp. 351–60, Jan. 1980.

[95] G. G. Naples, J. T. Mortimer, A. Scheiner, and J. D. Sweeney, "A spiral nerve cuff electrode for peripheral nerve stimulation.," *IEEE Trans. Biomed. Eng.*, vol. 35, no. 11, pp. 905–16, Nov. 1988.

[96] S. Raspopovic, J. Carpaneto, E. Udina, X. Navarro, and S. Micera, "On the identification of sensory information from mixed nerves by using single-channel cuff electrodes.," *J. Neuroeng. Rehabil.*, vol. 7, p. 17, Jan. 2010.

[97] M. Haugland, A. Lickel, J. Haase, and T. Sinkjaer, "Control of FES thumb force using slip information obtained from the cutaneous electroneurogram in quadriplegic man.," *IEEE Trans. Rehabil. Eng.*, vol. 7, no. 2, pp. 215–27, Jun. 1999.

[98] M. K. Haugland and T. Sinkjaer, "Cutaneous whole nerve recordings used for correction of footdrop in hemiplegic man," *IEEE Trans. Rehabil. Eng.*, vol. 3, no. 4, pp. 307–317, 1995.

[99] W. M. Grill and J. T. Mortimer, "Quantification of recruitment properties of multiple contact cuff electrodes.," *IEEE Trans. Rehabil. Eng.*, vol. 4, no. 2, pp. 49–62, Jun. 1996.

[100] W. M. Grill and J. T. Mortimer, "Stability of the input-output properties of chronically implanted multiple contact nerve cuff stimulating electrodes," *IEEE Trans. Rehabil. Eng.*, vol. 6, no. 4, pp. 364–373, 1998.

[101] R. L. Waters, D. R. McNeal, W. Faloon, and B. Clifford, "Functional electrical stimulation of the peroneal nerve for hemiplegia. Long-term clinical follow-up.," *J. Bone Joint Surg. Am.*, vol. 67, no. 5, pp. 792–3, Jun. 1985.

[102] A. V Caparso, D. M. Durand, and J. M. Mansour, "A nerve cuff electrode for controlled reshaping of nerve geometry.," *J. Biomater. Appl.*, vol. 24, no. 3, pp. 247–73, Sep. 2009.

[103] D. K. Leventhal, M. Cohen, and D. M. Durand, "Chronic histological effects of the flat interface nerve electrode.," *J. Neural Eng.*, vol. 3, no. 2, pp. 102–13, Jun. 2006.

[104] D. J. Tyler and D. M. Durand, “Chronic Response of the Rat Sciatic Nerve to the Flat Interface Nerve Electrode,” *Ann. Biomed. Eng.*, vol. 31, no. 6, pp. 633–642, Jun. 2003.

[105] M. A. Schiefer, M. Freeberg, G. J. C. Pinault, J. Anderson, H. Hoyen, D. J. Tyler, and R. J. Triolo, “Selective activation of the human tibial and common peroneal nerves with a flat interface nerve electrode.,” *J. Neural Eng.*, vol. 10, no. 5, p. 056006, Oct. 2013.

[106] X. Navarro, T. B. Krueger, N. Lago, S. Micera, T. Stieglitz, and P. Dario, “A critical review of interfaces with the peripheral nervous system for the control of neuroprostheses and hybrid bionic systems.,” *J. Peripher. Nerv. Syst.*, vol. 10, no. 3, pp. 229–58, Sep. 2005.

[107] K. Yoshida and R. B. Stein, “Characterization of signals and noise rejection with bipolar longitudinal intrafascicular electrodes.,” *IEEE Trans. Biomed. Eng.*, vol. 46, no. 2, pp. 226–34, Mar. 1999.

[108] S. M. Lawrence, G. S. Dhillon, W. Jensen, K. Yoshida, and K. W. Horch, “of Polymer-Based Longitudinal Intrafascicular Electrodes,” vol. 12, no. 3, pp. 345–348, 2004.

[109] T. Lefurge, E. Goodall, and K. Horch, “Chronically implanted intrafascicular recording electrodes,” *Ann. Biomed. …*, vol. 19, no. 12, pp. 197–207, 1991.

[110] J. a Malmstrom, T. G. McNaughton, and K. W. Horch, “Recording properties and biocompatibility of chronically implanted polymer-based intrafascicular electrodes.,” *Ann. Biomed. Eng.*, vol. 26, no. 6, pp. 1055–64, 1998.

[111] K. Yoshida and K. Horch, “Selective stimulation of peripheral nerve fibers using dual intrafascicular electrodes.,” *IEEE Trans. Biomed. Eng.*, vol. 40, no. 5, pp. 492–4, May 1993.

[112] K. Yoshida and M. Kurstjens, “Recording experience with the thin-film longitudinal intra-fascicular electrode, a multichannel peripheral nerve interface,” *… , 2007. ICORR 2007. …*, vol. 00, no. c, pp. 0–5, 2007.

[113] G. S. Dhillon, S. M. Lawrence, D. T. Hutchinson, and K. W. Horch, “Residual function in peripheral nerve stumps of amputees: implications for neural control of artificial limbs.,” *J. Hand Surg. Am.*, vol. 29, no. 4, pp. 605–15; discussion 616–8, Jul. 2004.

[114] G. S. Dhillon and K. W. Horch, “Direct neural sensory feedback and control of a prosthetic arm.,” *IEEE Trans. Neural Syst. Rehabil. Eng.*, vol. 13, no. 4, pp. 468–72, Dec. 2005.

[115] K. Horch, S. Meek, T. G. Taylor, and D. T. Hutchinson, “Object discrimination with an artificial hand using electrical stimulation of peripheral tactile and proprioceptive pathways with intrafascicular electrodes.,” *IEEE Trans. Neural Syst. Rehabil. Eng.*, vol. 19, no. 5, pp. 483–9, Oct. 2011.

[116] P. M. Rossini, S. Micera, A. Benvenuto, J. Carpaneto, G. Cavallo, L. Citi, C. Cipriani, L. Denaro, V. Denaro, G. Di Pino, F. Ferreri, E. Guglielmelli, K.-P. Hoffmann, S. Raspopovic, J. Rigosa, L. Rossini, M. Tombini, and P. Dario, “Double nerve intraneural interface

implant on a human amputee for robotic hand control.," *Clin. Neurophysiol.*, vol. 121, no. 5, pp. 777–83, May 2010.

[117] T. Boretius, J. Badia, A. Pascual-Font, M. Schuettler, X. Navarro, K. Yoshida, and T. Stieglitz, "A transverse intrafascicular multichannel electrode (TIME) to interface with the peripheral nerve.," *Biosens. Bioelectron.*, vol. 26, no. 1, pp. 62–9, Sep. 2010.

[118] J. Badia, T. Boretius, D. Andreu, C. Azevedo-Coste, T. Stieglitz, and X. Navarro, "Comparative analysis of transverse intrafascicular multichannel, longitudinal intrafascicular and multipolar cuff electrodes for the selective stimulation of nerve fascicles.," *J. Neural Eng.*, vol. 8, no. 3, p. 036023, Jun. 2011.

[119] S. Raspopovic, M. Capogrosso, and S. Micera, "A computational model for the stimulation of rat sciatic nerve using a transverse intrafascicular multichannel electrode.," *IEEE Trans. Neural Syst. Rehabil. Eng.*, vol. 19, no. 4, pp. 333–44, Aug. 2011.

[120] J. Badia, T. Boretius, A. Pascual-Font, E. Udina, T. Stieglitz, and X. Navarro, "Biocompatibility of chronically implanted transverse intrafascicular multichannel electrode (TIME) in the rat sciatic nerve.," *IEEE Trans. Biomed. Eng.*, vol. 58, no. 8, pp. 2324–2332, Aug. 2011.

[121] A. Kundu, K. R. Harreby, K. Yoshida, T. Boretius, T. Stieglitz, and W. Jensen, "Stimulation selectivity of the 'thin-film longitudinal intrafascicular electrode' (tfLIFE) and the 'transverse intrafascicular multi-channel electrode' (TIME) in the large nerve animal model.," *IEEE Trans. Neural Syst. Rehabil. Eng.*, vol. 22, no. 2, pp. 400–10, Mar. 2014.

[122] A. Branner, R. B. Stein, and R. A. Normann, "Selective Stimulation of Cat Sciatic Nerve Using an Array of Varying-Length Microelectrodes," *J Neurophysiol*, vol. 85, no. 4, pp. 1585–1594, Apr. 2001.

[123] C. T. Nordhausen, P. J. Rousche, and R. a Normann, "Optimizing recording capabilities of the Utah Intracortical Electrode Array.," *Brain Res.*, vol. 637, no. 1–2, pp. 27–36, Feb. 1994.

[124] Y. Aoyagi, R. B. Stein, A. Branner, K. G. Pearson, and R. a Normann, "Capabilities of a penetrating microelectrode array for recording single units in dorsal root ganglia of the cat," *J. Neurosci. Methods*, vol. 128, no. 1–2, pp. 9–20, Sep. 2003.

[125] R. B. Stein, D. J. Weber, Y. Aoyagi, a Prochazka, J. B. M. Wagenaar, S. Shoham, and R. a Normann, "Coding of position by simultaneously recorded sensory neurones in the cat dorsal root ganglion.," *J. Physiol.*, vol. 560, no. Pt 3, pp. 883–96, Nov. 2004.

[126] A. Branner and R. Stein, "Long-term stimulation and recording with a penetrating microelectrode array in cat sciatic nerve," *Biomed. …*, vol. 51, no. 1, pp. 146–57, Jan. 2004.

[127] R. A. Normann, D. McDonnall, G. A. Clark, R. B. Stein, and A. Branner, "Physiological activation of the hind limb muscles of the anesthetized cat using the Utah slanted electrode array," in *Proceedings. 2005 IEEE International Joint Conference on Neural Networks, 2005.*, 2005, vol. 5, pp. 3103–3108.

[128] G. a Clark, N. M. Ledbetter, D. J. Warren, and R. R. Harrison, “Recording sensory and motor information from peripheral nerves with Utah Slanted Electrode Arrays.,” *Conf. Proc. IEEE Eng. Med. Biol. Soc.*, vol. 2011, pp. 4641–4, Jan. 2011.

[129] H. a C. Wark, R. Sharma, K. S. Mathews, E. Fernandez, J. Yoo, B. Christensen, P. Tresco, L. Rieth, F. Solzbacher, R. a Normann, and P. Tathireddy, “A new high-density (25 electrodes/mm^2) penetrating microelectrode array for recording and stimulating sub-millimeter neuroanatomical structures.,” *J. Neural Eng.*, vol. 10, no. 4, p. 045003, Aug. 2013.

[130] M. Gasson, B. Hutt, I. Goodhew, P. Kyberd, and K. Warwick, “Invasive neural prosthesis for neural signal detection and nerve stimulation,” *Int. J. Adapt. Control Signal Process.*, no. December 2004, pp. 365–375, 2004.

[131] R. A. Normann, E. M. Maynard, P. J. Rousche, and D. J. Warren, “A neural interface for a cortical vision prosthesis,” *Vision Res.*, vol. 39, no. 15, pp. 2577–2587, Jul. 1999.

[132] H. A. C. Wark, B. R. Dowden, P. C. Cartwright, and R. A. Normann, “Selective Activation of the Muscles of Micturition Using Intrafascicular Stimulation of the Pudendal Nerve,” *IEEE J. Emerg. Sel. Top. Circuits Syst.*, vol. 1, no. 4, pp. 631–636, Dec. 2011.

[133] a Mannard, R. Stein, and D. Charles, “Regeneration electrode units: implants for recording from single peripheral nerve fibers in freely moving animals,” *Science (80-.).*, vol. 183, no. 4124, pp. 547–9, Feb. 1974.

[134] D. J. Edell, “A peripheral nerve information transducer for amputees: long-term multichannel recordings from rabbit peripheral nerves.,” *IEEE Trans. Biomed. Eng.*, vol. 33, no. 2, pp. 203–14, Feb. 1986.

[135] C. De Luca and L. Gilmore, “Long-term neuroelectric signal recording from severed nerves,” *Biomed. …*, no. 6, pp. 393–403, 1982.

[136] A. Mensinger and D. Anderson, “Chronic recording of regenerating VIIIth nerve axons with a sieve electrode,” *J. …*, pp. 611–615, 2000.

[137] R. M. Bradley, R. H. Smoke, T. Akin, and K. Najafi, “Functional regeneration of glossopharyngeal nerve through micromachined sieve electrode arrays.,” *Brain Res.*, vol. 594, no. 1, pp. 84–90, Oct. 1992.

[138] T. Akin, K. Najafi, R. H. Smoke, and R. M. Bradley, “A micromachined silicon sieve electrode for nerve regeneration applications.,” *IEEE Trans. Biomed. Eng.*, vol. 41, no. 4, pp. 305–13, Apr. 1994.

[139] R. M. Bradley, X. Cao, T. Akin, and K. Najafi, “Long term chronic recordings from peripheral sensory fibers using a sieve electrode array.,” *J. Neurosci. Methods*, vol. 73, no. 2, pp. 177–86, May 1997.

[140] T. Stieglitz, C. Blau, and J.-U. Meyer, “Flexible, light-weighted electrodes to contact the peripheral nervous system,” in *Proceedings of 18th Annual International Conference of the IEEE Engineering in Medicine and Biology Society*, vol. 1, pp. 363–364.

[141] Y. Shimatani, S. A. Nikles, K. Najafi, and R. M. Bradley, “Long-term recordings from afferent taste fibers.,” *Physiol. Behav.*, vol. 80, no. 2–3, pp. 309–15, Nov. 2003.

[142] A. Ramachandran, M. Schuettler, N. Lago, T. Doerge, K. P. Koch, X. Navarro, K.-P. Hoffmann, and T. Stieglitz, “Design, in vitro and in vivo assessment of a multi-channel sieve electrode with integrated multiplexer.,” *J. Neural Eng.*, vol. 3, no. 2, pp. 114–24, Jun. 2006.

[143] P. Negredo, J. Castro, N. Lago, X. Navarro, and C. Avendaño, “Differential growth of axons from sensory and motor neurons through a regenerative electrode: a stereological, retrograde tracer, and functional study in the rat.,” *Neuroscience*, vol. 128, no. 3, pp. 605–15, Jan. 2004.

[144] N. Lago, E. Udina, A. Ramachandran, and X. Navarro, “Neurobiological assessment of regenerative electrodes for bidirectional interfacing injured peripheral nerves.,” *IEEE Trans. Biomed. Eng.*, vol. 54, no. 6 Pt 1, pp. 1129–37, Jun. 2007.

[145] J. Castro, P. Negredo, and C. Avendaño, “Fiber composition of the rat sciatic nerve and its modification during regeneration through a sieve electrode.,” *Brain Res.*, vol. 1190, pp. 65–77, Jan. 2008.

[146] J. J. FitzGerald, N. Lago, S. Benmerah, J. Serra, C. P. Watling, R. E. Cameron, E. Tarte, S. P. Lacour, S. B. McMahon, and J. W. Fawcett, “A regenerative microchannel neural interface for recording from and stimulating peripheral axons in vivo.,” *J. Neural Eng.*, vol. 9, no. 1, p. 016010, Feb. 2012.

[147] I. R. Minev, D. J. Chew, E. Delivopoulos, J. W. Fawcett, and S. P. Lacour, “High sensitivity recording of afferent nerve activity using ultra-compliant microchannel electrodes: an acute in vivo validation.,” *J. Neural Eng.*, vol. 9, no. 2, p. 026005, Apr. 2012.

[148] D. J. Chew, L. Zhu, E. Delivopoulos, I. R. Minev, K. M. Musick, C. a. Mosse, M. Craggs, N. Donaldson, S. P. Lacour, S. B. McMahon, and J. W. Fawcett, “A Microchannel Neuroprosthesis for Bladder Control After Spinal Cord Injury in Rat,” *Sci. Transl. Med.*, vol. 5, no. 210, pp. 210ra155–210ra155, Nov. 2013.

[149] K. Garde, E. Keefer, B. Botterman, P. Galvan, and M. I. Romero, “Early interfaced neural activity from chronic amputated nerves.,” *Front. Neuroeng.*, vol. 2, p. 5, Jan. 2009.

[150] J. L. Seifert, V. Desai, R. C. Watson, T. Musa, Y.-T. Kim, E. W. Keefer, and M. I. Romero, “Normal molecular repair mechanisms in regenerative peripheral nerve interfaces allow recording of early spike activity despite immature myelination.,” *IEEE Trans. neural Syst. Rehabil. Eng. a Publ. IEEE Eng. Med. Biol. Soc.*, vol. 20, no. 2, pp. 220–7, 2012.

[151] M. a L. Nicolelis, D. Dimitrov, J. M. Carmena, R. Crist, G. Lehew, J. D. Kralik, and S. P. Wise, “Chronic, multisite, multielectrode recordings in macaque monkeys.,” *Proc. Natl. Acad. Sci. U. S. A.*, vol. 100, no. 19, pp. 11041–6, Sep. 2003.

[152] J. a Perge, M. L. Homer, W. Q. Malik, S. Cash, E. Eskandar, G. Friehs, J. P. Donoghue, and L. R. Hochberg, “Intra-day signal instabilities affect decoding performance in an intracortical neural interface system.,” *J. Neural Eng.*, vol. 10, no. 3, p. 036004, Jun. 2013.

[153] T. a Kung, R. a Bueno, G. K. Alkhalefah, N. B. Langhals, M. G. Urbanchek, and P. S. Cederna, “Innovations in prosthetic interfaces for the upper extremity.,” *Plast. Reconstr. Surg.*, vol. 132, no. 6, pp. 1515–23, Dec. 2013.

[154] G. E. Loeb and R. a Peck, “Cuff electrodes for chronic stimulation and recording of peripheral nerve activity.,” *J. Neurosci. Methods*, vol. 64, no. 1, pp. 95–103, Jan. 1996.

[155] S. Raspopovic, J. Carpaneto, E. Udina, X. Navarro, and S. Micera, “On the identification of sensory information from mixed nerves by using single-channel cuff electrodes.,” *J. Neuroeng. Rehabil.*, vol. 7, p. 17, Jan. 2010.

[156] G. S. Dhillon and K. W. Horch, “Direct neural sensory feedback and control of a prosthetic arm.,” *IEEE Trans. Neural Syst. Rehabil. Eng.*, vol. 13, no. 4, pp. 468–72, Dec. 2005.

[157] P. M. Rossini, S. Micera, A. Benvenuto, J. Carpaneto, G. Cavallo, L. Citi, C. Cipriani, L. Denaro, V. Denaro, G. Di Pino, F. Ferreri, E. Guglielmelli, K.-P. Hoffmann, S. Raspopovic, J. Rigosa, L. Rossini, M. Tombini, and P. Dario, “Double nerve intraneural interface implant on a human amputee for robotic hand control.,” *Clin. Neurophysiol.*, vol. 121, no. 5, pp. 777–83, May 2010.

[158] S. Micera, P. M. Rossini, J. Rigosa, L. Citi, J. Carpaneto, S. Raspopovic, M. Tombini, C. Cipriani, G. Assenza, M. C. Carrozza, K.-P. Hoffmann, K. Yoshida, X. Navarro, and P. Dario, “Decoding of grasping information from neural signals recorded using peripheral intrafascicular interfaces.,” *J. Neuroeng. Rehabil.*, vol. 8, no. D, p. 53, Jan. 2011.

[159] J. A. Malmstrom, T. G. McNaughton, and K. W. Horch, “Recording properties and biocompatibility of chronically implanted polymer-based intrafascicular electrodes.,” *Ann. Biomed. Eng.*, vol. 26, no. 6, pp. 1055–64.

[160] a Branner and R. a Normann, “A multielectrode array for intrafascicular recording and stimulation in sciatic nerve of cats.,” *Brain Res. Bull.*, vol. 51, no. 4, pp. 293–306, Mar. 2000.

[161] N. Lago, D. Ceballos, F. J. Rodríguez, T. Stieglitz, and X. Navarro, “Long term assessment of axonal regeneration through polyimide regenerative electrodes to interface the peripheral nerve.,” *Biomaterials*, vol. 26, no. 14, pp. 2021–31, May 2005.

[162] S. Musallam, M. J. Bak, P. R. Troyk, and R. A. Andersen, “A floating metal microelectrode array for chronic implantation.,” *J. Neurosci. Methods*, vol. 160, no. 1, pp. 122–7, Mar. 2007.

[163] P. J. Rousche and R. a Normann, “A method for pneumatically inserting an array of penetrating electrodes into cortical tissue.,” *Ann. Biomed. Eng.*, vol. 20, no. 4, pp. 413–22, Jan. 1992.

[164] F. Wood, M. J. Black, C. Vargas-Irwin, M. Fellows, and J. P. Donoghue, “On the variability of manual spike sorting.,” *IEEE Trans. Biomed. Eng.*, vol. 51, no. 6, pp. 912–8, Jun. 2004.

[165] R. Q. Quiroga, L. Reddy, G. Kreiman, C. Koch, and I. Fried, “Invariant visual representation by single neurons in the human brain.,” *Nature*, vol. 435, no. 7045, pp. 1102–7, Jun. 2005.

[166] K. A. Ludwig, J. D. Uram, J. Yang, D. C. Martin, and D. R. Kipke, “Chronic neural recordings using silicon microelectrode arrays electrochemically deposited with a poly(3,4-ethylenedioxythiophene) (PEDOT) film.,” *J. Neural Eng.*, vol. 3, no. 1, pp. 59–70, Mar. 2006.

[167] S. Suner, M. R. Fellows, C. Vargas-Irwin, G. K. Nakata, and J. P. Donoghue, “Reliability of signals from a chronically implanted, silicon-based electrode array in non-human primate primary motor cortex.,” *IEEE Trans. Neural Syst. Rehabil. Eng.*, vol. 13, no. 4, pp. 524–41, Dec. 2005.

[168] M. S. Fee, P. P. Mitra, and D. Kleinfeld, “Variability of extracellular spike waveforms of cortical neurons.,” *J. Neurophysiol.*, vol. 76, no. 6, pp. 3823–33, Dec. 1996.

[169] M. P. Ward, P. Rajdev, C. Ellison, and P. P. Irazoqui, “Toward a comparison of microelectrodes for acute and chronic recordings.,” *Brain Res.*, vol. 1282, pp. 183–200, Jul. 2009.

[170] S. Gibson, J. W. Judy, and D. Marković, “Technology-aware algorithm design for neural spike detection, feature extraction, and dimensionality reduction.,” *IEEE Trans. Neural Syst. Rehabil. Eng.*, vol. 18, no. 5, pp. 469–78, Oct. 2010.

[171] C. T. Nordhausen, P. J. Rousche, and R. a Normann, “Optimizing recording capabilities of the Utah Intracortical Electrode Array.,” *Brain Res.*, vol. 637, no. 1–2, pp. 27–36, Mar. 1994.

[172] R. Mancini, *Op Amps for Everyone*. Newnes, 2009, p. 648.

[173] J. Weis, R. May, and J. M. Schröder, “Fine structural and immunohistochemical identification of perineurial cells connecting proximal and distal stumps of transected peripheral nerves at early stages of regeneration in silicone tubes.,” *Acta Neuropathol.*, vol. 88, no. 2, pp. 159–65, Jan. 1994.

[174] X. Liu, D. B. McCreery, R. R. Carter, L. a Bullara, T. G. Yuen, and W. F. Agnew, “Stability of the interface between neural tissue and chronically implanted intracortical microelectrodes.,” *IEEE Trans. Rehabil. Eng.*, vol. 7, no. 3, pp. 315–26, Sep. 1999.

[175] C. a Chestek, V. Gilja, P. Nuyujukian, J. D. Foster, J. M. Fan, M. T. Kaufman, M. M. Churchland, Z. Rivera-Alvidrez, J. P. Cunningham, S. I. Ryu, and K. V Shenoy, “Long-term stability of neural prosthetic control signals from silicon cortical arrays in rhesus macaque motor cortex.,” *J. Neural Eng.*, vol. 8, no. 4, p. 045005, Aug. 2011.

[176] L. Karumbaiah, T. Saxena, D. Carlson, K. Patil, R. Patkar, E. a Gaupp, M. Betancur, G. B. Stanley, L. Carin, and R. V Bellamkonda, “Relationship between intracortical electrode design and chronic recording function.,” *Biomaterials*, vol. 34, no. 33, pp. 8061–74, Nov. 2013.

[177] B. Wodlinger, “Extracting Command Signals From Peripheral Nerve Recordings,” 2010.

[178] A. Branner, R. B. Stein, E. Fernandez, Y. Aoyagi, and R. A. Normann, “Long-term stimulation and recording with a penetrating microelectrode array in cat sciatic nerve.,” *IEEE Trans. Biomed. Eng.*, vol. 51, no. 1, pp. 146–57, Jan. 2004.

[179] R. M. Bradley, X. Cao, T. Akin, and K. Najafi, “Long term chronic recordings from peripheral sensory fibers using a sieve electrode array.,” *J. Neurosci. Methods*, vol. 73, no. 2, pp. 177–86, May 1997.

[180] S.-H. Cho, H. M. Lu, L. Cauller, M. I. Romero-Ortega, J.-B. Lee, and G. A. Hughes, “Biocompatible SU-8-Based Microprobes for Recording Neural Spike Signals From Regenerated Peripheral Nerve Fibers,” *IEEE Sens. J.*, vol. 8, no. 11, pp. 1830–1836, Nov. 2008.

[181] W. R. Patterson, M. Ieee, Y. Song, C. W. Bull, D. A. Borton, F. Laiwalla, S. Park, Y. Ming, and J. Aceros, “Listening to Brain Microcircuits for Interfacing With External World V Progress in Wireless Implantable Microelectronic Neuroengineering Devices,” vol. 98, no. 3, pp. 375–388, 2010.

[182] A. Sharma, L. Rieth, P. Tathireddy, R. Harrison, H. Oppermann, M. Klein, M. Töpper, E. Jung, R. Normann, G. Clark, and F. Solzbacher, “Long term in vitro functional stability and recording longevity of fully integrated wireless neural interfaces based on the Utah Slant Electrode Array.,” *J. Neural Eng.*, vol. 8, no. 4, p. 045004, Aug. 2011.

[183] J. Aceros, M. Yin, D. A. Borton, W. R. Patterson, C. Bull, and A. V Nurmikko, “Polymeric packaging for fully implantable wireless neural microsensors.,” *Conf. Proc. IEEE Eng. Med. Biol. Soc.*, vol. 2012, pp. 743–6, Jan. 2012.

[184] D. A. Borton, M. Yin, J. Aceros, and A. Nurmikko, “An implantable wireless neural interface for recording cortical circuit dynamics in moving primates.,” *J. Neural Eng.*, vol. 10, no. 2, p. 026010, Apr. 2013.

[185] N. Lago, E. Udina, A. Ramachandran, and X. Navarro, “Neurobiological assessment of regenerative electrodes for bidirectional interfacing injured peripheral nerves.,” *IEEE Trans. Biomed. Eng.*, vol. 54, no. 6 Pt 1, pp. 1129–37, Jun. 2007.

[186] X. Navarro, S. Calvet, M. Butí, N. Gómez, E. Cabruja, P. Garrido, R. Villa, and E. Valderrama, “Peripheral nerve regeneration through microelectrode arrays based on silicon technology.,” *Restor. Neurol. Neurosci.*, vol. 9, no. 3, pp. 151–60, Jan. 1996.

[187] Q. Zhao, J. Drott, T. Laurell, L. Wallman, kjell Lindström, L. M. Bjursten, G. Lundborg, L. Montelius, and N. Danielsen, “Rat sciatic nerve regeneration through a micromachined silicon chip,” *Biomaterials*, vol. 18, no. 1, pp. 75–80, Jan. 1997.

[188] D. Ceballos, A. Valero-Cabré, E. Valderrama, M. Schüttler, T. Stieglitz, and X. Navarro, “Morphologic and functional evaluation of peripheral nerve fibers regenerated through polyimide sieve electrodes over long-term implantation.,” *J. Biomed. Mater. Res.*, vol. 60, no. 4, pp. 517–28, Jun. 2002.

[189] M. D. Wood, S. W. P. Kemp, C. Weber, G. H. Borschel, and T. Gordon, “Outcome measures of peripheral nerve regeneration.,” *Ann. Anat.*, vol. 193, no. 4, pp. 321–33, Jul. 2011.

[190] M. A. M. Freire, E. Morya, J. Faber, J. R. Santos, J. S. Guimaraes, N. a M. Lemos, K. Sameshima, A. Pereira, S. Ribeiro, and M. a L. Nicolelis, “Comprehensive analysis of tissue preservation and recording quality from chronic multielectrode implants.,” *PLoS One*, vol. 6, no. 11, p. e27554, Jan. 2011.

[191] N. Khobragade, “Micromotion And Scarring Do Not Contribute To Failure Of Regenerative Peripheral Neural Interfacing.” Biomedical Engineering, 01-Jan-2011.

[192] J. Scadding, “Development of ongoing activity, mechanosensitivity, and adrenaline sensitivity in severed peripheral nerve axons,” *Exp. Neurol.*, vol. 364, pp. 345–364, 1981.

[193] W. Jänig, L. Grossmann, and N. Gorodetskaya, “Mechano- and thermosensitivity of regenerating cutaneous afferent nerve fibers.,” *Exp. Brain Res.*, vol. 196, no. 1, pp. 101–14, Jun. 2009.

[194] M. Michaelis, K. H. Blenk, W. Jänig, and C. Vogel, “Development of spontaneous activity and mechanosensitivity in axotomized afferent nerve fibers during the first hours after nerve transection in rats.,” *J. Neurophysiol.*, vol. 74, no. 3, pp. 1020–7, Sep. 1995.

[195] B. Zalc and R. D. Fields, “Do Action Potentials Regulate Myelination?,” *Neuroscientist*, vol. 6, no. 1, pp. 5–13, Feb. 2000.

[196] R. D. Fields, “Nerve impulses regulate myelination through purinergic signalling.,” *Novartis Found. Symp.*, vol. 276, pp. 148–58; discussion 158–61, 233–7, 275–81, Jan. 2006.

[197] G. Ming, J. Henley, M. Tessier-Lavigne, H. Song, and M. Poo, “Electrical activity modulates growth cone guidance by diffusible factors.,” *Neuron*, vol. 29, no. 2, pp. 441–52, Feb. 2001.

[198] J. W. Fawcett and R. J. Keynes, “Peripheral nerve regeneration.,” *Annu. Rev. Neurosci.*, vol. 13, pp. 43–60, Jan. 1990.

[199] G. Stoll and H. W. Müller, “Nerve injury, axonal degeneration and neural regeneration: basic insights.,” *Brain Pathol.*, vol. 9, no. 2, pp. 313–25, May 1999.

[200] N. Mokarram, A. Merchant, V. Mukhatyar, G. Patel, and R. V Bellamkonda, “Effect of modulating macrophage phenotype on peripheral nerve repair.,” *Biomaterials*, vol. 33, no. 34, pp. 8793–801, Dec. 2012.

[201] S. F. Lempka, M. D. Johnson, M. a Moffitt, K. J. Otto, D. R. Kipke, and C. C. McIntyre, “Theoretical analysis of intracortical microelectrode recordings.,” *J. Neural Eng.*, vol. 8, no. 4, p. 045006, Aug. 2011.

[202] K. A. Ludwig, J. D. Uram, J. Yang, D. C. Martin, and D. R. Kipke, “Chronic neural recordings using silicon microelectrode arrays electrochemically deposited with a poly(3,4-ethylenedioxythiophene) (PEDOT) film.,” *J. Neural Eng.*, vol. 3, no. 1, pp. 59–70, Mar. 2006.

[203] S. F. Cogan, “Neural stimulation and recording electrodes.,” *Annu. Rev. Biomed. Eng.*, vol. 10, pp. 275–309, Jan. 2008.

[204] Z. Yang, Q. Zhao, E. Keefer, and W. Liu, “Noise characterization, modeling, and reduction for in vivo neural recording,” *Adv. Neural …*, pp. 1–9, 2009.

[205] M. Johnson, K. Otto, and D. Kipke, “Repeated voltage biasing improves unit recordings by reducing resistive tissue impedances,” *Neural Syst. …*, vol. 13, no. 2, pp. 160–165, 2005.

[206] W. L. C. Rutten, “Selective electrical interfaces with the nervous system.,” *Annu. Rev. Biomed. Eng.*, vol. 4, pp. 407–52, Jan. 2002.

[207] J. C. Williams, J. a Hippensteel, J. Dilgen, W. Shain, and D. R. Kipke, “Complex impedance spectroscopy for monitoring tissue responses to inserted neural implants.,” *J. Neural Eng.*, vol. 4, no. 4, pp. 410–23, Dec. 2007.

[208] A. Prasad, Q.-S. Xue, R. Dieme, V. Sankar, R. C. Mayrand, T. Nishida, W. J. Streit, and J. C. Sanchez, “Abiotic-biotic characterization of Pt/Ir microelectrode arrays in chronic implants.,” *Front. Neuroeng.*, vol. 7, p. 2, Jan. 2014.

[209] E. Stark and M. Abeles, “Predicting movement from multiunit activity.,” *J. Neurosci.*, vol. 27, no. 31, pp. 8387–94, Aug. 2007.

[210] C. a Chestek, J. P. Cunningham, V. Gilja, P. Nuyujukian, S. I. Ryu, and K. V Shenoy, “Neural prosthetic systems: current problems and future directions.,” *Conf. Proc. IEEE Eng. Med. Biol. Soc.*, vol. 2009, pp. 3369–75, Jan. 2009.

[211] J. a Malmstrom, T. G. McNaughton, and K. W. Horch, “Recording properties and biocompatibility of chronically implanted polymer-based intrafascicular electrodes.,” *Ann. Biomed. Eng.*, vol. 26, no. 6, pp. 1055–64, 1998.

[212] A. S. Dickey, A. Suminski, Y. Amit, and N. G. Hatsopoulos, “Single-unit stability using chronically implanted multielectrode arrays.,” *J. Neurophysiol.*, vol. 102, no. 2, pp. 1331–9, Aug. 2009.

[213] C. W. Lu, P. G. Patil, and C. a Chestek, “Current challenges to the clinical translation of brain machine interface technology.,” *Int. Rev. Neurobiol.*, vol. 107, pp. 137–60, Jan. 2012.

[214] G. Di Pino, E. Guglielmelli, and P. M. Rossini, “Neuroplasticity in amputees: main implications on bidirectional interfacing of cybernetic hand prostheses.,” *Prog. Neurobiol.*, vol. 88, no. 2, pp. 114–26, Jun. 2009.

[215] J. Dargahi and S. Najarian, “Human tactile perception as a standard for artificial tactile sensing--a review.,” *Int. J. Med. Robot.*, vol. 1, no. 1, pp. 23–35, Jun. 2004.

[216] G. M. Manzano, L. M. P. Giuliano, and J. a M. Nóbrega, “A brief historical note on the classification of nerve fibers.,” *Arq. Neuropsiquiatr.*, vol. 66, no. 1, pp. 117–9, Mar. 2008.

[217] J. D. Stewart, “Peripheral nerve fascicles: anatomy and clinical relevance.,” *Muscle Nerve*, vol. 28, no. 5, pp. 525–41, Nov. 2003.

[218] J. Badia, A. Pascual-Font, M. Vivó, E. Udina, and X. Navarro, “Topographical distribution of motor fascicles in the sciatic-tibial nerve of the rat.,” *Muscle Nerve*, vol. 42, no. 2, pp. 192–201, Aug. 2010.

[219] G. Bernard, L. Bouyer, J. Provencher, and S. Rossignol, “Study of cutaneous reflex compensation during locomotion after nerve section in the cat.,” *J. Neurophysiol.*, vol. 97, no. 6, pp. 4173–85, Jun. 2007.

[220] J. E. Swett and C. J. Woolf, “The somatotopic organization of primary afferent terminals in the superficial laminae of the dorsal horn of the rat spinal cord.,” *J. Comp. Neurol.*, vol. 231, no. 1, pp. 66–77, Jan. 1985.

[221] S. Herbert, “The Classification of Nerve Fibers,” vol. 41, no. 3, pp. 145–159, 1941.

[222] D. P. C. Lloyd, “NEURON PATTERNS CONTROLLING TRANSMISSION OF IPSILATERAL HIND LIMB REFLEXES IN CAT,” *J Neurophysiol*, vol. 6, no. 4, pp. 293–315, Jul. 1943.

[223] “Cutaneous and Subcutaneous Somatic Sensory Receptors.” Sinauer Associates, 2001.

[224] S. W. Shaffer and A. L. Harrison, “Aging of the Somatosensory System: A Translational Perspective .”

[225] S. Raspopovic, M. Capogrosso, F. M. Petrini, M. Bonizzato, J. Rigosa, G. Di Pino, J. Carpaneto, M. Controzzi, T. Boretius, E. Fernandez, G. Granata, C. M. Oddo, L. Citi, A. L. Ciancio, C. Cipriani, M. C. Carrozza, W. Jensen, E. Guglielmelli, T. Stieglitz, P. M. Rossini, and S. Micera, “Restoring natural sensory feedback in real-time bidirectional hand prostheses.,” *Sci. Transl. Med.*, vol. 6, no. 222, p. 222ra19, Feb. 2014.

[226] S. Fu and T. Gordon, “Contributing factors to poor functional recovery after delayed nerve repair: prolonged denervation,” *J. Neurosci.*, vol. 15, no. 5, pp. 3886–3895, May 1995.

[227] E. Gutmann and F. K. Sanders, “Recovery of fibre numbers and diameters in the regeneration of peripheral nerves.,” *J. Physiol.*, vol. 101, no. 4, pp. 489–518, Mar. 1943.

[228] B. G. CRAGG and P. K. THOMAS, “THE CONDUCTION VELOCITY OF REGENERATED PERIPHERAL NERVE FIBRES.,” *J. Physiol.*, vol. 171, pp. 164–75, May 1964.

[229] T. Tandrup, C. J. Woolf, and R. E. Coggeshall, “Delayed loss of small dorsal root ganglion cells after transection of the rat sciatic nerve.,” *J. Comp. Neurol.*, vol. 422, no. 2, pp. 172–80, Jun. 2000.

[230] S. Y. Fu and T. Gordon, “The cellular and molecular basis of peripheral nerve regeneration.,” *Mol. Neurobiol.*, vol. 14, no. 1–2, pp. 67–116.

[231] H. Rönkkö, H. Göransson, P. Siironen, H. S. Taskinen, V. Vuorinen, and M. Röyttä, “The capacity of the distal stump of peripheral nerve to receive growing axons after two and six months denervation.,” *Scand. J. Surg.*, vol. 100, no. 3, pp. 223–9, Jan. 2011.

[232] S. N. Lawson, B. a Crepps, and E. R. Perl, “Relationship of substance P to afferent characteristics of dorsal root ganglion neurones in guinea-pig.,” *J. Physiol.*, vol. 505 (Pt 1, pp. 177–91, Nov. 1997.

[233] M. A. Ariano, R. B. Armstrong, and V. R. Edgerton, “Hindlimb muscle fiber populations of five mammals.,” *J. Histochem. Cytochem.*, vol. 21, no. 1, pp. 51–5, Jan. 1973.

[234] R. Hennig and T. Lømo, “Firing patterns of motor units in normal rats,” *Nature*, vol. 314, no. 6007, pp. 164–166, Mar. 1985.

[235] V. E. Abraira and D. D. Ginty, “The sensory neurons of touch.,” *Neuron*, vol. 79, no. 4, pp. 618–39, Aug. 2013.

[236] T. Milner and R. Stein, “Improved estimates of conduction velocity distributions using single unit action potentials.,” *J. Neurol. …*, vol. 44, no. 6, pp. 476–84, Jun. 1981.

[237] J. J. Struijk, “The extracellular potential of a myelinated nerve fiber in an unbounded medium and in nerve cuff models.,” *Biophys. J.*, vol. 72, no. 6, pp. 2457–69, Jun. 1997.

[238] C. H. Hakansson, “Conduction velocity and amplitude of the action potential as related to circumference in the isolated fibre of frog muscle.,” *Acta Physiol. Scand.*, vol. 37, no. 1, pp. 14–34, Jul. 1956.

[239] E. Blair and J. Erlanger, “A comparison of the characteristics of axons through their individual electrical responses,” *Am. J. Physiol. …*, 1933.

[240] D. Humphrey and E. Schmidt, “Extracellular single-unit recording methods,” *Neurophysiol. Tech.*, 1991.

[241] A. Towe and G. Harding, “Extracellular microelectrode sampling bias,” *Exp. Neurol.*, vol. 381, pp. 366–381, 1970.

[242] R. a Gaunt, J. a Hokanson, and D. J. Weber, “Microstimulation of primary afferent neurons in the L7 dorsal root ganglia using multielectrode arrays in anesthetized cats: thresholds and recruitment properties.,” *J. Neural Eng.*, vol. 6, no. 5, p. 055009, Oct. 2009.

[243] D. Bourbeau, J. Hokanson, J. E. Rubin, and D. Weber, “A computational model for estimating recruitment of primary afferent fibers by intraneural stimulation in the dorsal root ganglia.,” *J. Neural Eng.*, vol. 8, no. 5, p. 056009, 2011.

[244] L. Fisher and C. Ayers, “Chronic recruitment of primary afferent neurons by microstimulation in the feline dorsal root ganglia,” *J. neural …*, vol. 11, no. 3, p. 036007, Jun. 2014.

[245] V. G. Macefield, S. C. Gandevia, B. Bigland-Ritchie, R. B. Gorman, and D. Burke, “The firing rates of human motoneurones voluntarily activated in the absence of muscle afferent feedback.,” *J. Physiol.*, vol. 471, pp. 429–43, Nov. 1993.

[246] H. Schmalbruch, “Fiber composition of the rat sciatic nerve.,” *Anat. Rec.*, vol. 215, no. 1, pp. 71–81, May 1986.

[247] Y. Kawamura and P. J. Dyck, “Permanent axotomy by amputation results in loss of motor neurons in man.,” *J. Neuropathol. Exp. Neurol.*, vol. 40, no. 6, pp. 658–66, Nov. 1981.

[248] M. J. Furey, R. Midha, Q.-G. Xu, J. Belkas, and T. Gordon, “Prolonged target deprivation reduces the capacity of injured motoneurons to regenerate.,” *Neurosurgery*, vol. 60, no. 4, pp. 723–32; discussion 732–3, Apr. 2007.

[249] M. Capogrosso, N. Wenger, S. Raspopovic, P. Musienko, J. Beauparlant, L. Bassi Luciani, G. Courtine, and S. Micera, “A computational model for epidural electrical stimulation of spinal sensorimotor circuits.,” *J. Neurosci.*, vol. 33, no. 49, pp. 19326–40, Dec. 2013.

[250] K. G. Pearson, H. Acharya, and K. Fouad, “A new electrode configuration for recording electromyographic activity in behaving mice,” vol. 148, pp. 36–42, 2005.

[251] B. Elmer, “A Novel Device For The Establishment Of An Animal Model Mimicking Spinal Deformity Surgery For Neurological Deficit Risk Mitigation.” Biomedical Engineering, 01-Jan-2010.

[252] J. V Cichon, T. V McCaffrey, W. J. Litchy, and J. L. Knops, “The effect of botulinum toxin type A injection on compound muscle action potential in an in vivo rat model.,” *Laryngoscope*, vol. 105, no. 2, pp. 144–8, Feb. 1995.

[253] J. P. Cunningham, V. Gilja, S. I. Ryu, and K. V Shenoy, “Methods for estimating neural firing rates, and their application to brain-machine interfaces.,” *Neural Netw.*, vol. 22, no. 9, pp. 1235–46, Nov. 2009.

[254] C. R. Legéndy and M. Salcman, “Bursts and recurrences of bursts in the spike trains of spontaneously active striate cortex neurons.,” *J. Neurophysiol.*, vol. 53, no. 4, pp. 926–39, Apr. 1985.

[255] A. D. Dorval, “Probability distributions of the logarithm of inter-spike intervals yield accurate entropy estimates from small datasets.,” *J. Neurosci. Methods*, vol. 173, no. 1, pp. 129–39, Aug. 2008.

[256] M. MacKay-Lyons, “Central pattern generation of locomotion: a review of the evidence.,” *Phys. Ther.*, vol. 82, no. 1, pp. 69–83, Jan. 2002.

[257] A. Prochazka and P. Ellaway, “Sensory systems in the control of movement.,” *Compr. Physiol.*, vol. 2, no. 4, pp. 2615–27, Oct. 2012.

[258] Y. LAPORTE and D. P. C. LLOYD, “Nature and significance of the reflex connections established by large afferent fibers of muscular origin.,” *Am. J. Physiol.*, vol. 169, no. 3, pp. 609–21, Jun. 1952.

[259] E. R. PERL, “Effects of muscle stretch on excitability of contralateral motoneurones.,” *J. Physiol.*, vol. 145, no. 1, pp. 193–203, Jan. 1959.

[260] C. Chen, N. Stott, and H. Smith, “Effects of botulinum toxin A injection and exercise on the growth of juvenile rat gastrocnemius muscle,” *J. Appl. Physiol.*, vol. 93, no. 4, pp. 1437–47, Oct. 2002.

[261] F. A. Meunier, G. Schiavo, and J. Molgó, “Botulinum neurotoxins: from paralysis to recovery of functional neuromuscular transmission.,” *J. Physiol. Paris*, vol. 96, no. 1–2, pp. 105–13.

[262] G. M. Filippi, P. Errico, R. Santarelli, B. Bagolini, and E. Manni, “Botulinum A toxin effects on rat jaw muscle spindles.,” *Acta Otolaryngol.*, vol. 113, no. 3, pp. 400–4, May 1993.

[263] R. L. Rosales, “EXTRAFUSAL AND INTRAFUSAL BOTULINUM TOXIN-A INJECTION,” no. April, pp. 488–496, 1996.

[264] E. E. Fetz and D. V Finocchio, “Correlations between activity of motor cortex cells and arm muscles during operantly conditioned response patterns.,” *Exp. brain Res.*, vol. 23, no. 3, pp. 217–40, Sep. 1975.

[265] T. M. Bruns, J. B. Wagenaar, M. J. Bauman, R. a Gaunt, and D. J. Weber, “Real-time control of hind limb functional electrical stimulation using feedback from dorsal root ganglia recordings.,” *J. Neural Eng.*, vol. 10, no. 2, p. 026020, Apr. 2013.

[266] S. J. Bensmaia and L. E. Miller, “Restoring sensorimotor function through intracortical interfaces: progress and looming challenges.,” *Nat. Rev. Neurosci.*, vol. 15, no. 5, pp. 313–25, Apr. 2014.

[267] E. a Pohlmeyer, S. a Solla, E. J. Perreault, and L. E. Miller, “Prediction of upper limb muscle activity from motor cortical discharge during reaching.,” *J. Neural Eng.*, vol. 4, no. 4, pp. 369–79, Dec. 2007.

Biographical Information

Vidhi Desai, received a Bachelors in Biomedical Engineering from the Visvesvaraya Technological University, Belgaum, India in June 2009. Encouraged by her father to pursue advanced and globally competitive education, she started graduate studies at the University of Texas at Arlington in August 2009. A long term interest in neuroscience motivated her to join the Regenerative Neurobiology Laboratory of Dr. Mario Romero-Ortega to gain experience in the field of neural engineering. Her PhD dissertation explored the ability of regenerative interfaces to record from peripheral nerves with an in depth characterization of the acquired electrophysiological signals.